AD-A261 270

DOT/FAA/CT-90/22

FAA Technical Center
Atlantic City International Airport
N.J. 08405

A Model Study of the Aircraft Cabin Environment Resulting from In-Flight Fires

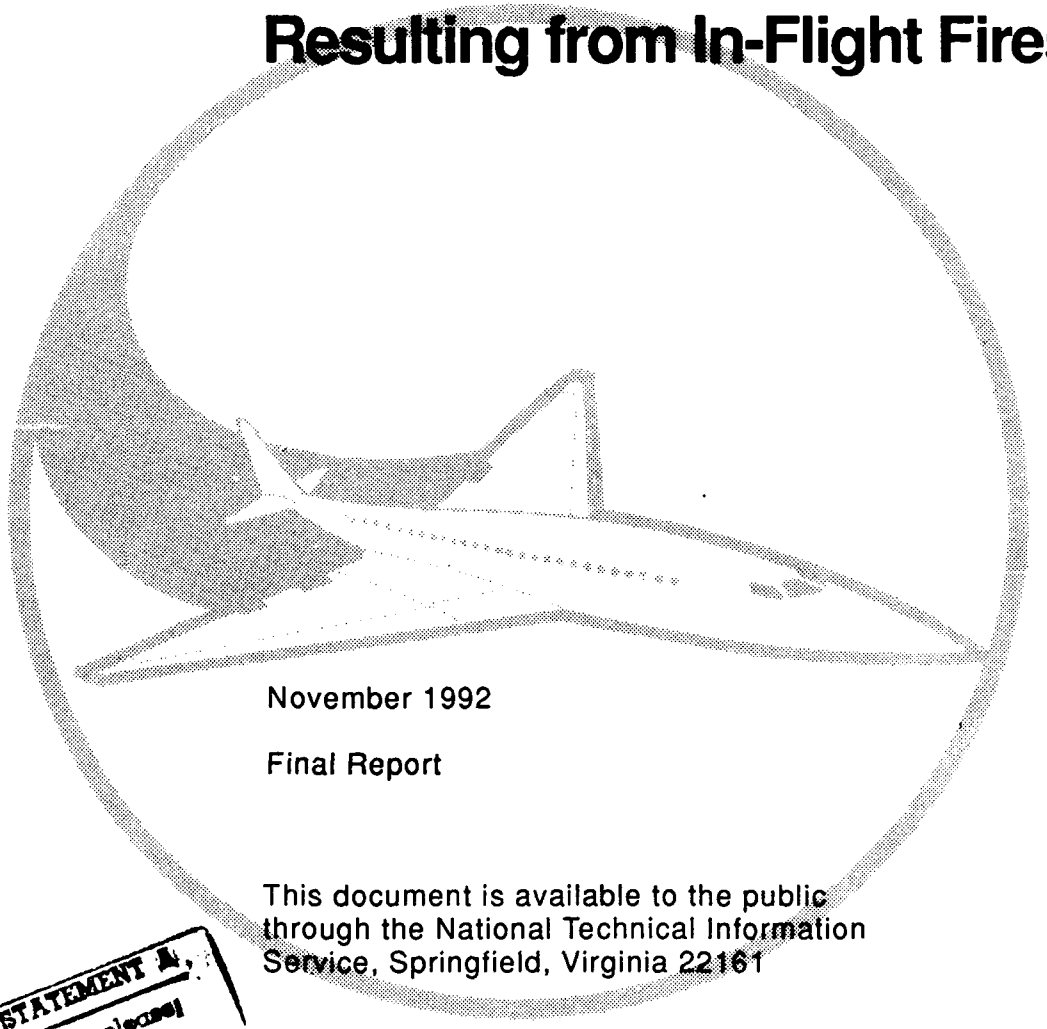

November 1992

Final Report

This document is available to the public through the National Technical Information Service, Springfield, Virginia 22161

DISTRIBUTION STATEMENT A
Approved for public release
Distribution Unlimited

U.S. Department of Transportation
Federal Aviation Administration

DTIC
ELECTE
FEB 25 1993
S D
B

93-03928

93 2 24 053

NOTICE

This document is disseminated under the sponsorship of the U. S. Department of Transportation in the interest of information exchange. The United States Government assumes no liability for the contents or use thereof.

The United States Government does not endorse products or manufacturers. Trade or manufacturers' names appear herein solely because they are considered essential to the objective of this report.

Technical Report Documentation Page

1. Report No.	2. Government Accession No	3. Recipient's Catalog No.
DOT/FAA/CT-90/22		

4. Title and Subtitle	5. Report Date
A MODEL STUDY OF THE AIRCRAFT CABIN ENVIRONMENT RESULTING FROM IN-FLIGHT FIRES	November 1992
	6. Performing Organization Code
7. Author(s) B. J. McCaffrey (U. of MD); King-Mon Tu, W. J. Rinkinen (NIST); and T. I. Eklund (FAA)	8. Performing Organization Report No. DOT/FAA/CT-90/22
9. Performing Organization Name and Address National Institute of Standards and Technology Gaithersburg, MD 20899	10. Work Unit No. (TRAIS)
	11. Contract or Grant No.
12. Sponsoring Agency Name and Address U.S. Department of Transportation Federal Aviation Administration Technical Center Atlantic City International Airport, NJ 08405	13. Type of Report and Period Covered Final Report
	14. Sponsoring Agency Code

15. Supplementary Notes

16. Abstract

A series of tests were conducted to examine the effect of the ventilation on the environment in an aircraft passenger cabin during an in-flight fire. These tests were run in a reduced scale mockup of an aircraft passenger cabin. A propane burner operating at 10 or 30 kilowatts served as the fire source. The simulated seats and the cabin lining material were both noncombustible. The vertical temperature and gas concentration profiles in the cabin were measured as a function of time. Reversing the normal ventilation flow direction by introducing the forced air at the floor level and exhausting it at the ceiling significantly reduced the measured temperatures and gas concentrations. Opening two 152- by 305-millimeter hatches in the end walls at the ceiling level to the outside air resulted in a significant reduction in the measured gas concentrations.

17. Key Words	18. Distribution Statement
Aircraft, Counterflow, Fire, Heat Transfer, Scale Model, Simulation, Ventilation	Document if available to the public through the National Technical Information Service, Springfield, Virginia 22161

19. Security Classif. (of this report)	20. Security Classif. (of this page)	21. No. of Pages	22. Price
Unclassified	Unclassified	126	

Form DOT F 1700.7 (8-72) Reproduction of completed page authorized

Table of Contents

DTIC QUALITY INSPECTED 3

Accession For
NTIS GRA&I ☑
DTIC TAB ☐
Unannounced ☐
Justification
By
Distribution/
Availability Codes
Dist | Special
A-1

EXECUTIVE SUMMARY

Fatal aircraft accidents resulting from in-flight fires have been characterized by deteriorating conditions within the passenger cabin. Visibility is lost as smoke accumulates, and the spread of noxious fumes can lead to passenger incapacitation. Improvements in capability to control or eliminate combustion products in the cabin depend in large measure on performance capability of the aircraft ventilation system. Past theoretical and experimental fire research is not directly applicable to the in-flight aircraft fire. Existing data pertain primarily to rooms, corridors, and warehouses wherein the spread of smoke is controlled primarily by the buoyancy of a fire plume rising into initially quiescent air. Air currents are driven by the fire itself. The flows in and out of enclosure openings are controlled by differential atmospheric head pressures.

In jet aircraft, air is supplied from engine compressors by a forced air ventilation system. Air is ducted to outlets in the cabin ceiling and is directed downward at the passengers. Air exits the cabin through exhaust grills along the lower cabin sidewalls. Air is exhausted from the aircraft primarily through pressure controlling outflow valves on the lower fuselage. The overall ventilation flow currents are from ceiling to floor, and the air exchange rate is once every 3 to 5 minutes.

A half-scale fuselage cabin section was fabricated as a test bed for quantifying the environment that develops from a fire in this type of forced ventilation. The test article was instrumented to measure the thermal environment, heat fluxes, gas concentrations, and ventilation rates. Interior fire size and ventilation rate were varied for these tests. Some alternate ventilation schemes were also tested for comparison with the standard ceiling-to-floor flow pattern. Test data were used to develop a semi-empirical model of heat transfer from the flowing combustion products to the enclosure ceiling.

Analysis of the experimental results yielded a number of significant findings. First, approximately 80 percent of the energy released by the fire was absorbed by the enclosure walls and ceilings. Only a small fraction of the energy was removed by ventilation air passing through the enclosure. Second, increases in ventilation rate had little effect on the temperature distribution within the enclosure although smoke and combustion product concentrations did decrease. Third, reversing the ventilation, so that air entered at floor level and exited at the ceiling, showed dramatic decreases in enclosure temperatures, smoke, and combustion product gas concentrations. Fourth, addition of various size vent hatches on the upper sidewall did little to improve the enclosure temperature profiles in these tests.

Chapter 1. Application of Model Tests to Aircraft

by

T.I. Eklund
Federal Aviation Administration

The vast majority of enclosure fire tests have involved burning materials under conditions of natural ventilation. They have usually involved ambient air being available from wall openings in the form of doors or windows. The fire in the enclosure causes a layer of hot gases to form at the ceiling and this results in a vertical hydrostatic pressure profile different in the enclosure from that outside. This pressure differential results in and controls the magnitude of the air inflow from the lower part of enclosure openings as well as the outflow of smoke from the top of the openings.

When fire is permitted to grow in these type tests, an event called flashover can usually be achieved. This event corresponds to an endpoint in occupant survivability in real world fires. In fully furnished compartments, the fire environment may change from overventilation (excess air over stoichiometric) to underventilated (inadequate air for complete combustion) during the flashover process.

Many postcrash aircraft cabin fire tests have demonstrated the same type phenomena as room fire tests (references 1, 2, 3). These tests also involved openings in the test fuselage which provided the only source of fresh air to the interior. In the aircraft tests cited, the safety objective was to delay flashover so as to allow more time for passenger evacuation from a burning aircraft. These tests all involved a large fuel fire burning adjacent to an

opening in the fuselage. Such a fire represents a powerful ignition source that results in relatively fast involvement of interior materials in the fire (of the order of minutes). Flashover has been demonstrated to be delayed in aircraft cabins through control of the heat release potential of interior materials such as seats and sidewalls.

Fire safety while an aircraft is in-flight involves ventilation and heat release rates and time scales, much different from those involved in post-crash fire tests. The ventilation rates are controlled by the aircraft environmental control system (ECS) rather than by fire induced pressure gradients across wall openings. The fire will usually start on a small scale and may grow very slowly compared to internal fire growth from a post-crash fire. Further, even over the continental United States, the time for landing and passenger evacuation can be expected to require tens of minutes. Rational improvements to aircraft fire safety require some elucidation of fire effects under the aircraft ventilation conditions in-flight.

Aircraft passenger cabin ventilation is provided by compressed air from the engines in all modern transports. This hot air is conditioned by means of heat exchangers, air cycle machines, water separators, and mixers to provide an adequate supply for occupant comfort as well as equipment cooling. The conditioned air is distributed through an array of ducts to air inlet devices to the cabin. These devices may be found on the upper sidewall, the passenger service units, and the ceiling. They take the form of slits, gaspers, and two-dimensional nozzles. Some may employ ejector design features to enhance their air circulation capability. The overall passenger cabin ventilation

involves air change rates of approximately once every three minutes. When recirculation is employed, the fresh air exchange rate might be every five minutes, while the combined fresh and recirculated air exchange rate remains approximately at the three minute value. These values exist when all ECS units are operating. If one of two units were shut down, the fresh air supply would be halved in most aircraft.

The ventilation air exits the passenger cabin through grills on the lower sidewall. It passes through spaces around the cargo compartments to one or more outflow valves on the fuselage below the cabin floor line. Overall it is apparent that the flow direction from ceiling to floor is opposite to that of fire induced flows documented in most enclosure fire tests. Additionally the ECS rather than the fire controls the air inflow.

The detailed data analysis comprising Chapters 2, 3, and 4 represent a systematic approach to characterize fire effects in such a counterflow environment. The test data was developed at the Center for Fire Research (CFR), National Institute of Standards and Technology (formerly NBS), in a mock-up that was roughly one-half aircraft scale on a width basis. Prior to these tests, expectations were that increased ventilation in an aircraft would strongly reduce heat and smoke from a fire in a fuselage. As noted in Chapter 2, fire test data for forced ventilated enclosures is scarce.

The mock-up tests represent a first step at evaluating enclosure fire environment in a counterflow environment. They provide a data base for estimating trends that might be expected from changing ventilation in an

actual aircraft. However, predictions of a real aircraft in-flight fire environment from these data might be questionable for a number of reasons. First, the interior lining materials of aircraft are different from the CFR model, and this could affect heat transfer to the walls and ceiling. Second, the air flowing into the real aircraft is through slits and nozzles that are designed to throw a turbulent jet with penetration and entrainment adequate for the comfort of a seated occupant. The CFR tests were not scaled to this level of detail, and it is problematic whether any scaled down tests could incorporate such details. Finally, the CFR tests simulated an aircraft cabin fire from a fire source on the floor. Effects due to fire locations beneath the floor or near the ceiling were not within the scope of the effort. Also neither conditions at the onset of flashover nor under ventilated fires were examined.

Within the context of classical Froude modeling, the time scales are affected by the square root of the length scales. Thus an air change rate in the half scale of five minutes would correspond to an air change rate of seven minutes in full-scale.

Chapter 2 provides a detailed analysis of the thermal budget from the experimental data collected in the model tests. The major overall finding is that regardless of ventilation rates studied, the bulk of the heat is absorbed by the enclosure itself - particularly the ceiling - and a relatively small proportion is exhausted through the outflow. The analysis further shows how the heat transfer to the ceiling can be correlated on a local basis. That is, the area directly above the fire absorbs most heat, and the ceiling heat

absorption drops off radially from this area. For the test data analyzed, the heat transfer to the ceiling was proportional to fire size. Additionally, the addition of mock-up seats did not materially affect the findings. The test data and analysis of Chapter 2 indicate that modest increases in cabin ventilation (factor of 2) will not improve the cabin environment insofar as thermal effects are concerned.

The thermal data further show that, in spite of the counterflow ventilation configuration, the enclosure evidenced strong thermal stratification with hot gas staying near the ceiling and cooler gas near the floor. The tests were all run at fire sizes that would keep the upper air temperatures lower than about 400°F. These fire sizes were selected to represent cases where the cabin environment would deteriorate prior to catastrophic damage to aircraft systems.

Chapter 3 provides data on gas species in the enclosure as well as effects of adding vents at the top of the wall to the outside. Regardless of ventilation rates, the level of carbon dioxide approximately doubles from floor level to ceiling. The same holds true for oxygen depletion. These data demonstrate that the gas species demonstrate stratification just as the thermal data does.

The addition of hatches on the upper part of the sidewall had an inconsequential effect on the enclosure thermal profiles. The hatches could cause a roughly thirty percent drop in the enclosure gas species (carbon dioxide and oxygen depletion). This may be extremely significant because of the particular way these hatch tests were performed. The exhaust ducts at the

bottom of the enclosure were ducted to another duct which ran to an exhaust fan to pull the enclosure gases out of the test building. Thus, the exhaust ducts of the enclosure were subjected to a slight vacuum from the building exhaust fan. Because all the hatch tests were conducted with this exhaust fan operating, approximately sixty percent of the ventilation air was going out the bottom of the enclosure with the remaining forty percent going out the hatches. If one hundred percent of the gases were to leave through the hatches, further significant effects on the enclosure gas specie concentrations might have been achieved. Additionally, there might have been more pronounced effects on the enclosure thermal profiles.

The actual carbon dioxide levels for these tests varied between 0.3 percent and 3.0 percent depending on sampling location, fire size, and ventilation rate. These numbers represent cabin environmental degradation but not levels needed for incapacitation of occupants over lengthy time periods of exposure.

Chapter 4 presents data for temperature, gas species, and smoke obscuration for tests where ventilation flow was reversed in the enclosure. In these tests, air entered the enclosure through the floor vents and exited through the ceiling vents. There were also some tests with reverse flow along with open hatches in the upper walls. With no hatches, reversing the flow resulted in roughly a fifty percent reduction in carbon dioxide in the upper layer from the concentrations found in normal flow. When hatches were open, there was an additional slight reduction over the entire height of the enclosure. The overall reduction in gas species was more dramatic because under reverse flow conditions, the bottom half of the enclosure was virtually free of any

combustion products. Under normal ventilation, the specie concentration at floor level is roughly fifty percent of that at the ceiling.

Reversing the flow substantially changes the temperature profile in a similar fashion as the bottom three-quarters of the height suffers an inconsequential temperature rise. Changing the ventilation rate under reverse flow has little effect on the temperature profiles.

The main overall results may be summarized through separate treatment of the thermal environment from the gas species environment. In the tests described in Chapters 2, 3, and 4, the thermal environment was not affected substantively by changes of ventilation or the addition of hatches. The only tests that showed major lowering of internal temperatures were the ones involving reverse flow. In these reverse flow tests, the flow direction rather than the ventilation rate caused the lower temperatures.

In contrast to the thermal environment, the gas specie profiles were affected significantly by all three parameters. The specie concentration at a given point was inversely proportional to an increase in ventilation rate. Addition of hatches significantly reduced specie concentration over the entire height of the enclosure. Reversing the flow reduced specie concentration by approximately fifty percent in the upper half of the enclosure and maintained the lower half virtually free of combustion products.

The findings of the model tests and the analysis, to the extent that they apply to in-flight fires, indicate that changes in or enhancements of the

aircraft ventilation characteristics can provide improvements in the cabin environment as far as toxic gases and smoke are concerned.

REFERENCES

1. Sarkos, C.P., Hill, R.G., and Howell, W.D., The Development and Application of a Full-Scale Wide-Body Test Article to Study the Behavior of Interior Materials During a Postcrash Fuel Fire, AGARD Lecture Series No. 123 on Aircraft Fire Safety, AGARD-LS-123, June 1982.

2. Quintiere, J.G., et al, The Role of Aircraft Panel Materials in Cabin Fires and their Properties, Federal Aviation Administration, Report DOT/FAA/CT-84/30, June 1985.

3. Hill, R.G., Eklund, T.I., Sarkos, C.P., Aircraft Interior Panel Test Criteria Derived from Full-Scale Fire Tests, Federal Aviation Administration , Report COT/FAA/CT-85/23, September 1985.

Chapter 2. Aircraft Cabin Fire Environment In Counter flow Ventilation

by

B.J. McCaffrey
University of Maryland
Baltimore, MD

and

W.J. Rinkinen
Center for Fire Research
National Institute of Standards and Technology

1.0 Introduction

The effects of normal aircraft ventilation on the growth of an incipient inflight fire as well as on the spread of smoke and toxic products in the cabin has not been systematically studied to any great degree. In an effort to establish an improved data base on in-flight fires and smoke removal, the Federal Aviation Administration has been sponsoring studies both at their laboratories and through contracts with airframe manufacturers fire research organizations aimed at elucidating the phenomena and gaining the required scientific understanding. These studies may offer near-term benefit, for example, insight for recommendations and guidelines for crew action in the event of fire, and they might in addition offer the rational basis for estimating the possible benefits of proposed future design changes, for example, emergency venting of smoke.

One such study, the subject of this report, took place at the Center for Fire Research (CFR), National Bureau of Standards. This study involved an

experimental program in a 1/2-scale section of a simulated wide body aircraft, to address the effects of ventilation on the fire environment. (Aircraft cabins are generally ventilated from top to bottom. Fresh air is forced in at the ceiling of the fuselage and exhausted near the floor. Fires create hot gases with buoyant forces which are in the opposite direction from that of the ventilation flow. The inability to analytically characterize the resulting large scale eddy mixing process is one cause for the uncertainty surrounding the fire question.)

This report describes the following tasks:

i) the design and instrumentation of a 1/2- scale test article simulating the interior and ventilation pattern in commercial aircraft;

ii) the collection of the data required to determine the effects of "counterflow" ventilation on the thermal environment;

iii) heat transfer to the ceiling of the test article. It became apparent soon after the initiation of the study that a major portion of the energy release rate of the fire was not getting exhausted through the floor vents. Rather, the energy was being transferred to the ceiling, and hence it was necessary to study carefully the implications of that heat transfer.

Throughout this study it must be kept in mind that only trends and phenomena are being investigated. Caution must be exercised in interpreting the small scale measurements. For example in the case of exchange rates, Froude number scaling analysis would yield differences of $\sqrt{2}$ in event times between model and full scale. See Quintiere (1978) for a full discussion of this point.

Surprisingly in the past there have been few studies which have attempted to predict the fire environment in a moderately sealed enclosure for any sort of forced ventilation. For aircraft specifically, Sarkos and Hill (1985) noted substantial differences in hazard histories at different points throughout the cabin between a controlled ventilation, in-flight fire scenario case (the present configuration) compared with the postcrash tests where the cabin was ventilated naturally through fuselage openings. Apparently because of mixing the former tended to distribute the seat fire hazards throughout the airplane, i.e. hazard conditions existed at a station as much as 12 m (40 ft) from the source at an elevation as low as 1.7 m (5 ft 6 in) prior to flashover. In contrast hazardous conditions were limited to the ceiling layer in the naturally ventilated, post crash test up until the point of flashover.

Until very recently calculations involving numerical solutions of the conservation equations with radiation and elaborate turbulence models, quite successful in reasonably high velocity, forced convective flows, have not yielded the same kinds of successes for highly buoyant, low speed flows. The large scale structure responsible for the major share of the mixing has not been properly modelled. DeSouza, Yang and Lloyd (1985) in a two-dimensional calculation show that flows with velocities equal to 0.1 m/s have little

effect and flows at 1 m/s have drastic effects on the stability of the hot upper layer. Unfortunately, there are non-negligible three-dimensional effects associated with the flow field and the actual aircraft flow velocities fall precisely between these two extremes. Mitler (1984) has attempted forced ventilation calculations using zone models and indicates clearly the weaknesses of that approach because of the lack of a good mixing algorithm for the incoming stream. Finally, using a well-stirred reactor analysis Eklund (1984 a,b) has shown the importance of ventilation with regard to fire hazard development including visibility.

One experimental study of fire growth in a sealed container with ventilation, worth noting, is that of a nuclear containment vessel at the Lawrence Livermore National Laboratory. The resulting correlations were presented by Foote, Pagni, and Alvares (1986). In that study the representative upper level gas temperature rise varied with the ventilation flow rate to a not immodest -0.36 power. Cox, Kumar, and Markatos (1986) were able to do a reasonable job in reproducing some of these results using more modern three-dimensional field modelling techniques. Unfortunately however, their ventilation flow direction was in the same direction as the buoyant flow, i.e., in at the bottom and out at the top, the same direction as the normally generated flows due to the fire - the hot gases simply get pushed along by the vent flow.

There appears to be no systematic study in the literature of the desired configuration. Evidence suggests that mixing of the upper layer is significant (Sarkos and Hill 1985) and for the reversely ventilated (in at the

bottom out at the top) case the thermal environment is medium to strongly dependent on the ventilation rate. For the counterflow situation, the direction of interest here, little guidelines exist - the present experimental program was carried out to fill this void.

2.0 Experimental

A view of one-half of the test article is shown schematically in Fig. 1. It was constructed of two symmetrical chambers built on a raised frame with wheels so that the interior could be accessed easily, and with the two halves clamped together formed a reasonably sealed enclosure. Each chamber was approximately 2.4 m long by 2.4 m wide by 1.2 m high (8x8x4 ft) thus simulating to approximately 1/2-scale a closed section of aircraft 9.8 m (32 ft) long by 4.9 m (16 ft) wide by 2.4 m (8 ft) high. The skin was of 24 gauge (0.7 mm thick) galvanized sheet and the frame was constructed of 38 x 38 mm and 51 x 51 mm angle and channel members 3.2 mm thick of hot rolled, AISI C-1020 metal. The skin was riveted to the frame, and the joints were overlapped sheet, sealed with high temperature silicone adhesives. High temperature gasket material was used in the clamped butted joint where the two chambers were connected. The reproducibility of the seal after movement of the chambers could be determined by checking the pressure transducer reading at a given ventilation flow rate. Windows in the walls provided visual observation of the fire behavior.

The floor and ceiling were composed of sheets of calcium silicate board ("marinite") which, positioned approximately 10 cm off the skin, formed a

plenum with slit openings to provide for the airflow, as shown in figure 1. Fresh air was pumped from the laboratory into a top center aperture in both halves of the box. It filled the plenum and flowed out more or less uniformly, since the slit area was a small fraction of the plenum cross section. The air flowed out of the two slits in the marinite for either of the two configurations 'wall' or 'central' into the cabin proper. At the floor the air flowed out through the slits into the lower plenum and was collected through two apertures in the bottom skin and continued out of the building through ducting. The two apertures in the bottom skin were exact replicas of those in the top skin. Fans located upstream of the top aperture provided flow and positive pressure in the box. The building exhaust system provided slight negative pressure near the outlet of the ducts leading from the bottom apertures.

The table in the Appendix provides the complete list of instruments and the correspondence with locations and instrument type can be determined from Figure 1. Not shown on the figure are the inlet airflow velocity measurements, cabin pressure relative to the laboratory, gas sampling instruments and smoke meters.

For the work reported here both fire size (a steady flow of C_3H_8 through a 0.15 m diameter glass bead burner located at the floor. Fig 1) and ventilation were steady in time. The procedure was quite straightforward. The ventilation fans were started and flow rates selected and several minutes were allotted before steady conditions were assured. At that point the computer was started, instructing the data scanner to begin reading the various

channels and writing the data to memory. After about one minute of data taking the ignition system was activated and the propane flow rate was set to the desired constant heat release rate value. The remainder of the experimental procedure consisted in simply waiting for the desired run duration time to elapse.

Most of the initial study consisted of experiments performed in an empty enclosure. In order to evaluate the effect of additional thermal energy storage capacity in the cabin, simulated seats were constructed and placed symmetrically in the cabin since it turned out that a large fraction of the fire heat release was not being exhausted. In addition the effects on the environment of any large scale fluid motion could possibly be evaluated since blockage due to the presence of the seats would provide a different cabin flow pattern. They were 32 in number and consisted of bent sheets of aluminum with the seat and back composed of 13 mm thick sheets of marinite (Fig. 2). If required, material with different thermal capacitance could be accommodated.

3.0 Results

Table 1 presents the set of experiments for the thermal environment portion of the study and gives condition of ventilation in terms of time for one air exchange, i.e., 4.9 x 2.4 x 1.2 = 14.1 m^3; ceiling ventilation position, either at the wall or at positions 0.6 m in from the wall (see Fig. 1); heat release rate and seating configuration.

The complete set of reduced data for one run, F1202 is shown in the Appendix. Data in the same form, i.e., 2-D arrays of time in seconds, and instrument output, reduced to appropriate engineering units, was developed under each test condition and formed the basis for the analytical findings on the aircraft cabin fire environment.

The results will show first the effect of ventilation rate on the environment in the cabin for a fixed fire size and vent location. The air supply vent position will then be changed and the effect noted. The next section contains the work relating to the effect of the fire size for a fixed ventilation rate and contains considerable analysis of ceiling heat transfer rates in order that the results may be generalized to different materials and scale. Finally a section on stratification completes the thermal portion of the study.

Ventilation rates varied from 2 to 4 1/2 minutes as the time for one volume airchange. Keep in mind any scale factor when interpreting these rates for full scale. These are consistent with cabin ventilation values for the commercial fleet. It was not necessary to vary the rate (nor the inlet position) beyond these limits because of the nature of the results - the

buoyancy forces of the fire were dominating over ventilation rate as regards exhausting heat generated by the fire. The extent of mixing however may depend on the venting rate and position.

Heat release rates varied from 6 to 60 kW in the experiments or if Froude number scaling is assumed, 30 to 350 kW. This would correspond to full scale heat release rates of 2 raised to the 5/2 power. The 350 kW fire is representative of about a fully involved seat fire.

Table 1: Experiment Parameters

Run ID	Ventilation Exchange Time (min.)	Ventilation Inlet Location	Heat Release Rate (kW)	Seating Configuration
F0402	2.0	WALL	30	None
F1102	2.0	WALL	30	None
F1202	2.4	WALL	30	None
F1902	4.5	WALL	30	None
F2502	2.4	CENTRAL	30	None
F0403	2.4	CENTRAL	30	None
F0503	2.4	CENTRAL	20	None
F1203	2.4	CENTRAL	10	None
F1803	2.4	CENTRAL	6	None
F1903	2.4	CENTRAL	40	None
F2603	2.4	CENTRAL	60	None
F0206	2.4	CENTRAL	30	32 Seats

The set of graphs of the data, contained in the appendix, is typical for all the tests. They are for F1202, which had an intermediate fire size and ventilation level, and which had the air inlets adjacent to the sidewalls. The first four figures, Fig. 3 - 6, are for the thermocouple (TC) trees or gas temperature around the cabin. They rise rapidly as the fire is turned on,

approximately 60 s after start of data collection, and except for their level the behavior in time of all the trees is nearly identical - no transit delay time could be ascertained. (The TC's are visually protected from any flame radiation by their angular location relative to the support rod.) The front of the thermal wave is moving fast enough that only if the TC's were being sampled at a rate such that the time between scans is less than one second could transit times be actually measured. Obviously in a real situation where the aspect ratio could involve the entire length of the aircraft, spatial variation will become a factor. Phenomenologically however this should not create a problem - the same things will be happening at later times downstream.

The actual level of temperatures in different parts of the cabin will be discussed in the section on the effect of fire size. Not surprisingly the TC closest to the ceiling reaches the highest temperature and the furthest away or lowest reaches the lowest temperature with the remainders ranked accordingly. The glaring exception, TC 1 & 2 on tree A, can be explained by structural blockage (see section on upper level gas temperatures). This is an important point. In spite of the external ventilation which will cause mixing and stirring, the upper layer is perfectly stratified - i.e. temperature increases monotonically with height. From figures 3-6 it can be seen that as the fire is turned off the high to low ranking remains in spite of the fact that the ventilation is running. The ventilation can not overcome the residual buoyancy in the gases - the cabin is still stratified. One however can argue that the difference between high and low in that case may not be very significant.

The point of all this speculation about stirring has to do with the ability of the ventilation system to flush out adequately smoke and hot gases from the cabin during a fire situation. Recall the exhaust is going out at the floor level. If the buoyancy of the fire gases is such that only relatively cool and clean air is remaining near the floor, then the system cannot be expected to perform adequately. What size of buoyant forces, or fire condition can overcome the plane's ventilation system will need to be addressed. A small smoldering fire (like a whole group of smokers) can obviously be handled by the present system, however it is not clear whether or not toxic products associated with the temperatures seen on Figs. 3- 6 could be adequately flushed from the cabin in a reasonable amount of time using the same ventilation system.

Fig. 7 shows the temperature of the thermocouples located in the two ventilation exhaust lines and confirms the contention made above that only cool gas is being removed in times of interest for this case. The level hardly reached 50°C at 450 seconds, when the fire was turned off. (Fig. 7 and the previous figures indicate significant thermal stratification, in themselves however they cannot indicate the level of mixing of conserved species such as carbon dioxide and oxygen.) The much more gradual rise in gas temperature shown in Fig. 7 indicates the delay in "filling" the entire cabin from the top down before any warm gas appears in the exhaust.

Fig. 8, shows the time history of the ceiling TC's which like the gas temperature show a rapid rise in temperature. The TC's were peened into the

marinite ceiling and offer a reasonable measure of surface temperature rise with time. The level of temperature attained varies inversely with distance from the fire. The TC's were exposed to the full brunt of the fire plume gases and are critical in determining heat transfer rates, as discussed later in the analysis.

Fig. 9 contains the traces of the output of four TC's mounted on the inside walls at various positions around the cabin. The time histories are notably different from the gas and ceiling time history in regards rapid temperature rise and exhibit more the characteristic of the exhaust gases but at higher temperature levels. These TC's are fastened to the metal walls with screws and their slower response vs the ceiling TC's is attributed to the lower convective coefficient due to lower gas velocities on the sidewalls, a finite filling time to bring hot gases to the lower position on the walls and finally the high thermal conductivity of the wall material. Additionally, for the ventilation configuration with air inlets along the wall, the flow field is rather complex with the cold jet running down the side along with a portion of the ceiling jet which due to sufficient momentum has made the turn and starts heading downward adjacent to the measuring station. The last effect can be checked with the results of a "central" ventilation run which ought to present a different local flow velocity to the probe. Comparison of Fig. 9 with its counterpart for run F0403, identical to F1202 except for location of the vent inlet, shows little difference in temperature signal.

Wall temperature and heat transfer from exterior measurements can be seen on Figs. 10 and 11 which show on the same scale, gauge heat flux in kW/m^2 and

temperature rise above ambient. There is a pair of signals for each of the four stations, the smoother of the two is the thermopile temperature output. Note before the fire is turned on there are some non-zero signals. Prior to this run, an experiment took place and even after the period of time allowed for cooling, the box still retained some small differential energy. For single runs in a day these transducers registered negligible initial signal. The time histories seen on Figs. 10 and 11 are similar to those seen on the interior thermocouples, Fig. 9. The data seen on Figs. 10 and 11 can be used for validating heat transfer model calculation for these wall flows.

Fig. 12 shows the output of the velocity measuring transducers in the inlet ventilation ducts converted to volumetric flow rate and the static differential pressure measurement, cabin to laboratory. The velocity profile across the duct has been measured and documented and the use of a single centerline measurement corrected accordingly. The non-uniformity of the flow signals represent asymmetry between the two halves of the enclosure as do the two exhaust temperature measurements on Fig. 7.

The behavior of the enclosure regarding pressure is interesting. As the fire is turned on the spike in pressure signal due to expansion is clearly evident. As heat is added continually at a constant rate it takes quite a while for the cabin to equilibrate back to the initial, prior to fire, value. During other tests with smaller fires and hence longer running times that equilibration was assured to a high degree of accuracy. There is no doubt as to when the fire is turned off as a mirror image of the process occurs. There are analyses

available which predict pressure rise in closed vessels due to the onset of a fire using simple First Law Thermodynamic concepts.

The above offers a description of the kinds of data that have been obtained and a general discussion of the implications of the data. The remainder of the report presents detailed analyses appropriate to the problem at hand, namely the effect of aircraft ventilation on the fire environment.

3.1 Effect of Ventilation Rate and Position on Gas Ceiling, and Wall Temperature

At a fixed fire size (30 kW) there results little change in either gas temperature (Figs. 13 and 14) or in ceiling or wall temperature (Figs. 15, 16 and 17) due to changes in the air exchange rate from 4½ min to 2 min per airchange. (Note that unlike Figs. 3 through 12, for the remaining graphs the identification numbers on the right hand side of the curves do not necessarily correspond to the channel numbers). In fact the wall heat transfer rates (Figs. 16 and 17) are just slightly higher in the higher exchange rate case perhaps due to better contact of the hot gases with the wall surface. The bulk gas temperatures (Figs. 13 and 14) themselves however, appear to follow the more intuitive direction, i.e. higher level temperature for lower flow rates.

Fig. 18 shows the exhaust flow thermocouple readings for the high and low flow rates. There are two exhaust positions and hence two traces per experiment. One can easily do a quick calculation of the enthalpy leaving in the exhaust

gases. The enclosure volume is 4x8x16 ft^3, (14.5 m^3) or for the 2 min. exchange rate, the volume flow rate is 14.5/2/60 = 0.12 m^3/s. At about 540s, as the fire is turned off, the maximum temperature rise for the 2 min. case is about 25 K. Hence

$$Q = \dot{V}\rho C_p \Delta T = 0.12x1.2x1x1x25 = 3.6 \text{ kW}$$

(using properties of room air, ρ = 1.2 kg/m^3; C_p = 1 kJ/kg·K). For the 4.5 min. case, the flow is 0.054 m^3/s, the temperature rise is about 18 K and hence the enthalpy leaving at about 500 s is .054x1.2x1x 18 = 1.2 kW. Note the falloff of the temperature signal compared to the gas or ceiling temperatures when the fire is extinguished. In the latter cases the temperature drops immediately. For the exhaust flow temperature only slight decreases are noted as the gases containing stored energy in the enclosure continues to flow out. Note also in the rising portion of the traces the much more slowly rising signal than, for example, the gas or ceiling traces. That is, the 3.6 and 1.2 kW figures, representing 12% and 4% respectively, of the energy source, will continue to rise with time much more so than the more asymptotically looking gas temperature traces.

Instead of comparing the two cases at approximately the same absolute time perhaps it would be more appropriate to compare the signals at comparable characteristic flow times. For example 540 s for the 4.5 min. case is about 1.8 flow times or equal to somewhere around 280 s for the 2 min. case. That ΔT would be closer to 15 K or about 2.2 kW or 7% of heat release rate. At times corresponding to a few airchanges, only a small amount of energy is being carried down and out through the ventilation.

The amount of energy through the metal side walls can be estimated using the measurements of wall heat flux seen on Figs. 16 and 17. Heat flux values from Fig. 16 and 17, and here no difference between the two cases will be assumed, bunch around 0.2 to 0.3 kW/m^2 for three of the sensors and for the remaining one, 0.7 to 0.8 kW/m^2. Assume that the wall area can be divided into a hot upper central region (3 m^2) to go with the high flux and the remainder of the area (15 m^2) for the lower values. The total flux through the walls at the time the fire is turned off is

$$Q = q'' \times A = 0.75x3+0.25x15 = 6kW$$

or about 20% of the total heat release rate of the fire. Like the ventilation thermocouples, the signals on Figs. 16 and 17 fall gradually after the fire is turned off. This indicates significant dissipation of a lot of stored energy.

The above indicates that approximately 30% of the total energy created by the fire leaves through the walls and ventilation flow in times equal to several airchanges. Therefore, 70% must remain. In the configuration without seats only the floor and ceiling have the capability to store energy. These internal components are separated by plenums from the actual metal floor and ceiling skin. Over these times, the external metal floor and ceiling skin do not get very warm. Therefore, their energy transfer paths have been ignored. (The metal skin above the marinite ceiling is exposed to the incoming cool

air. The rise of the metal floor interior temperature will be reflected in Fig. 18.)

Considering then that the floor and ceiling are the primary absorbers, the thermal capacity is equal to

$$mC_p = (8x16/12)/(3.281)^3 \times 700 \times 1.1 = 233 \text{ kJ/K}$$

(where 700 kg/m^3 and 1.1 kJ/kg K are representative of the density and specific heat of the material). If the heat transfer rate was assumed constant over the 540-60 = 480 s time that the fire was turned on and assuming 70% of the 30 kW was being stored then an average temperature rise of the interior would be 21/(233/480) = 43 K.

Observation of the ceiling surface temperature as the fire is turned off on Fig. 15 indicates that a 40 K rise in ceiling temperature is not an unreasonable number. To transfer all the energy the 12 m^2 ceiling would require an average heat flux of 21/12 = 1.8 kW/m^2. Derived heat transfer coefficients (see Ceiling Temperature section) are in the range .02 to .07 kW/m^{2}K making the average temperature difference between gas and ceiling 25 to 90 K - a reasonable number, not unlike the more detailed calculation result. Obviously a more accurate partitioning of energy around the interior requires the more detailed result. Since a large fraction of the energy does not get removed in the present configuration, knowledge of the thermal characteristics of the enclosure will be very important.

The conclusions reached above appear to be independent of the position of the inlet "slit" at least as regards the "wall" and "central" configurations. Experiment F1202, the "wall" ventilation case discussed earlier can be compared to F0403 which is an identical run except for position - this is a "central" case. To first approximation the results are identical - the graphs of all the variables can be superimposed within the noise or normal fluctuation of the signal. Some very minor differences are perceptible, e.g. the ceiling temperature "T2" on Fig. 1 is on the order of ten degrees higher for the wall ventilated case, as are the upper TC's on trees D and B slightly higher. One might postulate a cooling curtain effect in the central case. Again however these are very small changes, and to reasonably high confidence the position of the vent had little effect on the measurements recorded.

3.2 Effect of Seats

The effect of seats is to exacerbate the problem of trying to exhaust hot gases by the normal ventilation, i.e. out the bottom. Either through additional energy transfer to the seats or by the blockage of large scale flows the gas temperature in the lower regions is cooler and more stratified i.e., the gradient of temperature is larger. And this is reflected in the level of exhaust gas temperature. For a given case, F0206 with seats vs F0403 without seats, everything else identical, there is about a factor of two decrease in the differential temperature of the exhaust gases between the configuration with seats opposed to that without seats at comparable flow times. The remaining transducers are not greatly affected with some minor differences e.g., exterior wall heat transfer in the lower regions is somewhat

less in the with-seat configuration. Upper level gas & ceiling temperatures are similar in the two cases.

3.3 Effect of Fire Size

Gas, wall, ceiling, and exhaust gas temperatures all vary significantly with heat release rate.

i) Ceiling Temperatures (T1-T4)

An excellent fit of the temperature rise - time data of the ceiling thermocouple signal is:

$$\frac{\Delta T}{\Delta T_m} = 1 - \exp\left[h^2 \frac{t}{\rho c k}\right] \cdot \operatorname{erfc}\left[h \sqrt{\frac{t}{\rho c k}}\right] \tag{1}$$

which is the solution for the surface temperature history for one-dimensional heat conduction through a semi-infinite slab exposed at t=0 to a large mass of fluid of temperature T_m. Surface resistance is indicated through the, film coefficient, h, which is assumed constant. The governing differential equation is the familiar diffusion equation with the given initial and boundary conditions:

$$\frac{\partial T}{\partial t} = \alpha \frac{\partial^2 T}{\partial x^2} \tag{2}$$

$$t \le 0 \qquad T = T_0 \tag{3}$$

$$t > 0, \; x = 0 \qquad -k \frac{\partial T}{\partial x} = h(T_m - T) \tag{4}$$

The adequacy of Eq. (1) as a fit to a typical data set can be judged by observation of Figs. 19 through 22. They show temperature rise-time data for the four ceiling positions with the best least squares fit determined by Eq. (1) shown by the smooth curves. Note the data set includes only that portion with the fire "on". The point here is to generalize the data and perhaps garner something of the physics of the fire-ceiling interactions. Eq. (1) is essentially a two parameter data-fit expression. The parameters are ΔT_m and $h \bullet (\rho ck)^{-\frac{1}{2}}$. We do a least squares fit of the data to the Eq. (1) form and derive the best constants. Using the simple semi-infinite transient conduction model, Eqs. (1)-(4), one can associate or relate the derived ΔT_m with the measured fluid or gas temperatures determined independently by the thermocouple trees; the ρck portion with the thermal properties of the given "inert" ceiling material; and finally, the derived or best h, an effective heat transfer coefficient, with the thermo-fluid mechanical environment experienced by the ceiling.

It is an "effective" coefficient because of the simplicity of the thermal model, i.e. no reradiation through the hot layer to the colder floor, the loss of the semi-infinite approximation at longer times (small fires) due to the finite thickness of the ceiling material and also the transient nature of the gas temperature rise, to name just a few restrictions.

Having now a reasonable "model" for fire-ceiling interaction or at least a reasonable analytical fit to the data, one is able to see how these parameters change as a function of fire size. The results of least squares fitting of

all the ceiling temperature data for a fixed configuration in the form of Eq. (1) led to several observations. For a fixed fire size, Q, ΔT_m and h varied considerably with position or location relative to the fire. At a fixed position ΔT_m varied almost linearly with fire size and h varied much more weakly with Q.

In order to systematize the data analysis more easily a functional form of the h variation with Q was chosen. Because of the nature of Eq. (1) and the data sets, a range of ΔT_m and h values could yield similarly accurate least squares fits. On a plot of the sum of the squares of the differences between calculated values and actual data values vs h, the minimum of the curve (which will be the best value for the fit) was rather broad. A very sharp minimum would have dictated a unique pair. Therefore a range of h and corresponding ΔT_m values would all give statistically similar results. Visual examination of the plots could not differentiate which pair within the range yielded better results.

The effective film coefficient h, was chosen to vary with Reynolds number to the 1/2 power. This dependence is characteristic of an extremely wide range of geometries from convective heat transfer studies. Velocities from buoyant plumes and real fires vary with heat release to the 1/3 power, and hence h will be allowed to vary with Q to the 1/6 power, a result totally consistent within the experimental data scatter. (A larger Reynolds number exponent could have been chosen if the lower portion of the flame zones where the dependence on fire size becomes weaker, i.e. 1/5 in the intermittent and 0 in the continuous flame, were controlling the phenomena. Irrespective of what

model is chosen the data dictates a weak h dependence on Q, which must be satisfied.)

The efficacy of choosing a fixed power for the h-Q variation can be demonstrated by considering the ΔT_m vs Q data before and after fixing the 1/6 power for h vs. Q. The correlation coefficients for the power fits of ΔT_m vs Q in four ceiling positions ranged from 0.89 to 0.98 in the arbitrary situation. By letting h vary with $Q^{1/6}$, going back to the fitting routines and obtaining the new ΔT_m it turns out that those ΔT_m vs Q fits now have all four correlation coefficients greater than 0.99!

The results of all the curve fittings are contained in Table 2 and illustrated in Fig. 23 which shows how ΔT_m (open symbols) and C or h (filled symbols) vary with position in the cabin. Note that $C/Q^{1/6}$, i.e. the film coefficient, ($C = h/\sqrt{\rho ck}$) varies inversely with position from the fire, a not unexpected result given that the fire generated gas flow velocities will be decreasing as one moves further from the fire. The same is true, in general, as regards ΔT_m. The exception is for position T1 which is slightly further from the fire than position T2 and for all the central ventilation data (square symbols) exhibits higher temperatures. With ventilation at the edge or wall position, T1 drops below T2 following the trend of cooler regions being further from the fire (triangle symbols). The curtain of cool air falling between the fire and the positions of T4 and T2 in the former case may provide disturbance to a decreasing thermal stress with distance from the fire trend, that is, if one can ignore the enclosure asymmetry to begin with. The hash marks on the figure indicate the length and breath of the compartment. Perhaps T3 and T1

ought to be compared separately from T4 and T2 for the central configuration cases.

The lower part of Fig. 23 yields for the present center ventilation configuration a film coefficient h of between about 5 and 80 W/m^2K. The lower number is typical for free convection with the higher value ($r/H \rightarrow 0$) well into the forced convective range for gases. The data also bounds that found by Quintiere (1978) for a ceiling in a corridor just outside a burn room.

To construct figure 23, an average n equal to 0.933 was chosen from Table 2. The $\Delta T_m = AQ^n$ was recalculated to yield a new A and compared to the temperature levels at each position irrespective of slight changes in Table 2 values of n. The triangles on the figure are for the one data set with wall ventilation. These data have not gone through the extensive analysis that the central ventilation or squares have, i.e. $h \alpha Q^{1/6}$. Quite large decreases in h could result in small increases in ΔT_m and still preserve the goodness of the least squares fit. In other words the impression that h for the wall ventilation case is twice that for the central ventilation may not be a correct one. To convert C to h a value of $\rho ck = 0.1$ $(kw/m^2/K)^2 \cdot s$ was chosen for the ceiling material. How well the derived bulk "bath" temperatures, ΔT_m, compare to actual measured gas temperatures will be presented in the next section.

TABLE 2: CEILING TEMPERATURE CORRELATION PARAMETERS[1]

			T3		T4		T2		T1	
RUN I.D.	Q(kW)		ΔT_m(K)	C($s^{-½}$)	ΔT_m	C	ΔT_m	C	ΔT_m	C
F0403	30		221	.166	136	.109	128	.0363	162	.0226
F0503	20		140	.155	93	.101	93	.0339	115	.0211
F1203	10		73.5	.138	48.3	.0904	47.6	.0302	57.5	.0188
F1803	6		44	.127	25.2	.0830	28	.0278	35.3	.0173
F1903	40		259	.174	172	.114	164	.0381	200	.0237
F2603	60		378	.186	248	.122	237	.0408	273	.0253
			$C/Q^{1/6}$	.0942		.0616		.0206		.0128
		A		8.43		4.74		5.61		7.34
	$\Delta T_m = AQ^n$	n		0.937		0.978		.919		0.897

[1] Least Squares Fit to $\Delta T/\Delta T_m = 1 - e^{C^2 t}$ erfc $C\sqrt{t}$ (No seats, central ventilation, 2.4 min^{-1})

ii) Upper Level Gas Temperatures (A2, B1, C1, D1)

Time histories of the uppermost thermocouple (TC) temperature rise for the four TC trees are shown in Figs. 24-27. (Note for tree "A" that the second TC is used since, due to blockage by a structural rib on the ceiling, the topmost TC on that pole was somewhat shielded from the hottest gases and consistently recorded a temperature slightly less than the second from the top.) For want of any other particular method the data was correlated using the semi-infinite error function analysis used previously. Observation of Fig. 24-27 seems to indicate that it is adequately representing the data. The ΔT_m and C's shown on the traces are the determined least squares fit of Eq. (1).

Table 3 contains the results of the curve fitting analysis for the other five fire sizes. The results of the variations with fire size or heat release rate, Q, were similar to the ceiling analysis. That is, ΔT_m varied, nearly linearly with Q; while C, scattering considerably, varied very weakly with Q. As before, to systematize the data analysis, C was made to vary with $Q^{1/6}$, and the analysis fitting was repeated to obtain the best ΔT_m for that new C. (Here the similarity to an actual convective film coefficient may be more tenuous since gas or rather the TC's are being heated, not a semi infinite plate). An example of exactly how things change by this manipulation is to consider Fig. 24-27. The ΔT_m and C's shown on the figures are the "raw" or best values. Those in the table have been "processed", e.g., ΔT_m for D1 went from 206 to 205 K while C increased from .085 to .0897 $s^{-1/2}$, etc. Meanwhile the sum of the squares of the deviations does not change appreciably. The big

TABLE 3: UPPER GAS LEVEL TEMPERATURE CORRELATION PARAMETERS[2]

		D1		A2		B1		C1	
RUN I.D.	Q(kW)	ΔT_m(K)	C($s^{-½}$)	ΔT_m	C	ΔT_m	C	ΔT_m	C
F0403	30	163	.0855	180	.0860	145	.0506	144	.0569
F0503	20	113	.0799	125	.0804	99	.0473	104	.0532
F1203	10	61	.0712	68	.0716	54.5	.0421	58	.0474
F1803	6	43	.0654	44	.0658	35.5	.0387	36	.0435
F1903	40	205	.0897	226	.0902	185	.0531	184	.0597
F2603	60	260	.0960	301	.0966	242	.0568	243	.0639
		$C/Q^{1/6}$	.0485		.0488		.0287		.0323
$\Delta T_m = AQ^n$		A	9.89		9.74		7.77		8.37
		n	.812		.848		.851		.833

[2] Least Squares Fit to $\Delta T/\Delta T_m = 1 - e^{C^2 t}$ erfc $C\sqrt{t}$ (No seats, central ventilation, 2.4 min^{-1})

difference again came about when considering ΔT_m vs Q. In all cases the correlation coefficient increases to over 0.99 with the formalized $C\text{-}Q^{1/6}$ variation.

From Table 3 the mean power for gas variation, 0.836 is measurably lower and the data is less scattered than the ceiling temperature rise variation, i.e. n=0.933. Fig. 28 shows the radial variation of $\Delta T_m/Q^{.836}$ with again the numbers reworked using the constant n. For comparison the ceiling variation with distance using 0.933 is also shown. Heat transfer to the ceiling as a function of position (as well as with time) can be determined from the plot. Additional information required is contained in figure 28 which shows $C/Q^{1/6}$ for the gas as well as the ceiling. Here they are left in the "C" form, a simple data fitting constant, as opposed to conversion of the ceiling value to h as on Fig. 23.

The gas values of C appear to be less dependent on position than those of the ceiling. For the ceiling C increases significantly as one gets closer to the fire indicating a smaller time constant or smaller time to reach ΔT_m. Here the analog with a film or heat transfer coefficient makes sense - the plume velocities will be highest in the stagnation - turning region of the ceiling.

We now have the ceiling temperature rise as well as a representative upper level gas temperature rise due to a fire in a cabin ventilated from above. As a function of time,

$$\Delta T = \Delta T_m \left[1 - \exp(C^2 t) \bullet \operatorname{erfc}(C\sqrt{t})\right] \qquad (5)$$

with

$$\Delta T_m = A_i Q^{n_i} \tag{6}$$

for

$$i = \text{gas} \qquad n_i = .836$$

$$i = \text{ceiling} \quad n_i = .933$$

$$C = B_i \, Q^{1/6} \tag{7}$$

where A_i and B_i are each functions of (r/H) and are contained on the upper and lower portions of Fig. 28 respectively.

3.4 Ceiling Heat Transfer

At any radial position the heat transfer rate, gas to ceiling, is from the simple model

$$\dot{q}'' = h_c (T_m - T_{CEILING}) \tag{8}$$

For the film coefficient, h_c, derived using the semi-infinite analysis, T_m was assumed to be the constant bath temperature into which one side of the ceiling was suddenly exposed. In reality the gas temperature itself is rising. Additionally from Fig. 28 the independent experimentally derived ΔT_m for the gas is somewhat higher. It will be useful to see the effect on heat transfer of using the higher and transient gas temperature.

Using the data representation, Eq. (1), the above becomes

$$\dot{q}''/h_c = \Delta T_{mg} - \Delta T_{mc} \left[1 - \exp(C_c^2 t) \cdot \mathrm{erfc}(C_c \sqrt{t})\right] \qquad (9)$$

where the additional subscripts g and c indicate gas and ceiling respectively. Note that if the ceiling maximum temperature (the semi-infinite approx.) is used for the bath or gas temperature then Eq. (9) reduces to

$$\dot{q}'' = h_c \Delta T_{mc} \exp(C_c^2 t) \cdot \mathrm{erfc}(C_c \sqrt{t})] \qquad (10)$$

or at short times, say to 30 seconds for C_c of order 0.05 $s^{-1/2}$, we can approximate the erfc expression and obtain the convenient

$$\dot{q}'' = h_c \Delta T_{mc} \ (1 - C_c \sqrt{t}) \qquad (11)$$

The complete solution can be expressed as (Abramowitz and Stegun 1965):

$$\dot{q}''/h_c = (\Delta T_{mg} - \Delta T_{mc}) + \Delta T_{mc} \ (a_1 t_c + a_2 t_c^{\,2} + a_3 t_c^{\,3}) \qquad (12)$$

where $t_c = \dfrac{1}{1 + pC_c \sqrt{t}}$

and $a_1 = .3480242$, $a_2 = -.0958798$, $a_3 = .7478556$, $p = .47047$

Note the first term, a sort of compensation for weaknesses in the semi-infinite model since the experimental gas temperatures always come out higher than the bath temperature of the model, represents a value of order 10% or less of the second term for times of interest here and hence Eq. (10) (and Eq. (11) for short times) ought to be adequate in predicting heat transfer to the ceiling. That is, even though from Fig. 28 the gas temperatures are

higher than the derived ceiling temperature the effect on ceiling heat transfer is small.

The maximum value, i.e. when $t \to o$, is from (11):

$$q'' = h_c \Delta T_{mc} \tag{13}$$

From Fig. 23 or Table 2 we can find the variation of q" with fire size, i.e. 1/6 + .93, not a great deal different from direct proportionality. This is a significant finding. It is of interest to determine the partitioning of energy throughout the various modes independent of fire size since perfect scaling will not have been obtained in simulation. That is, it is important to know that, for example, the enthalpy leaving through the lower vents represents some particular fraction of the heat release over the whole range of possible fire sizes and not, for example, just for small or just for large fires. Proportionality insures that the ceiling heat transfer, representing a large fraction of the energy, does indeed scale with fire size.

From Fig. 23 the variations with position are seen to be, not surprisingly, very significant. If one extrapolates the four central ventilation points for h and the two more-central ΔT_m points (T_3 and T_1) to $r/H \to 0$, the maximum values of ceiling heat transfer may be estimated.

$$h/Q^{1/6} = 0.043 \tag{14}$$

$$\Delta T_m/Q^{.93} = 9.5 \tag{15}$$

in SI units (kW, K, and m).

For the 30 kW heat release rate example, Eq. (13) will yield $.043 \times 9.5 \times 30^{1.1} = 17\ kW/m^2$. At r/H = 1 this reduces to about $7kW/m^2$ and so on, decreasing strongly with distance from the fire. With heat transfer rates of this order it is quite plausible for the approx. 70% figure of the energy to be absorbed by the ceiling.

How the heat transfer rate falls in time can be seen on Fig. 29 which shows the above example case, the 30kW fire, for the two r/H positions. Initially there is quite a dramatic reduction. Things begin to level off approximately at times corresponding to when the exhaust TC'S are beginning to sense warm air coming out. (Fig. 18).

The generalized form of the solution of the semi-infinite model Eq. (10) is shown on figure 30 where the non-dimensional heat transfer rate $\dot{q}''/(h_c \Delta T_m)$ is plotted vs. dimensionless time, $C\sqrt{t}$. The early times solution Eq. (11) is also shown for convenience. The quantities, h and C, are related according to $C = h/\sqrt{\rho ck}$.

3.5 Stratification

Fig. 31 shows eight traces of thermocouple readings, top-to-bottom, for tree D during a 40kW, central ventilation, 2.4 min rate, no seat test configuration. At arbitrary times one can look at the distribution of temperature with

elevation. Fig. 32 presents six such profiles at times equal to 30 s through 460 s after ignition. Obviously, hotter gases are at the top with the entire profile rising in time.

The question now arises as to how to generalize such a plot. The easiest method is to normalize each trace to some value that is representative of that time. Since all the information has been gathered and correlated for the top or maximum reading thermocouples, the trace of that thermocouple would be the obvious choice. Using the erfc model (Fig. 24-27) and the parameters from Table 3 we can, first subtracting out the initial ambient temperature, divide each of the readings of the profiles by the calculated maximum temperature for that time.

Fig. 33 shows the normalized profiles, the fraction of the maximum temperature at the time, that maximum being calculated via Eq. 1 using ΔT_m = 205K and C = 0.0897 $s^{-1/2}$. At long times a somewhat universal profile is achieved. The level of scatter is about ± 10% at the top. However we do clearly see the enclosure "filling" as the 30 s profile falls much lower than the one at 60 s which is lower than that at 120 s. The 120 s profile is beginning to approach the longer time result where temporal non-uniformity tends to disappear, and the whole bulk of gas or each strata moves upward in temperature simultaneously. Before this point is reached, times less than 120 s, the upper gases get hotter quickly and the lower gases slowly - there is definite temporal non-uniformity - the rates of rise are different in the upper and lower regions.

4.0 Conclusions

Three broad conclusions for the thermal field portion of these studies can be stated.

(1) Within times of interest, i.e., a few airchanges, the bulk of the fire produced energy was not being exhausted through the normal floor ventilation. The hot gases were accumulating close to the ceiling and except for some local mixing, were hardly affected by the incoming cold streams. As time progressed and the cabin began to fill from the top downward and heat transfer rates decreased as the ceiling and walls heated, only then did significant temperature levels begin to appear in the outflow stream.

(2) In the present apparatus most of the energy of the fire is transiently being stored in the "marinite" ceiling. The results have been generalized in terms of a semi-infinite slab model exposed to a high temperature constant bath, a function of fire size, through a constant convective film coefficient, h, dependent on position in the cabin and weakly on fire size.

(3) Heat transfer to the cabin ceiling was found to scale with fire size through almost direct proportionality thus insuring the generality of the present experiments. The behavior of different ceiling materials ought to be reflected through different ρck values.

5.0 Acknowledgements

Dan Madrzykowski with some help from Bob Vettori converted a conceptual design into a very durable excellently operating experimental apparatus in the form of the 1/2 scale, simulated wide body aircraft cabin. Without their friendly cooperation and hard work this task could not have been completed. Thanks are also due the technical coordinator at FAA, Dr. Thor Eklund, who from the broader view of the entire cabin fire problem was able to guide this work effectively suggesting which and how best to approach each of the problems.

6.0 References

1. Cox, G., Kumar, S., Markatos, N.C., (1986) "Some Field Model Validation Studies, Fire Safety Science-Proceedings of the First International Symposium", Hemisphere Publishing Corp. p. 159.

2. DeSouza, B.P., Yang, K.T., Lloyd, J.R., (1985) "Numerical Simulations of the Effect of Floor and Ceiling Venting on Fire and Smoke Spread in Aircraft Cabins", NBS-GCR-84-479, National Bureau of Standards, Gaithersburg, MD.

3. Eklund, T.I., (1984 a) "Effects of Ventilation and Panel Properties on Temperature Rise from Aircraft Fires", DOT/FAA/CT - TN 83/63 FAA Technical Note, Technical Center, Atlantic City.

   Eklund, T.I., (1984 b) "An Analysis for Relating Visibility to Smoke Production and Ventilation", DOT/FAA/CT-TN 84/22.

4. Foote, K.L., Pagni, P.J., Alvares, N.J., (1986) "Temperature Correlations for Forced-Ventilated Compartment Fires, Fire Safety Science-Proceedings of the First International Symposium", Hemisphere Publishing Corp. p.139.

5. Mitler, H.E., (1984) "Zone Modeling of Forced Ventilation Fires", Combustion Science and Technology 39, 83.

6. Quintiere, J., McCaffrey, B.J., and Kashiwagi, T., (1978) A Scaling Study of a Corridor Subject to a Room Fire, Combustion Science and Technology 18, pp 1-19.

7. Sarkos, C.P. and Hill, R.G.(1985), "Evaluation of Aircraft Interior Panels Under Full-Scale Cabin Fire Test Conditions", AIAA 23rd Aerospace Sciences Meeting, Reno.

8. Abramowitz, M. and Stegun, I.A., Handbook of Mathematical Functions, National Bureau of Standards Applied Math Series 55, 1965.

LIST OF FIGURES

25) ERFC-like Curve Fits to Gas Temperature Data. C1

26) ERFC-like Curve Fits to Gas Temperature Data. A2

27) ERFC-like Curve Fits to Gas Temperature Data. D1

28) Ceiling and Gas Thermal Characteristics and Heat Transfer Coefficient vs. position.

29) Calculated Ceiling Heat Transfer Decay for 30kW Fire at r/H = 0, 1

30) Normalized Solution and Small Time Approximation.

31) Gas Temperature-Time Trace, TC Tree D, 40kW Fire

32) Vertical Temperature Profiles (selected times)

33) Normalized Temperature Profile

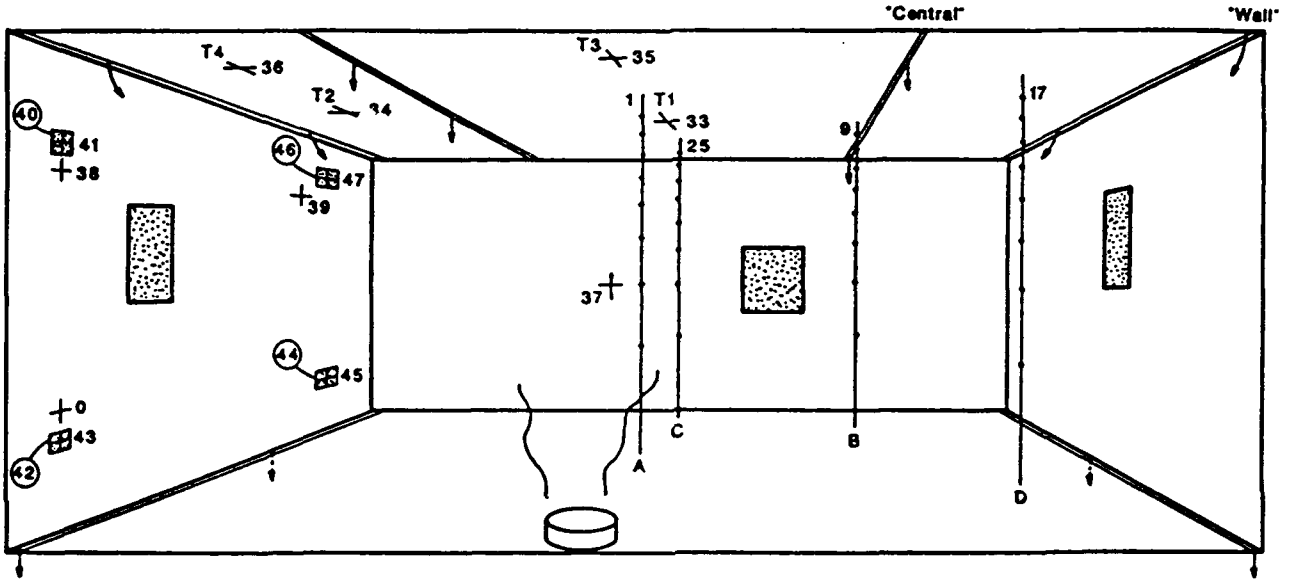

Fig. 1 Interior View of One Half of Symmetric Enclosure.

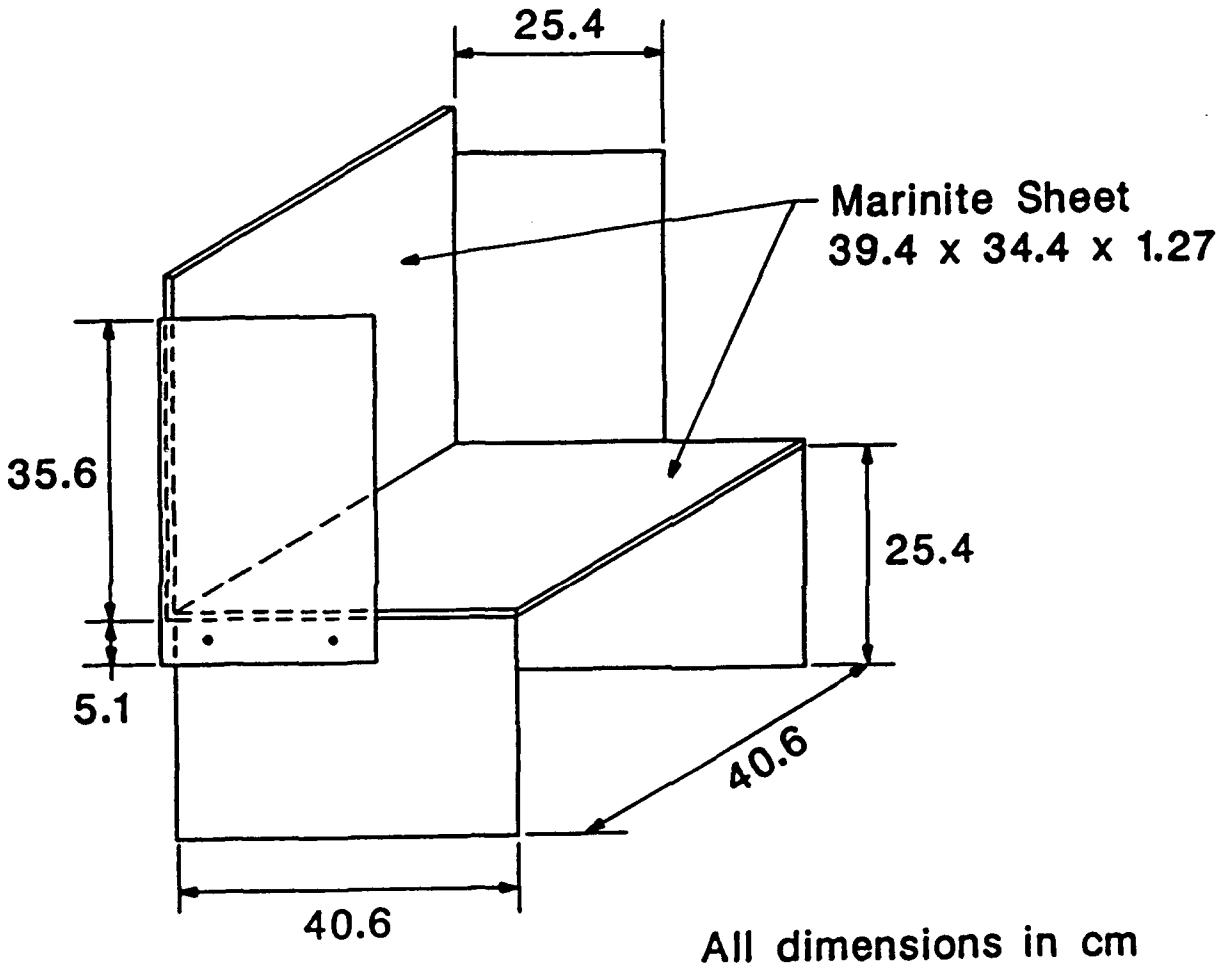

Fig. 2 Typical Seat.

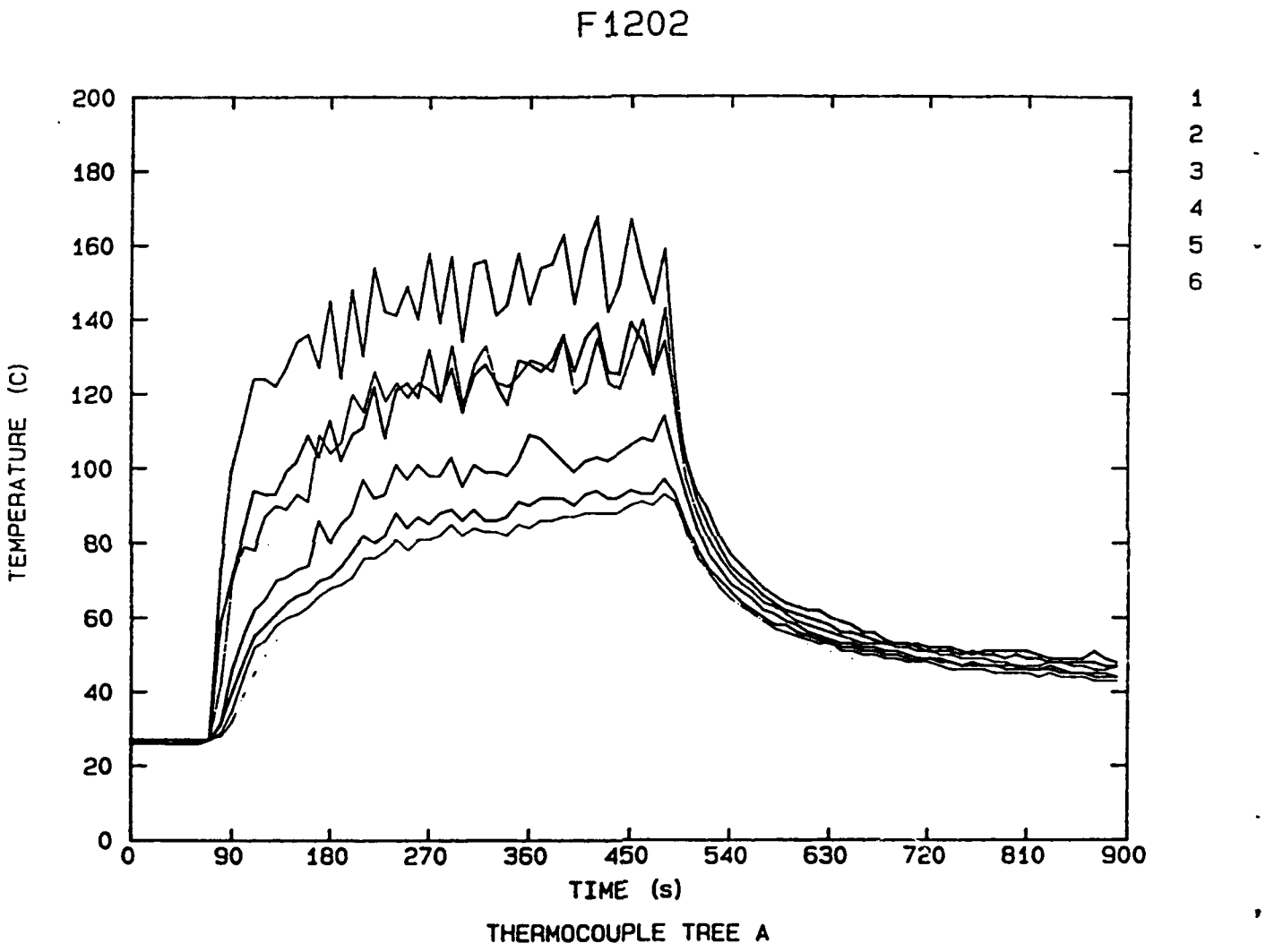

Fig. 3 Time Histories TC Tree A F1202

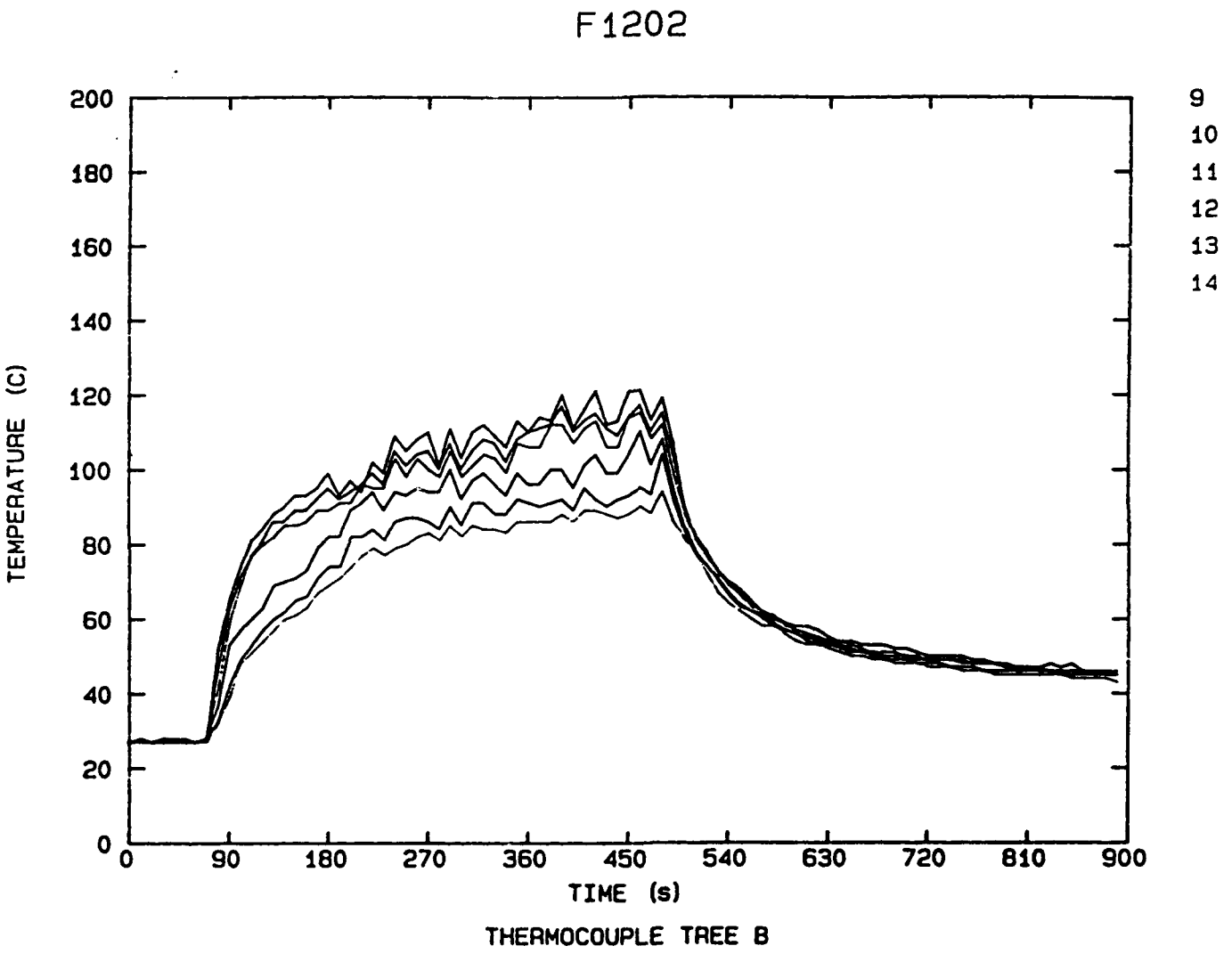

Fig. 4 Time Histories TC Tree B F1202

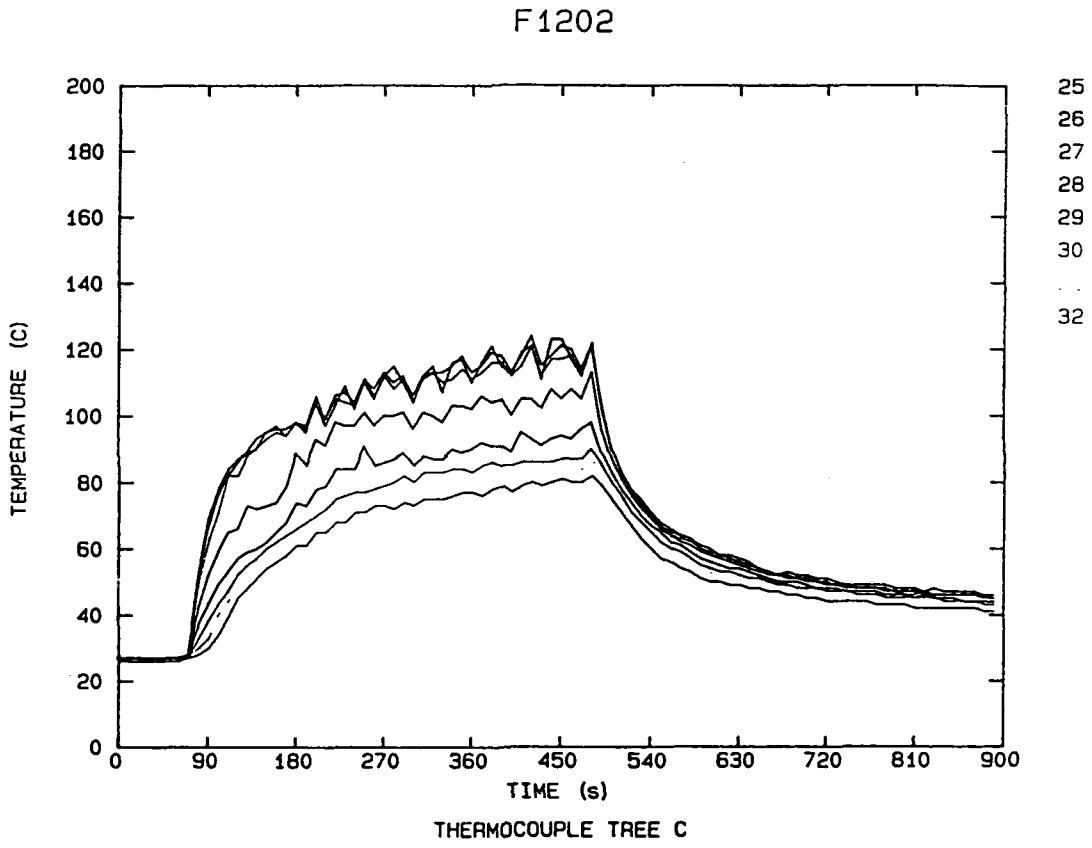

Fig. 5 Time Histories TC Tree C F1202

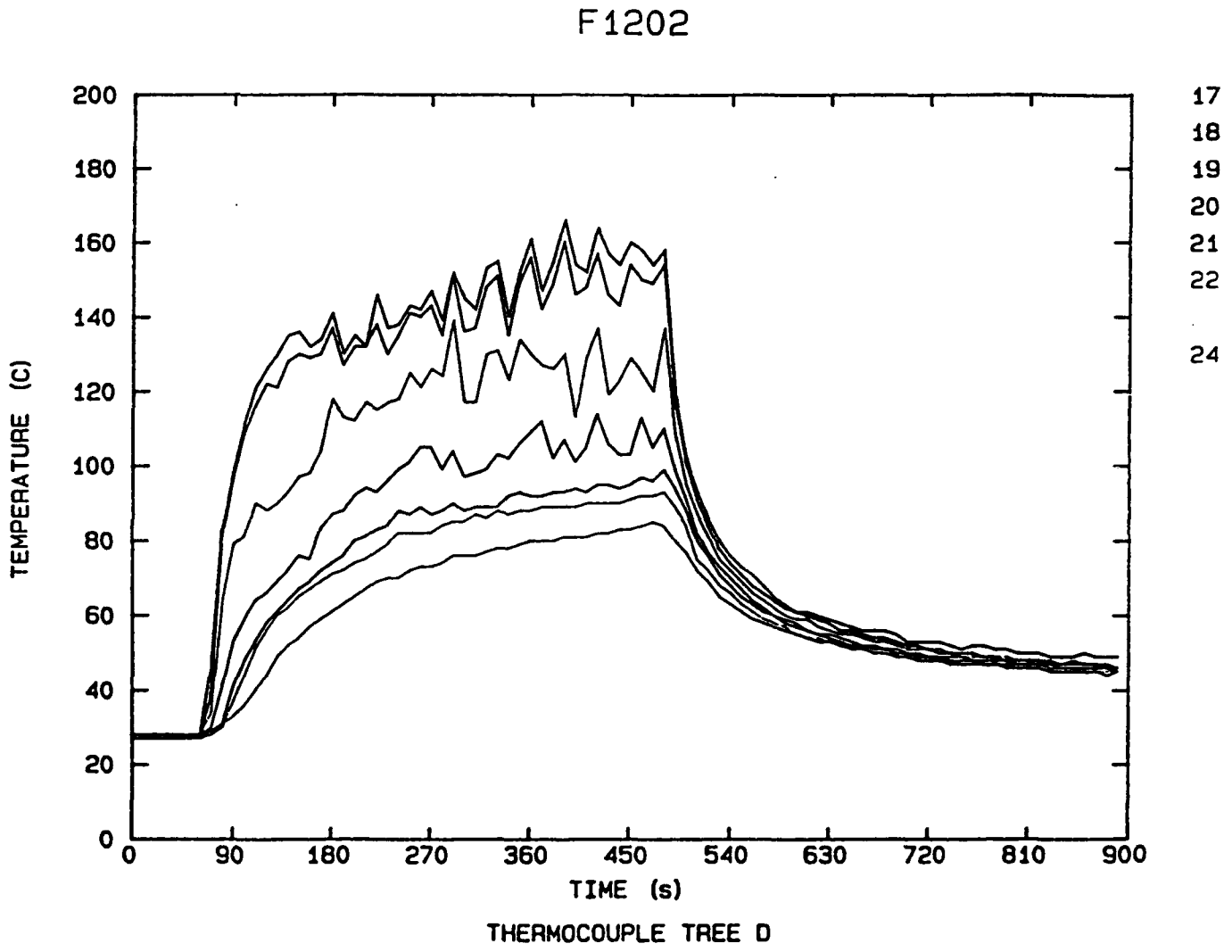

Fig. 6 Time Histories TC Tree D F1202

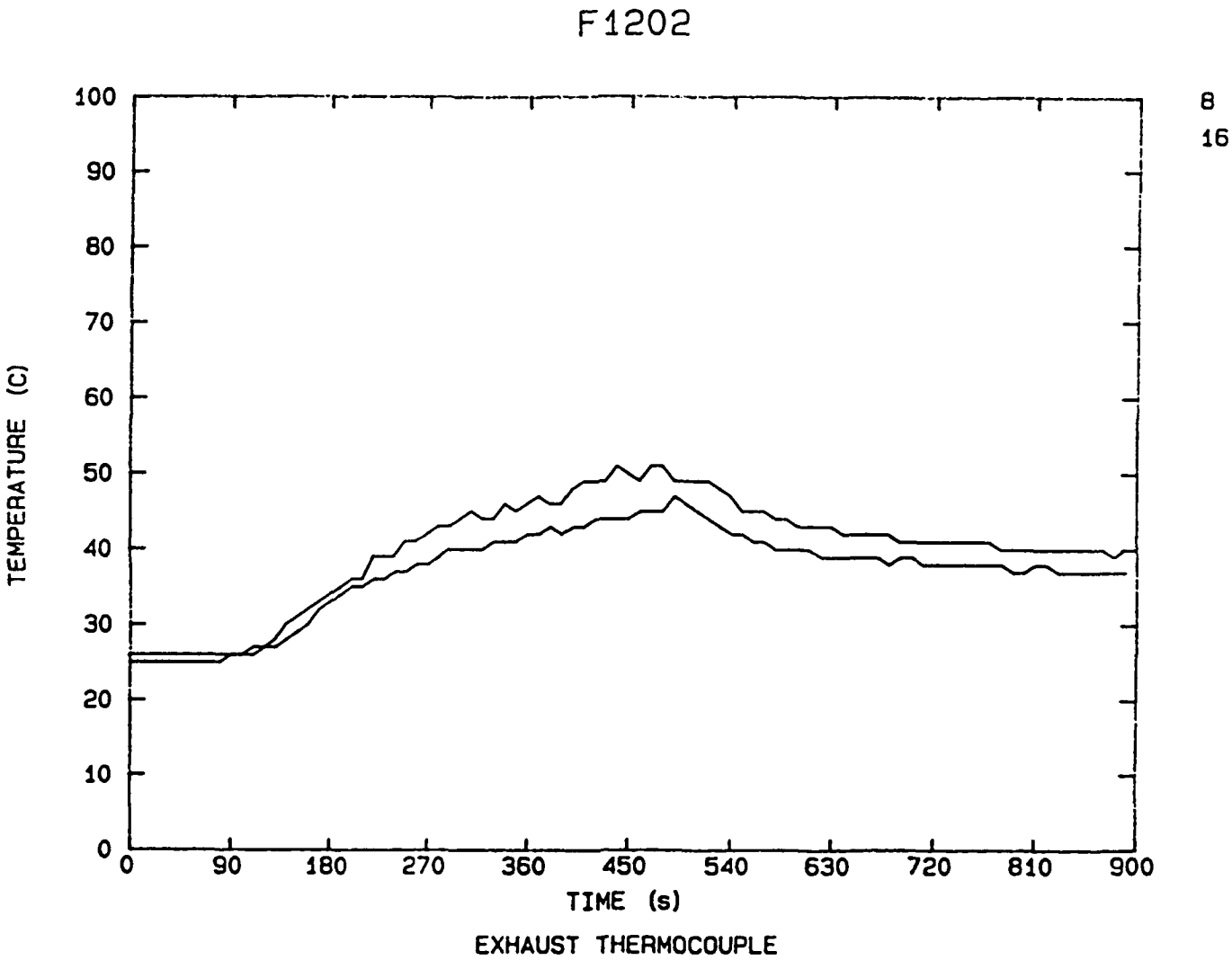

Fig. 7 Exhaust Gas TC Histories F1202

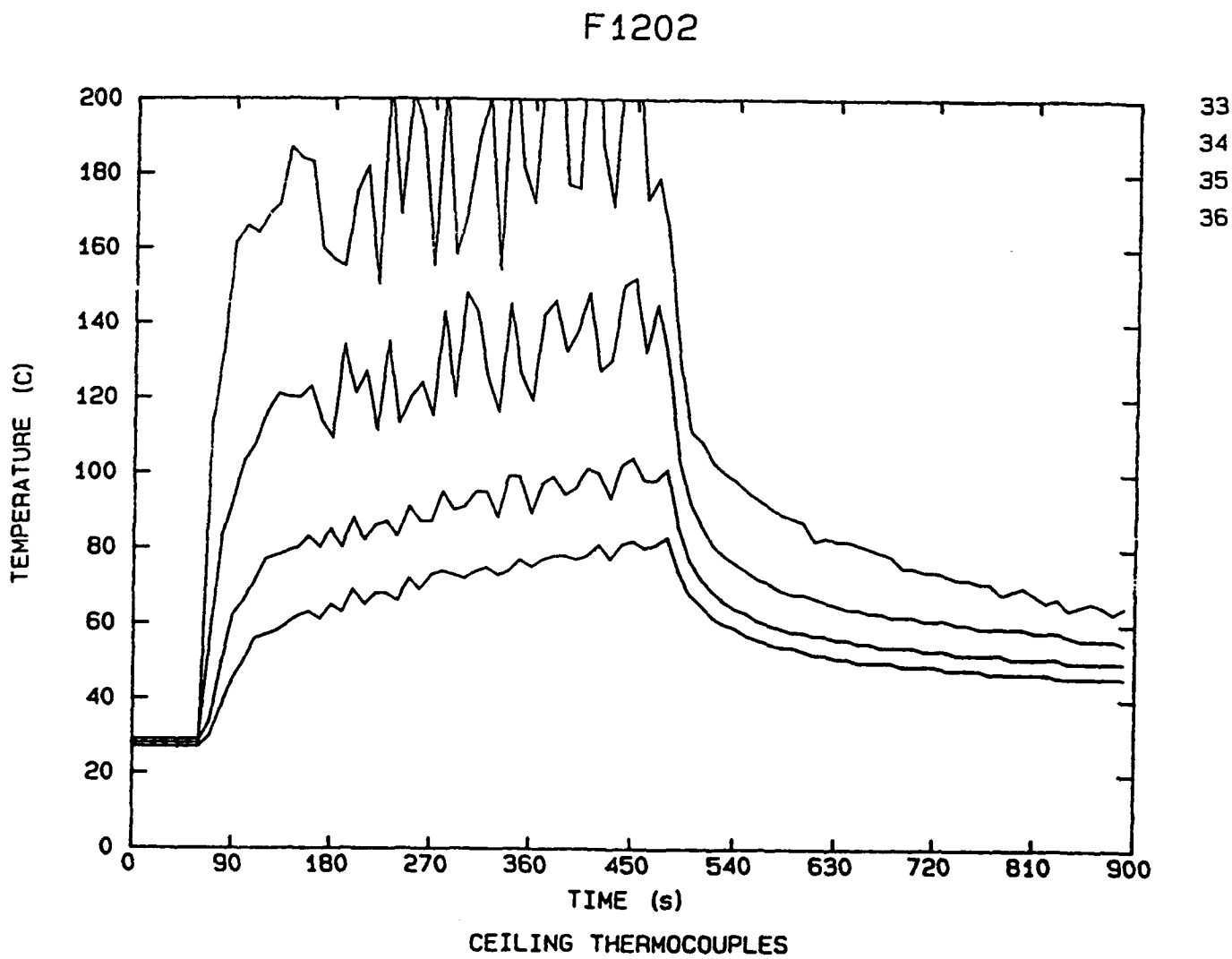

Fig. 8 Ceiling Temperatures Histories F1202

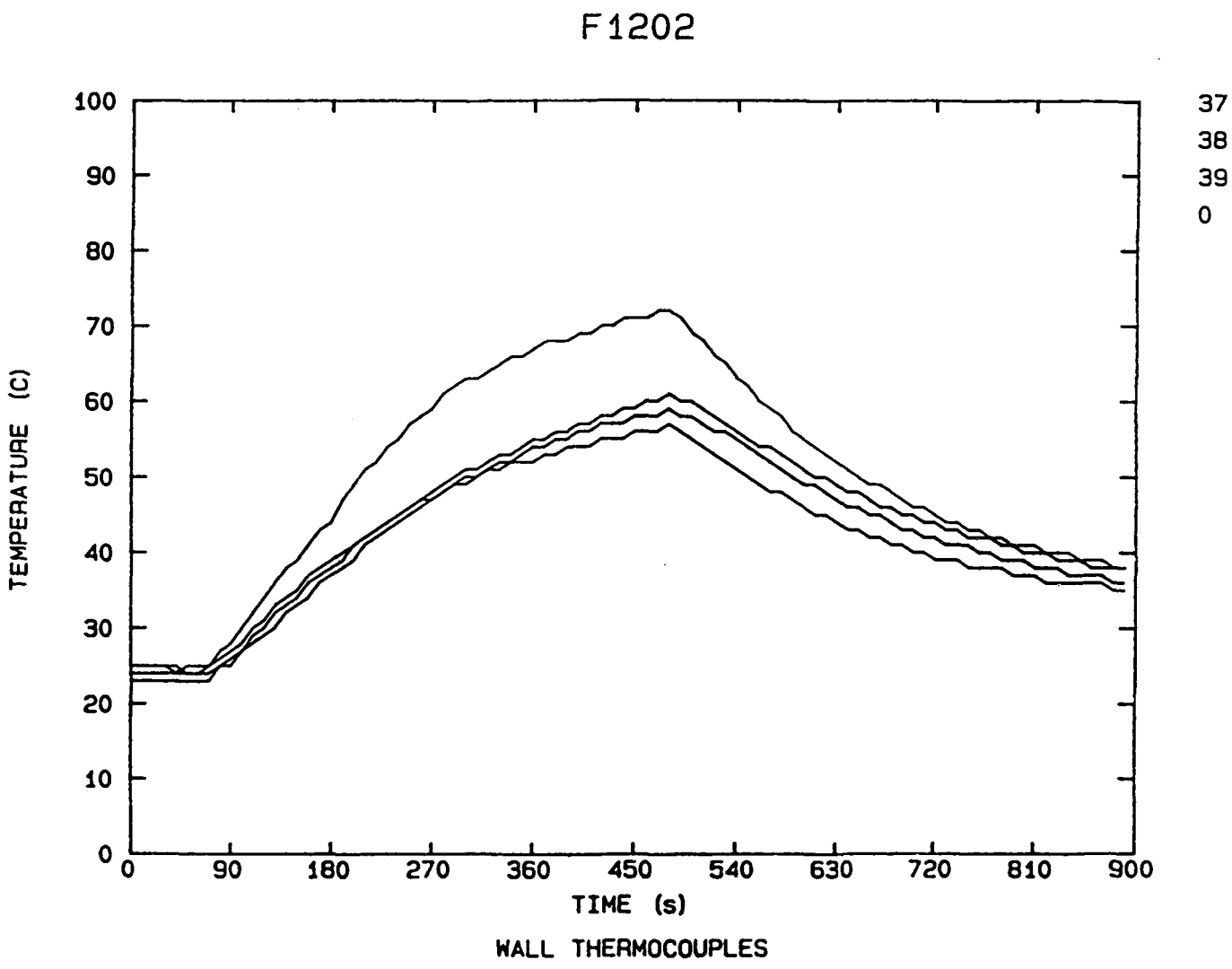

Fig. 9 Interior Wall TC Traces F1202

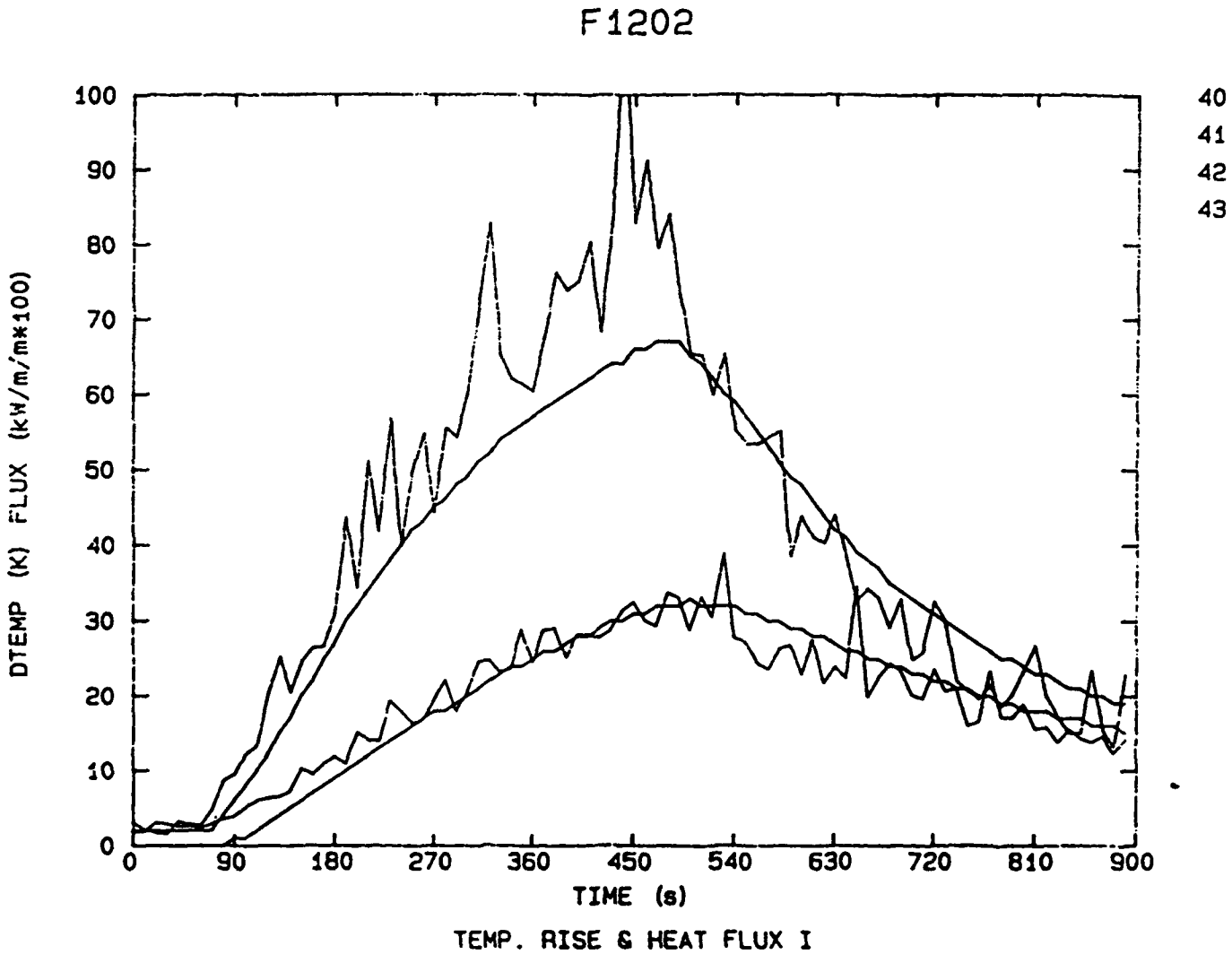

Fig. 10 Exterior Temperature Rise and Heat Flux Histories F1202

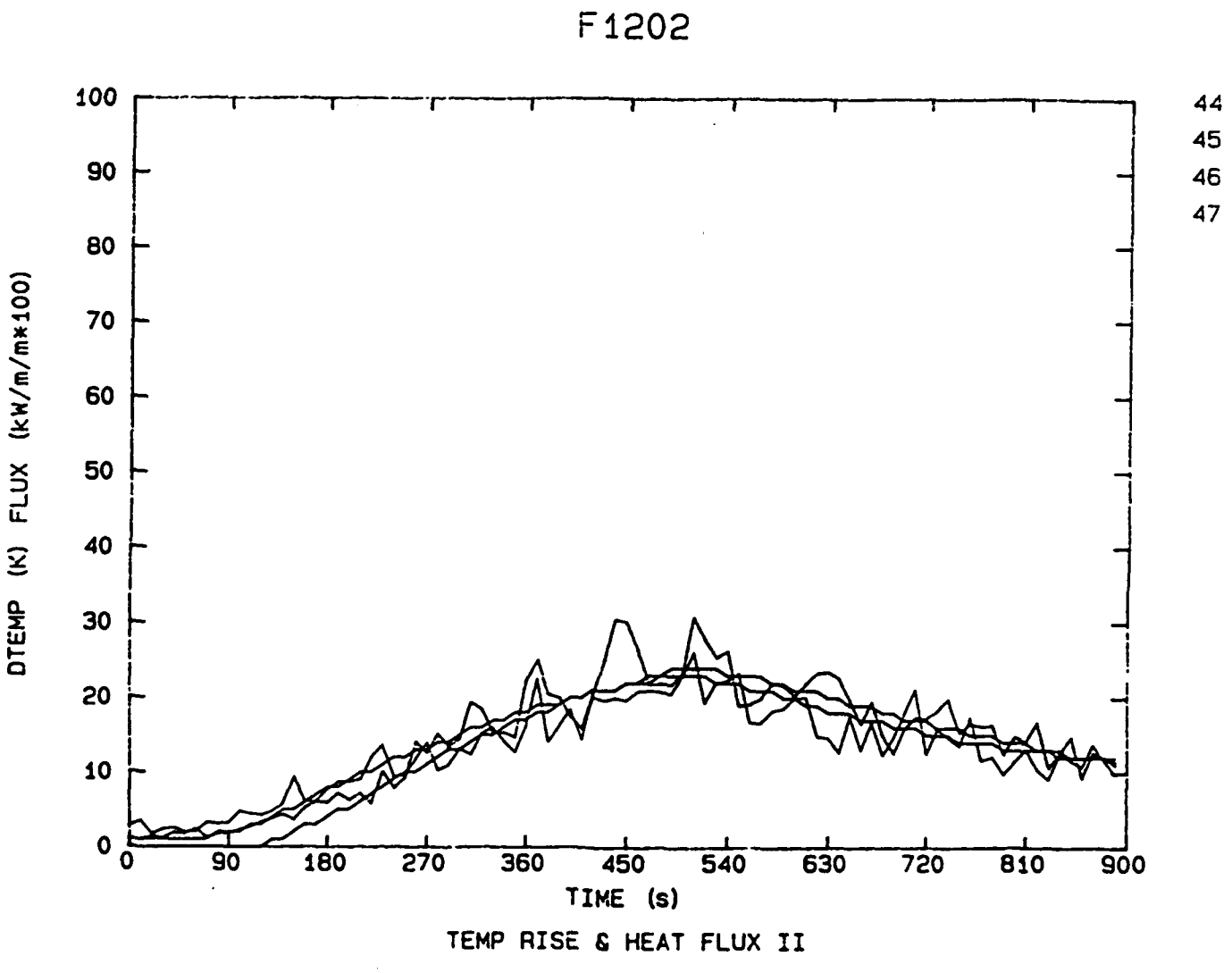

Fig. 11 Exterior Temperature Rise and Heat Flux Histories F1202

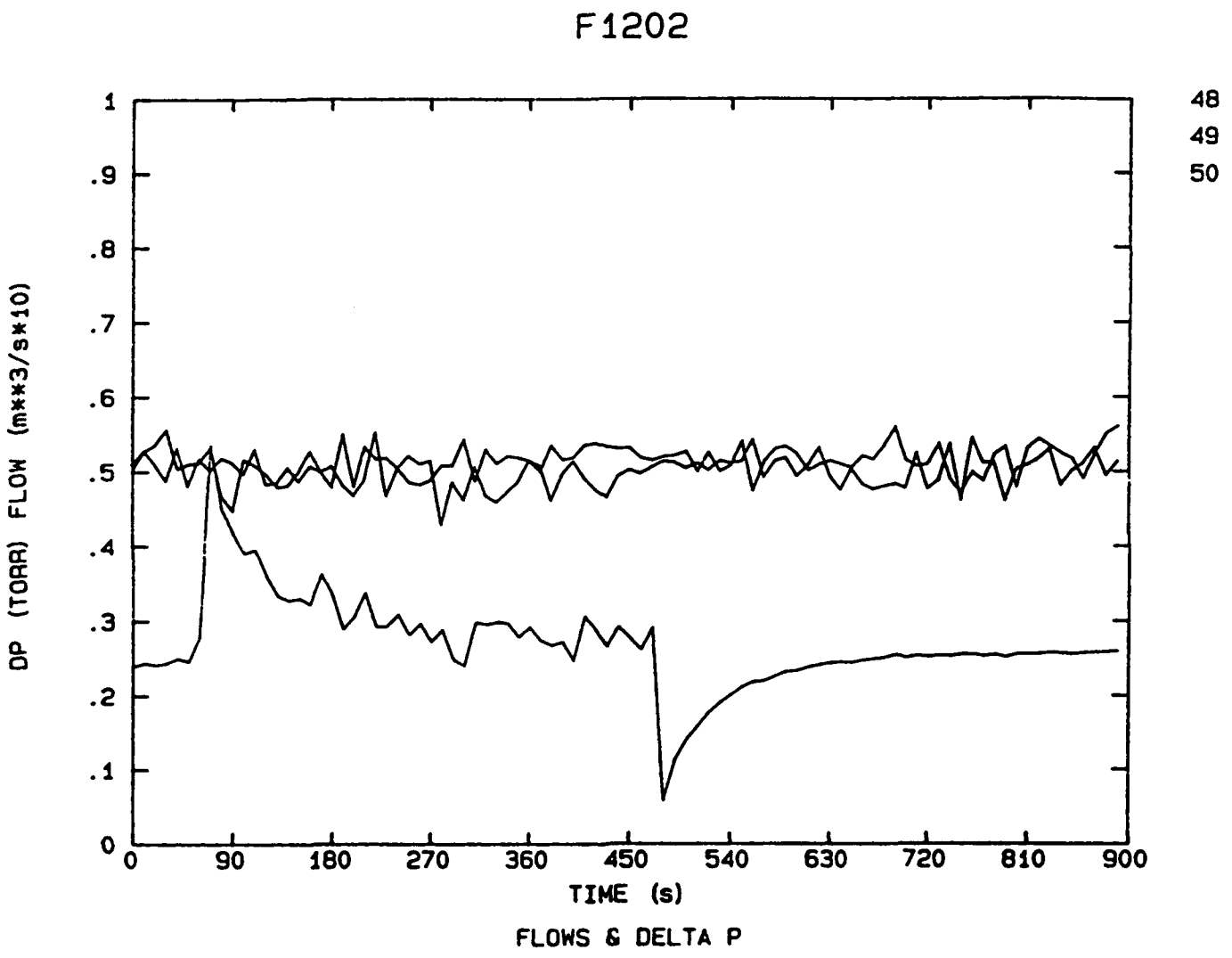

Fig. 12 Ventilation Flow Rates and Cabin Differential Pressure Histories F1202

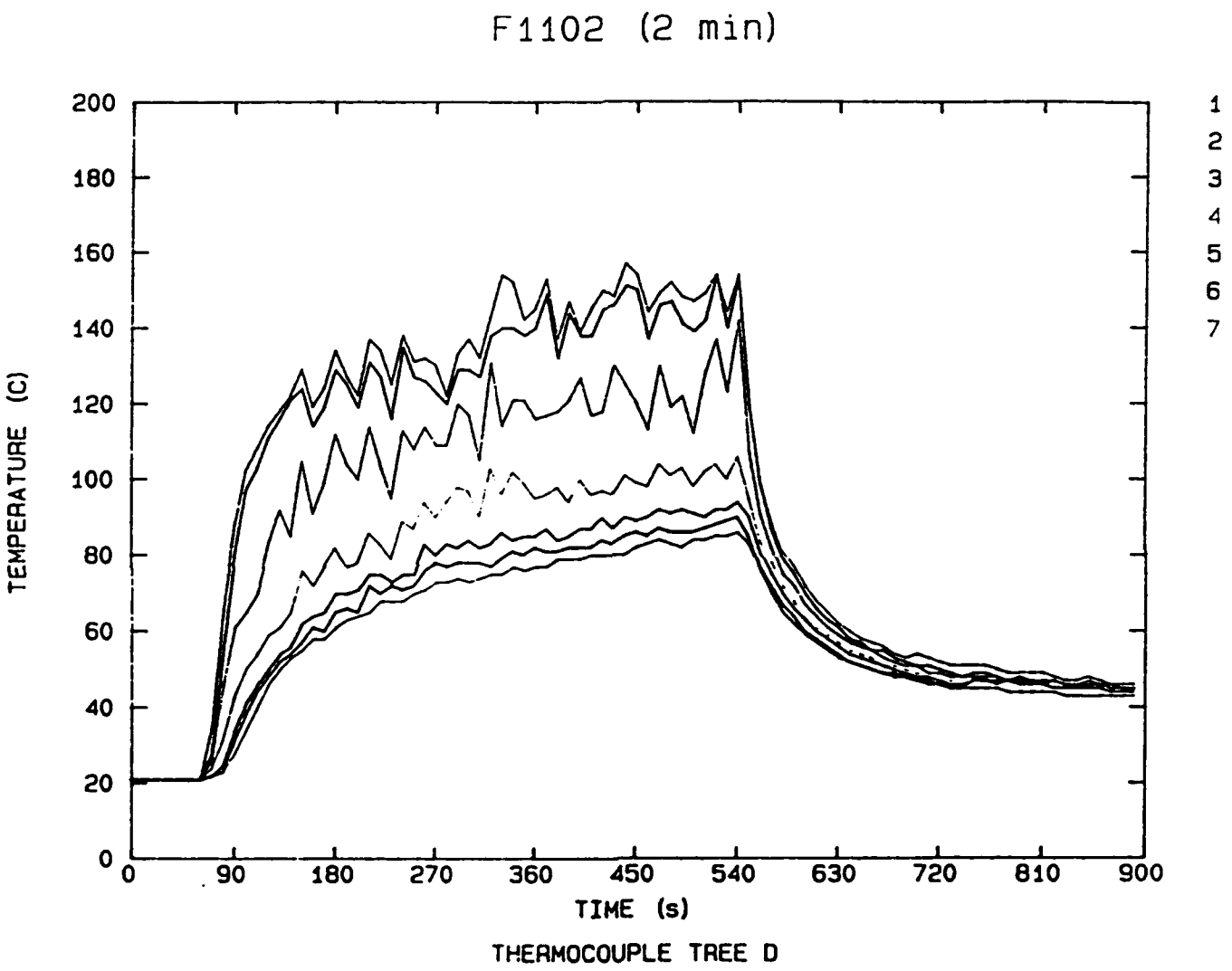

Fig. 13 Gas Temperature-Time Traces. TC Tree D, 30kW Fire 2 min Rate

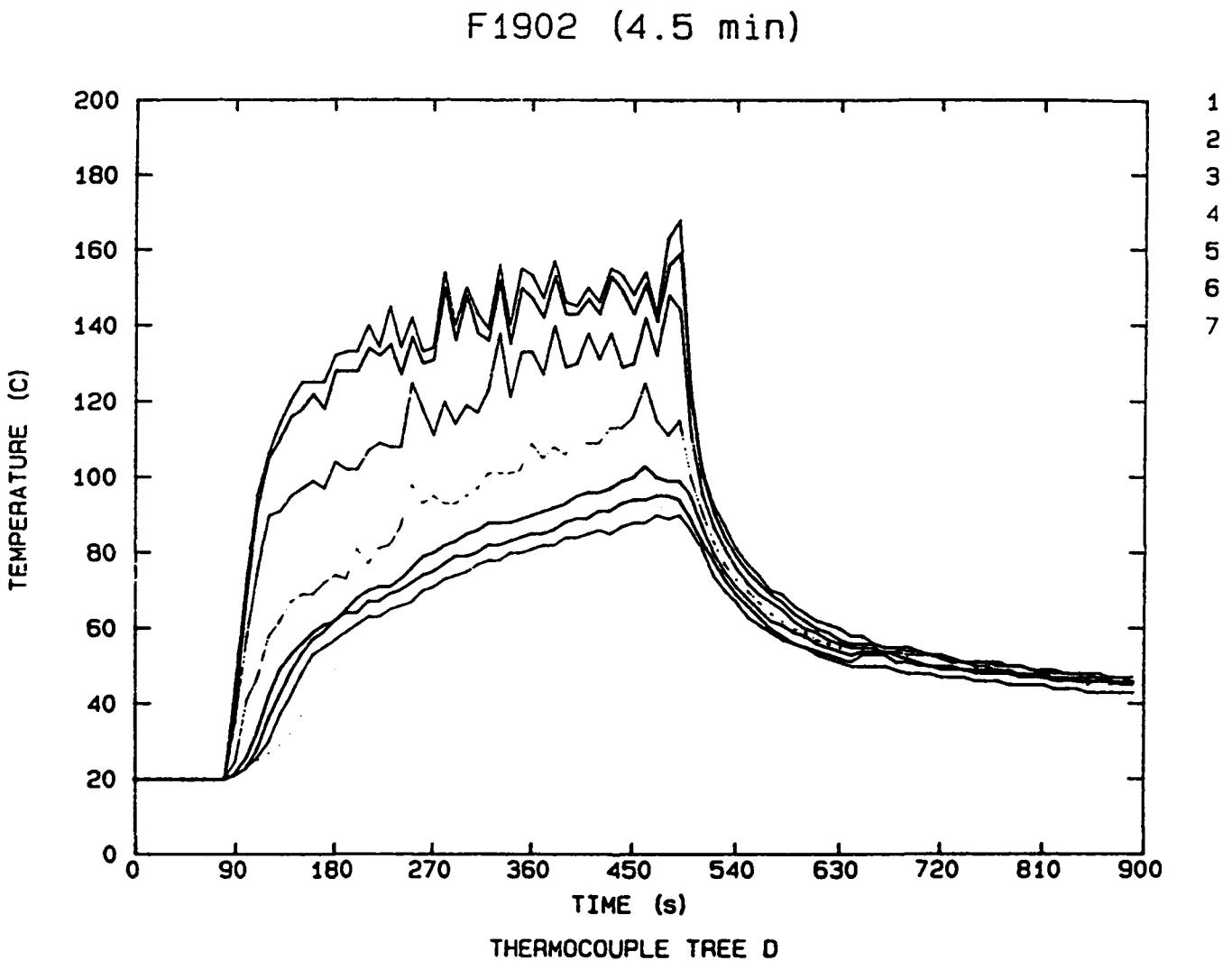

Fig. 14 Gas Temperature-Time Traces. TC Tree D, 30kW Fire 4.5 min Rate

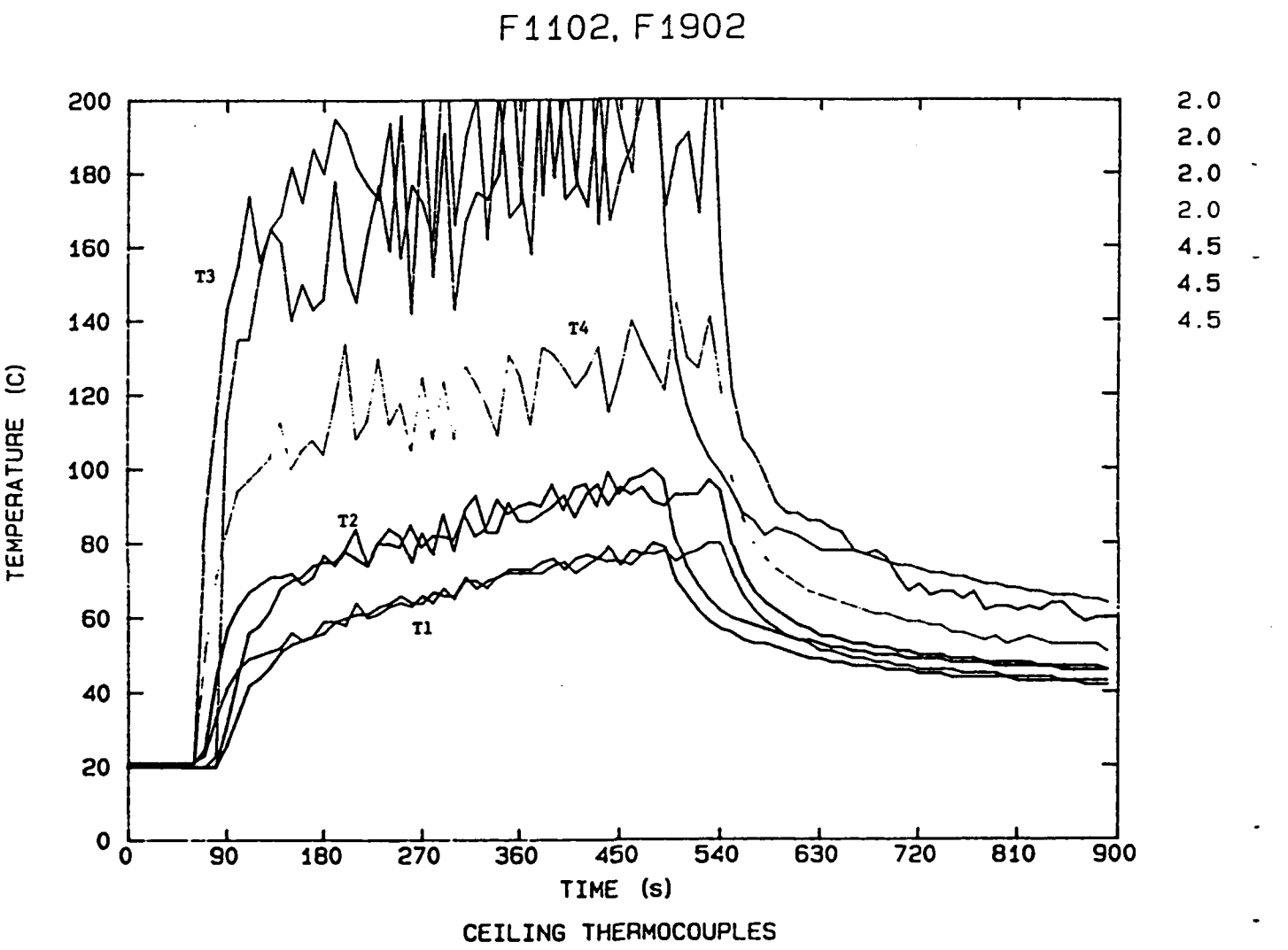

Fig. 15 Ceiling Temperature-Time Traces. 4 Positions, 30 kW, Two Ventilation Rates.

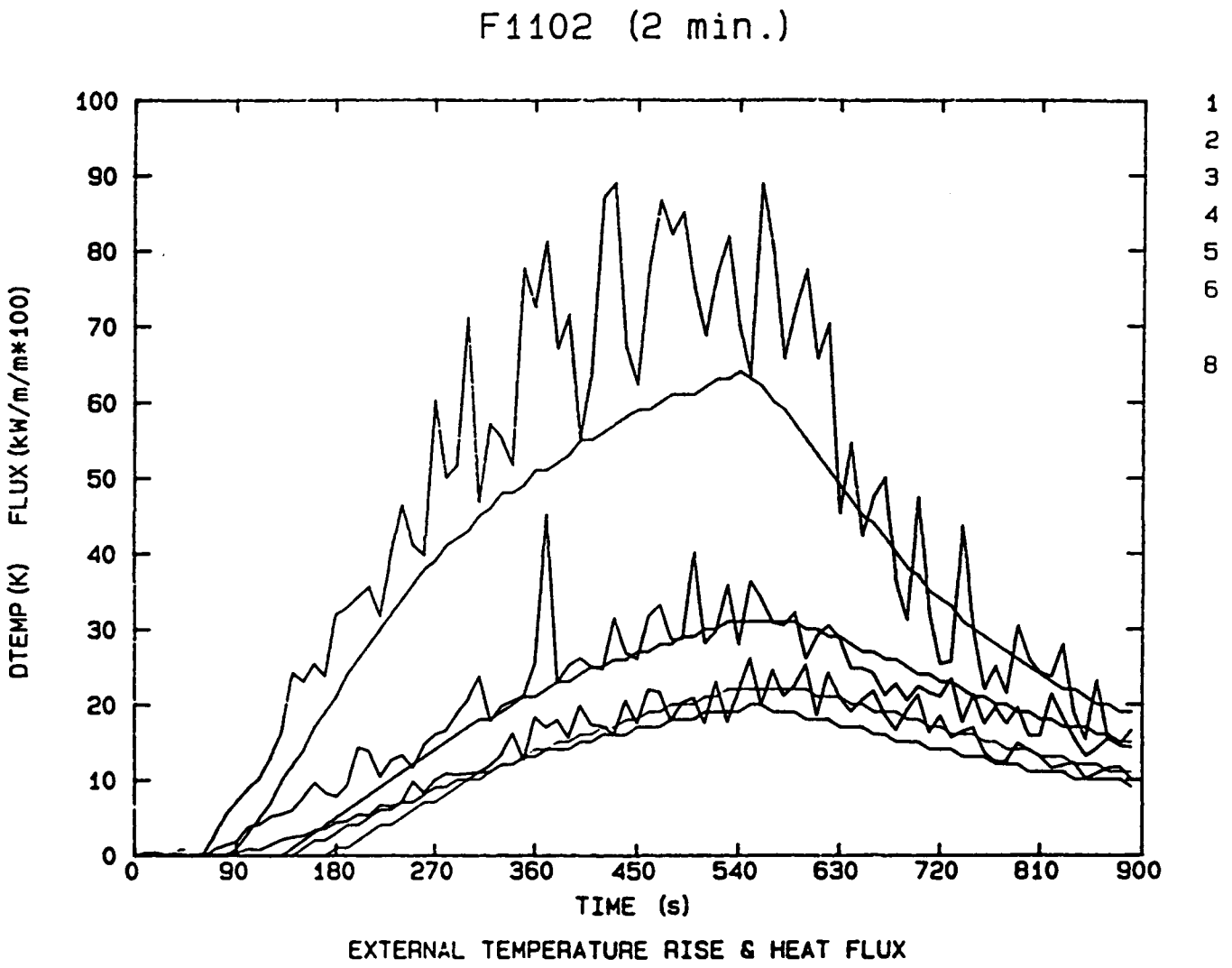

Fig. 16 External Wall Temperature, Heat Flux-Time Plots. 30 kW, 2 min Rate

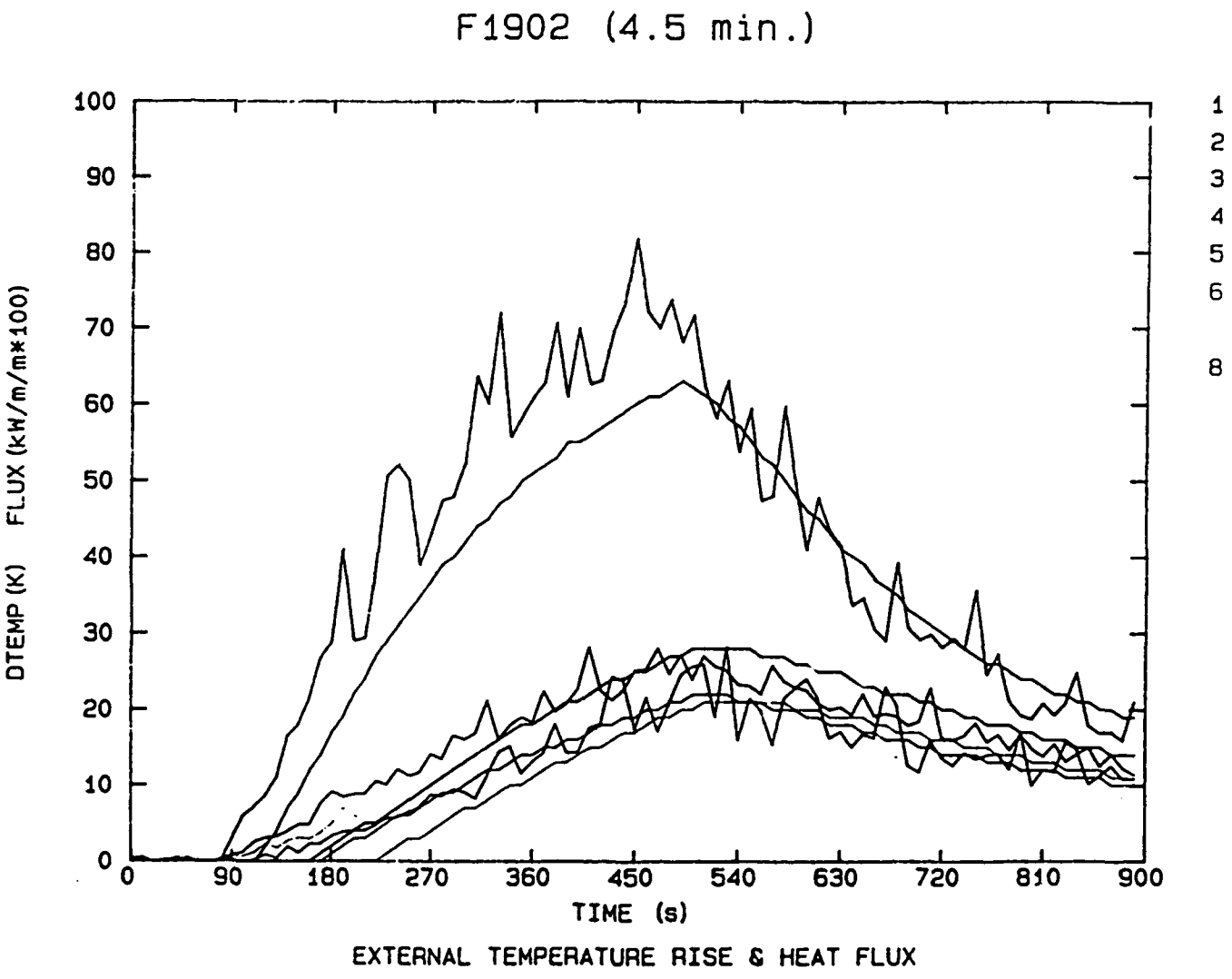

Fig. 17 External Wall Temperature, Heat Flux-Time Plots. 30 kW, 4.5 min Rate

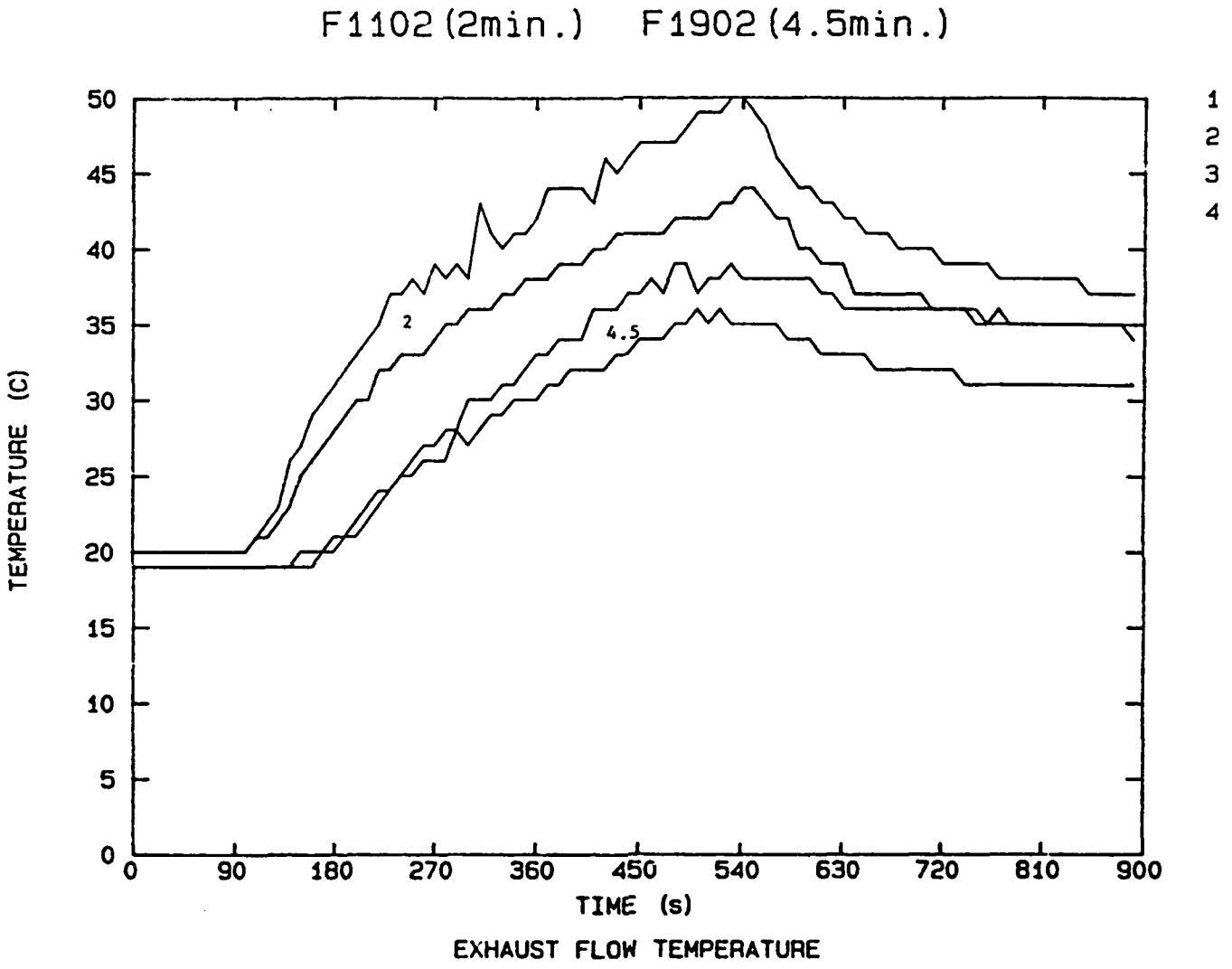

Fig. 18 Exhaust Flow TC Readings. Two Ventilation Rates, Two per run.

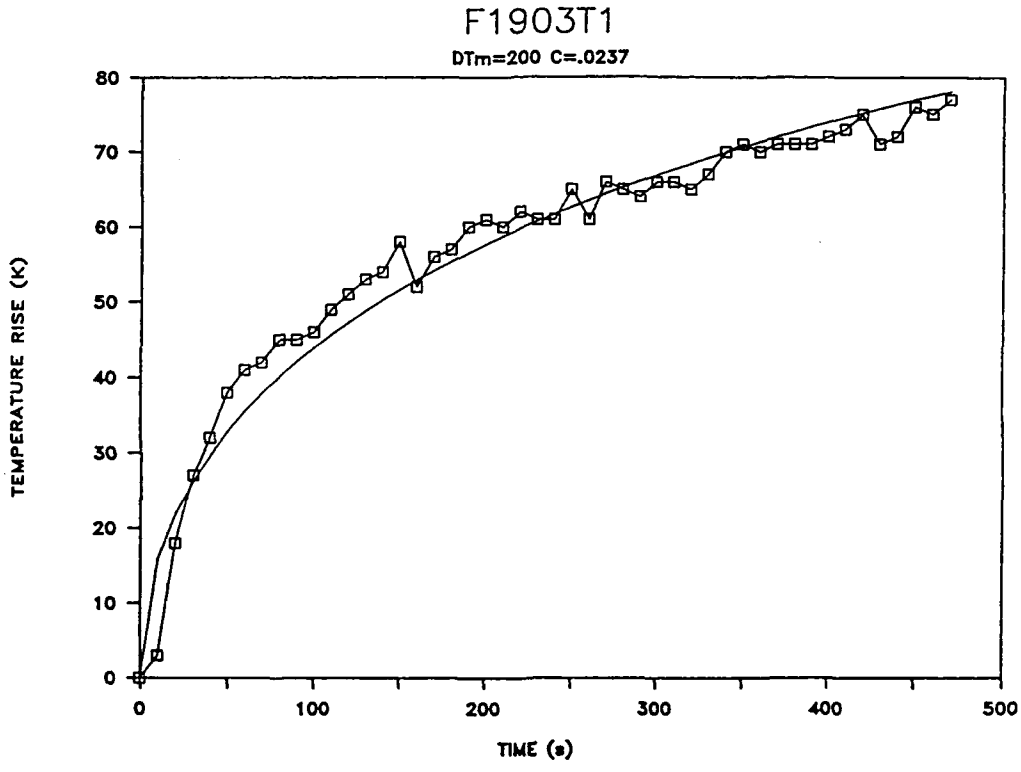

Fig. 19 ERFC-like Curve Fits to Ceiling Temperature Data. T1

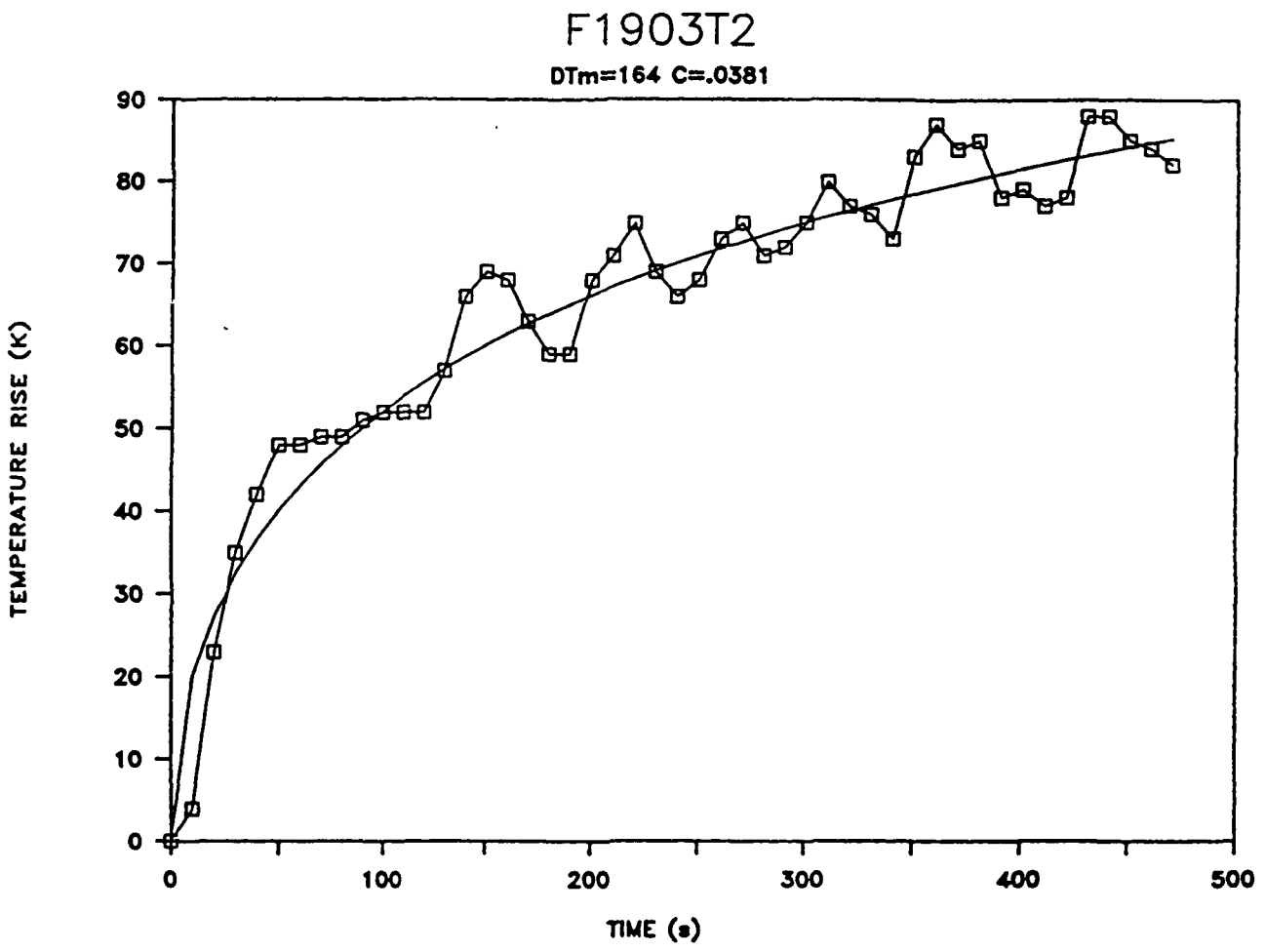

Fig. 20 ERFC-like Curve Fits to Ceiling Temperature Data. T2

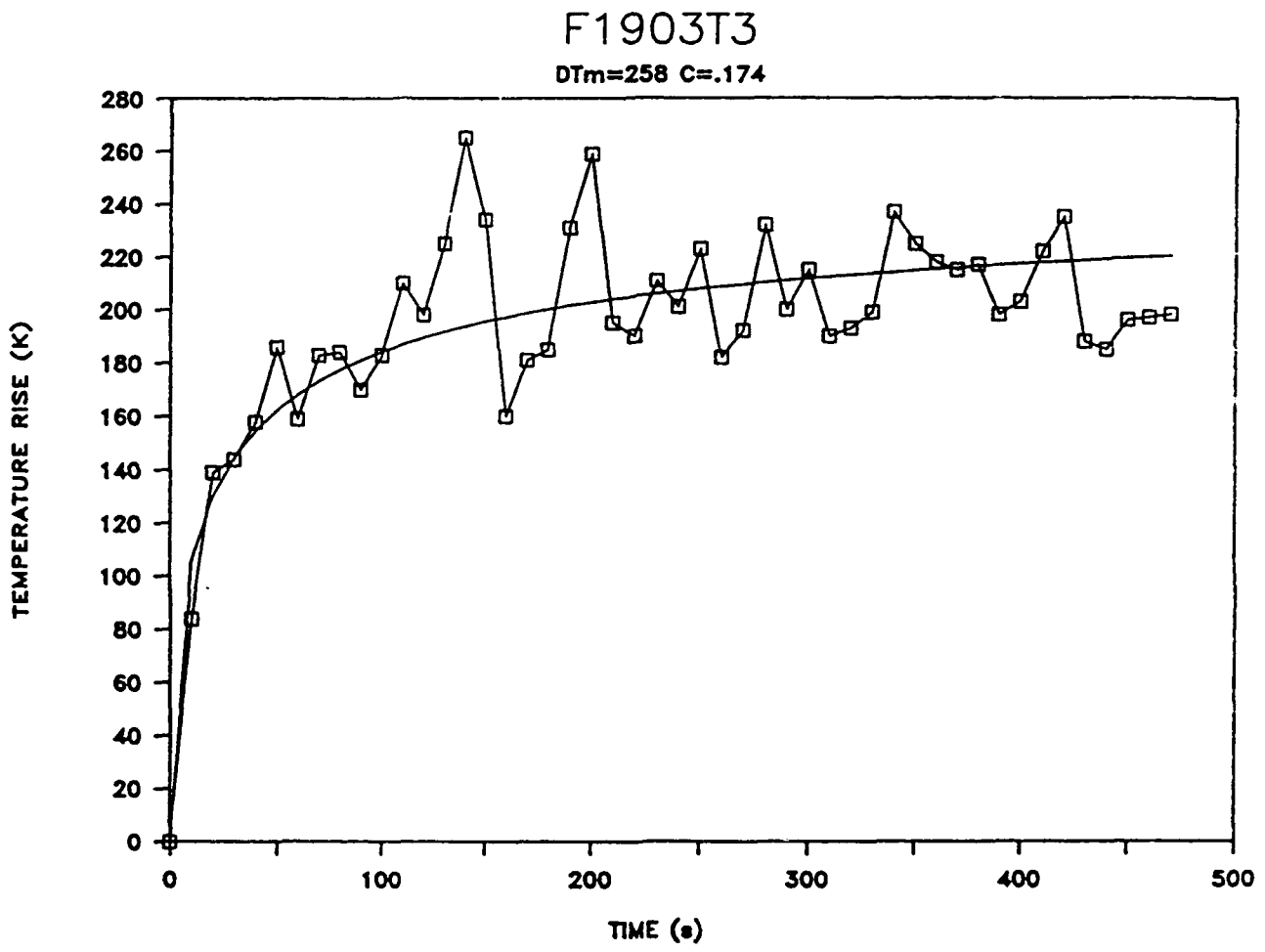

Fig. 21 ERFC-like Curve Fits to Ceiling Temperature Data. T3

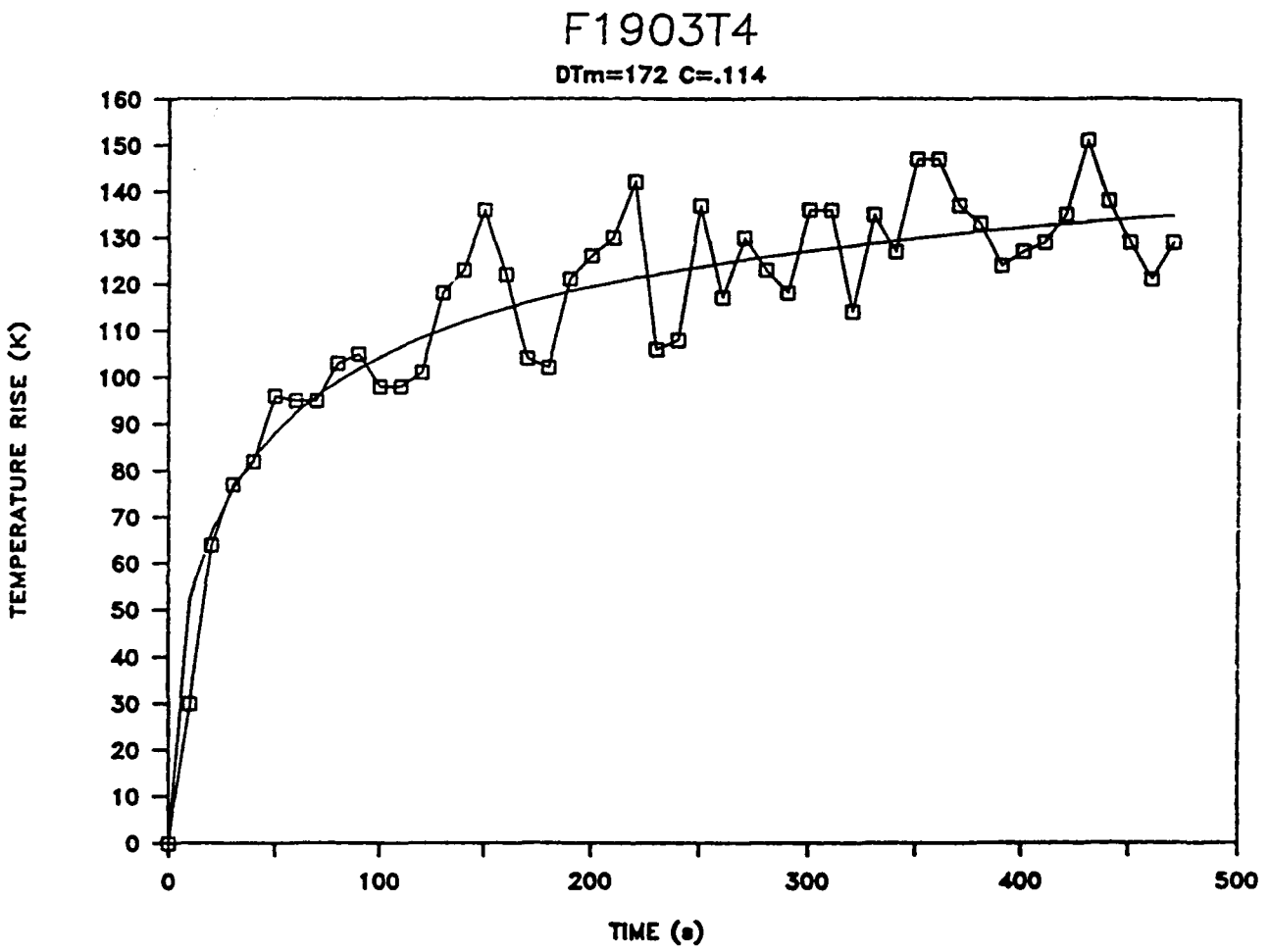

Fig. 22 ERFC-like Curve Fits to Ceiling Temperature Data. T4

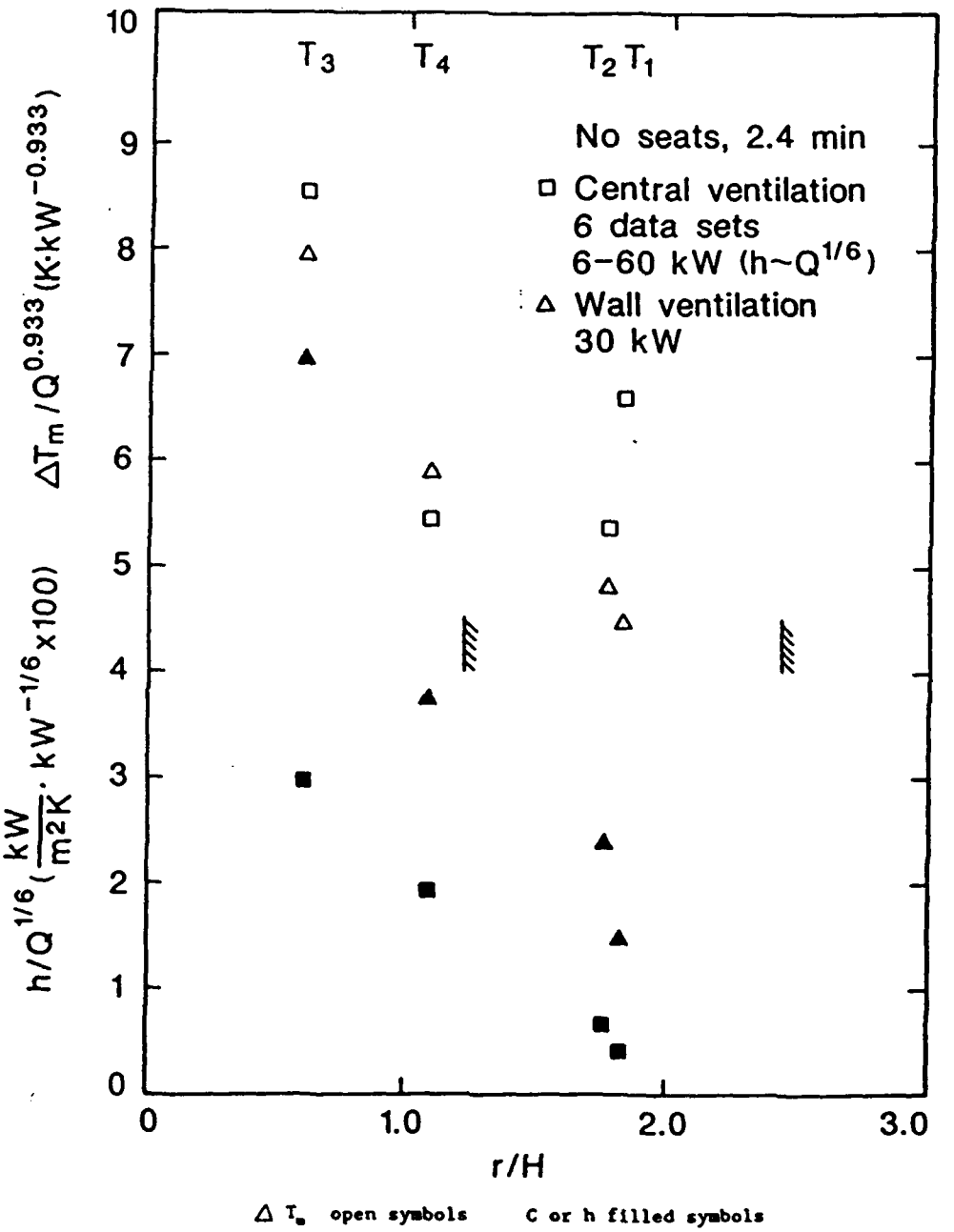

Fig. 23 Ceiling Thermal Characteristics, ΔT_m and h vs Q and r/H.

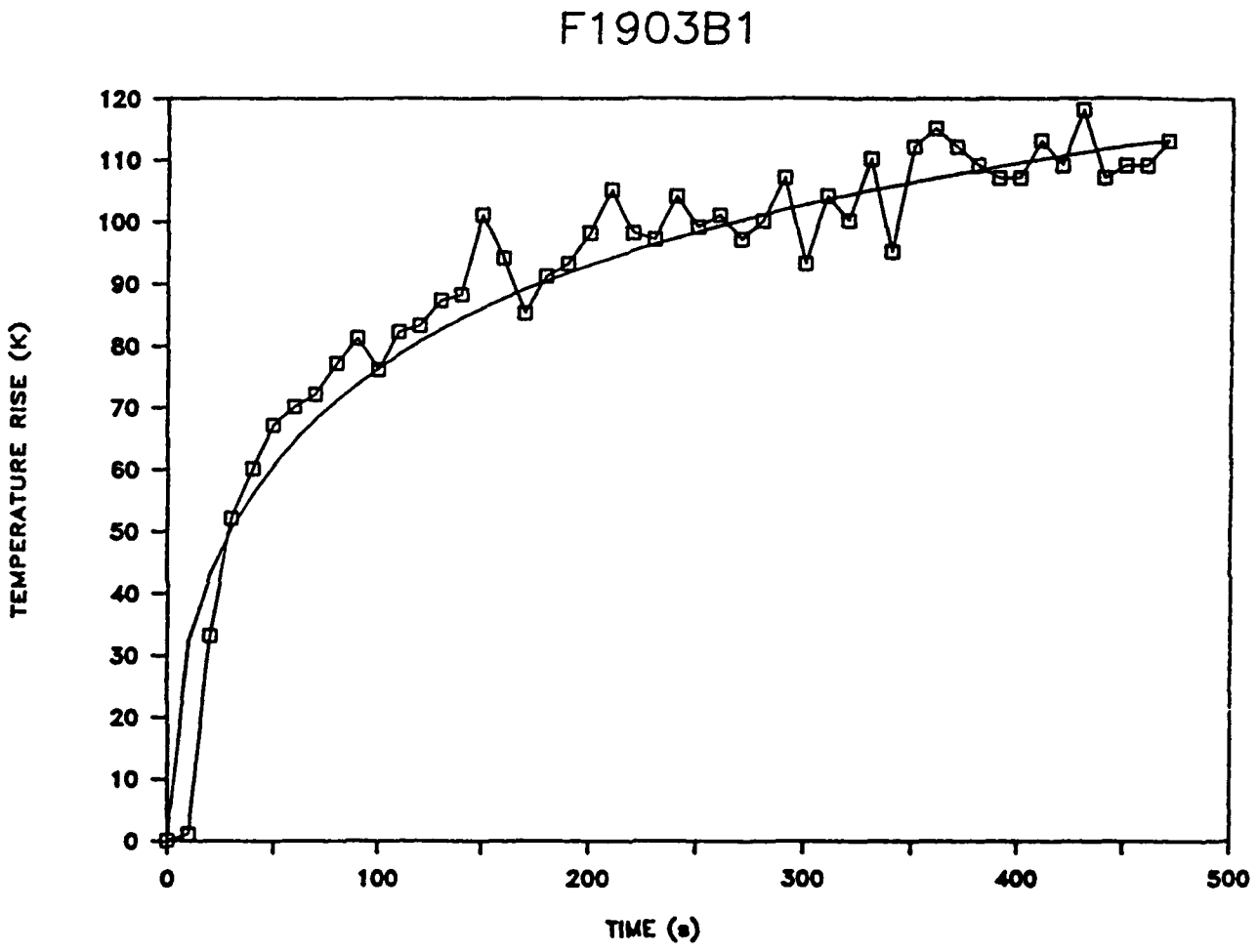

Fig. 24 ERFC-like Curve Fits to Gas Temperature Data. B1

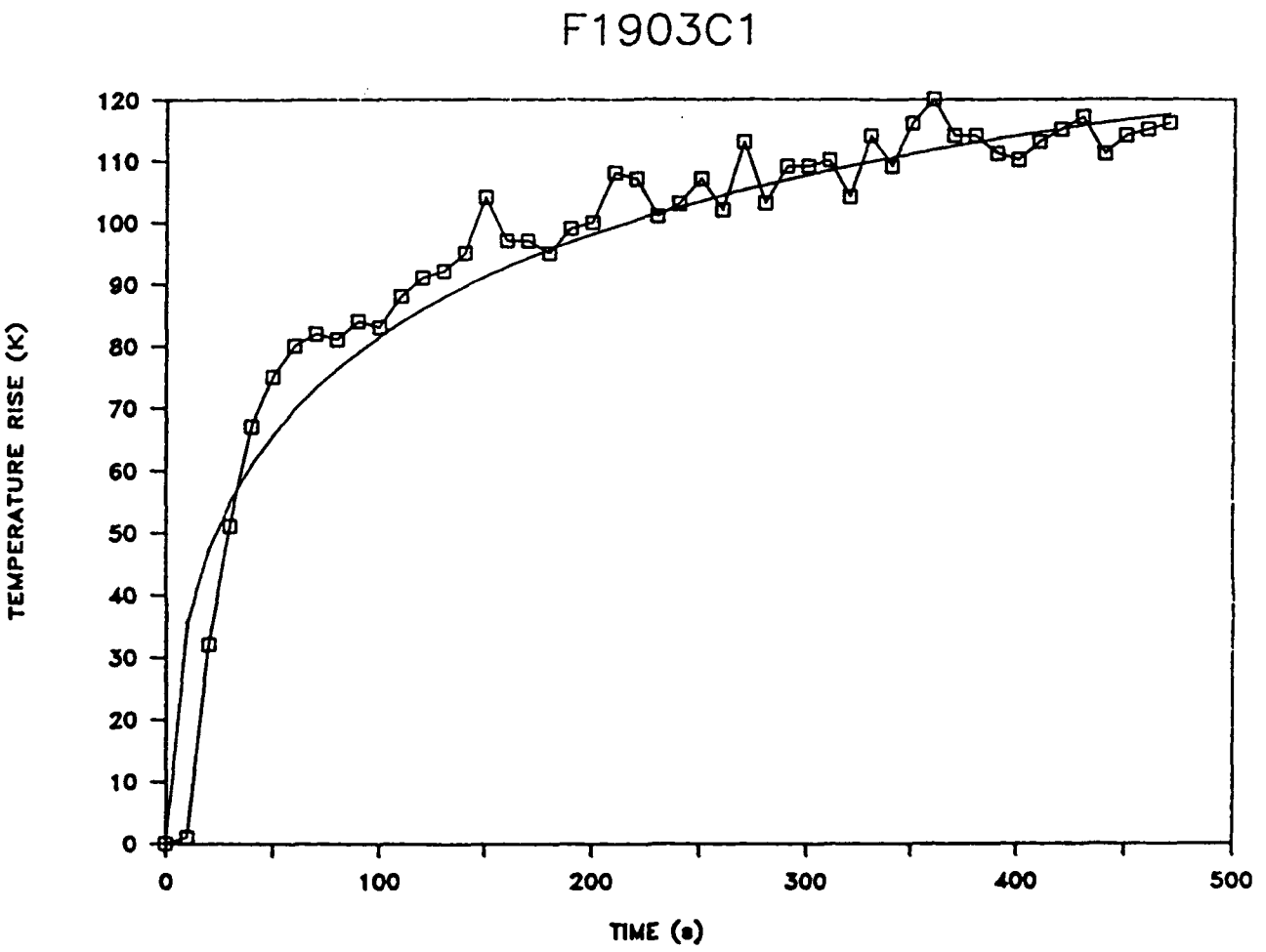

Fig. 25 ERFC-like Curve Fits to Gas Temperature Data. C1

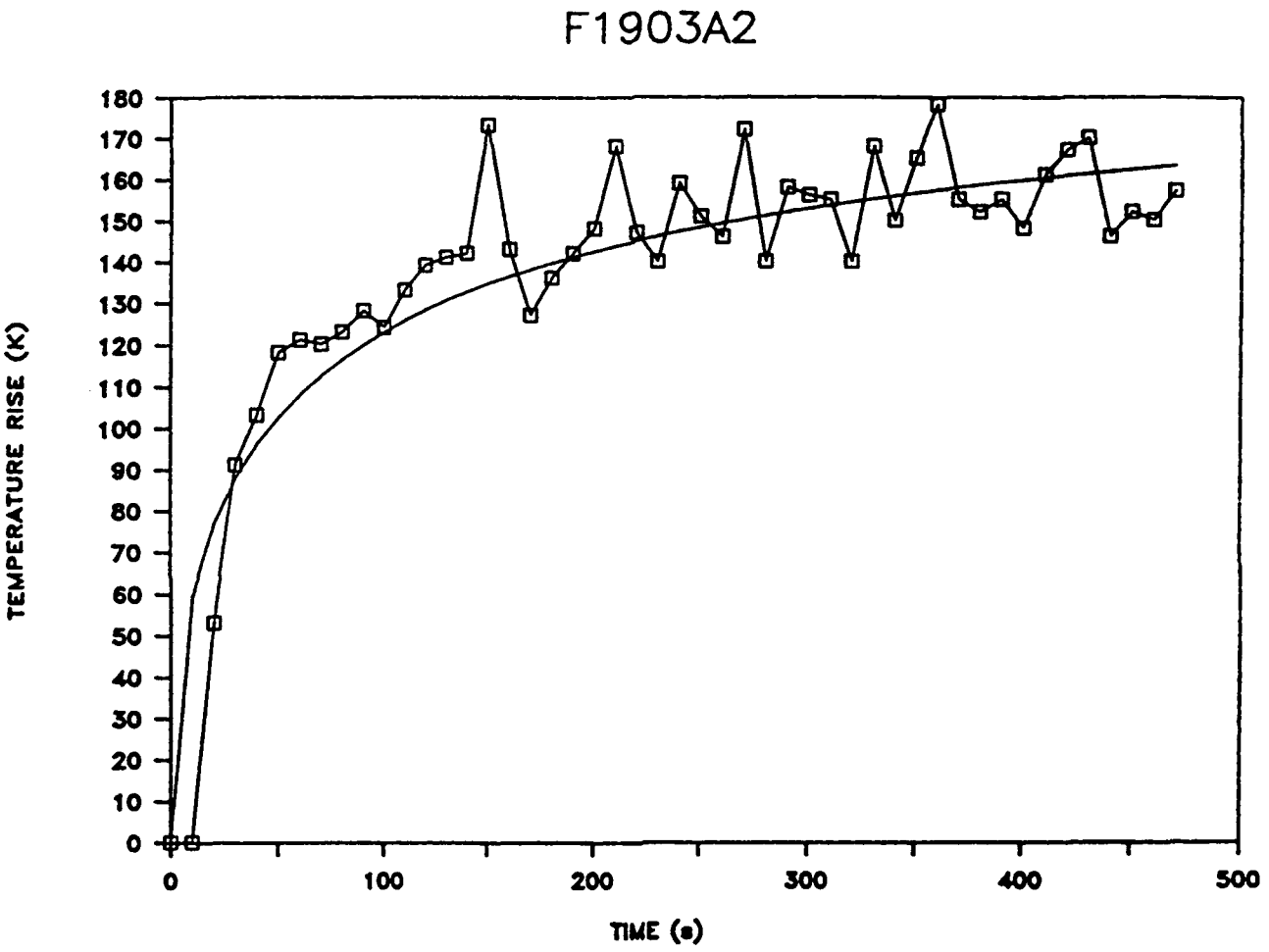

Fig. 26 ERFC-like Curve Fits to Gas Temperature Data. A2

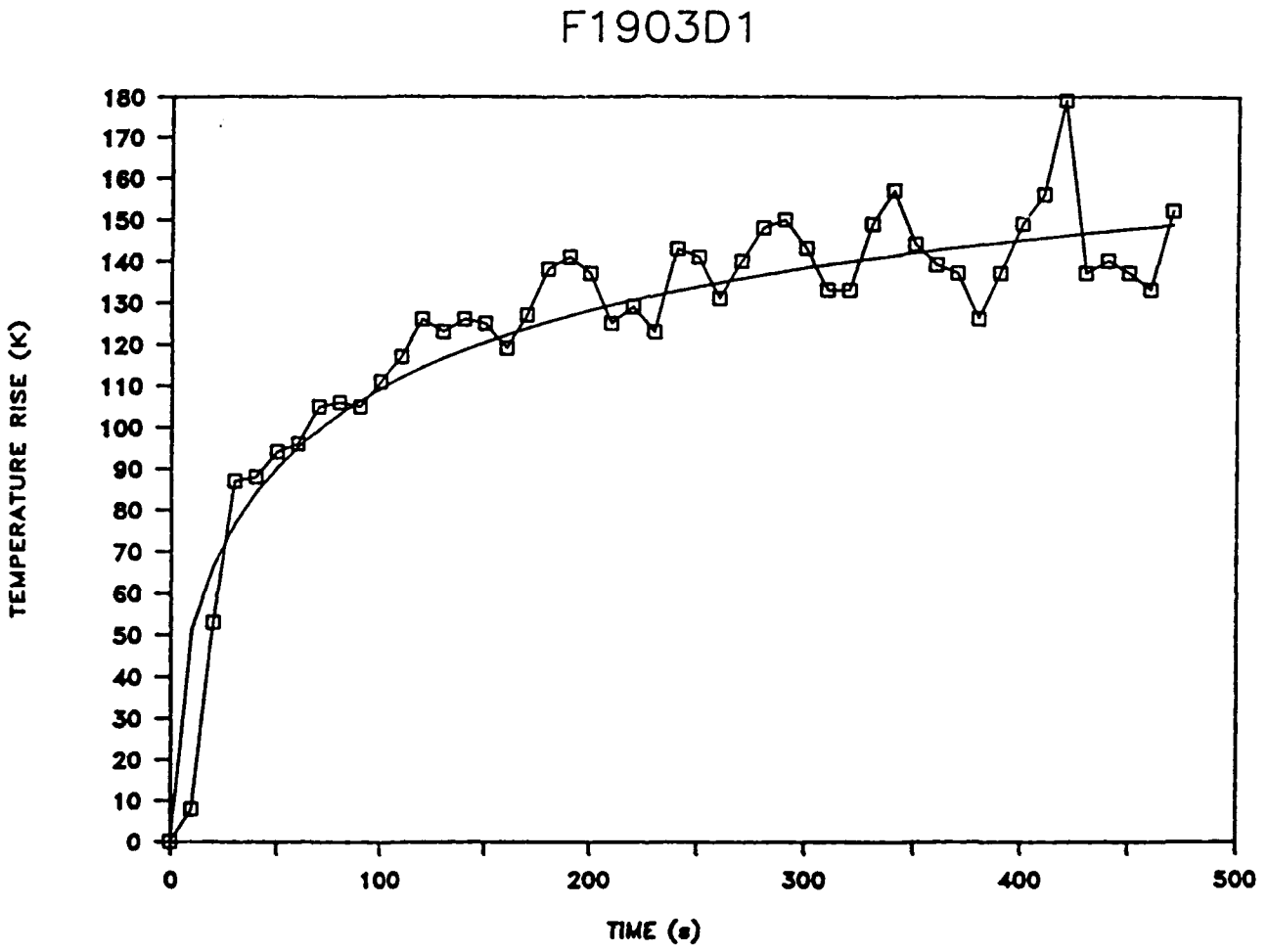

Fig. 27 ERFC-like Curve Fits to Gas Temperature Data. D1

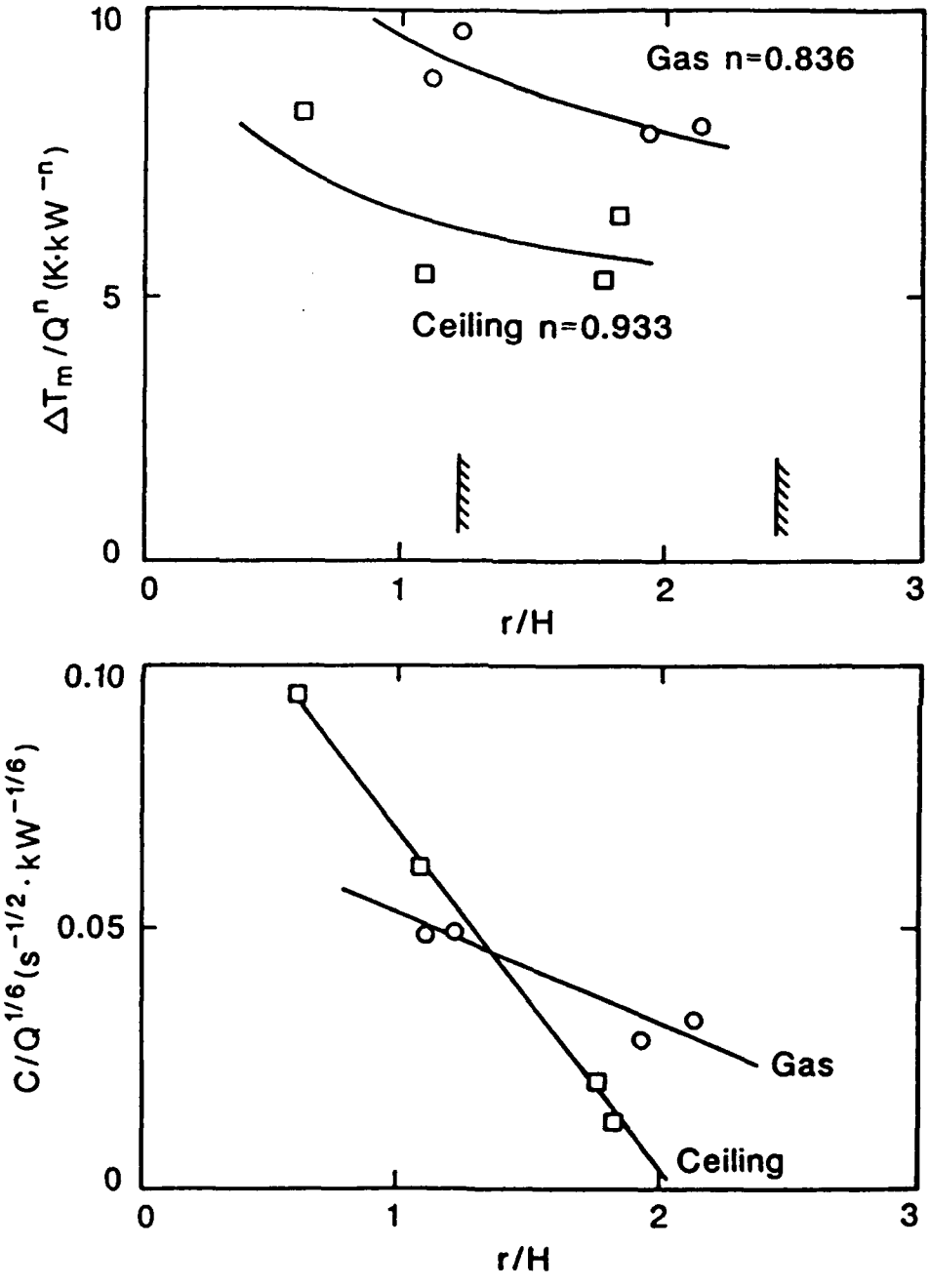

Fig. 28 Ceiling and Gas Thermal Characteristics and Heat Transfer Coefficient vs. position.

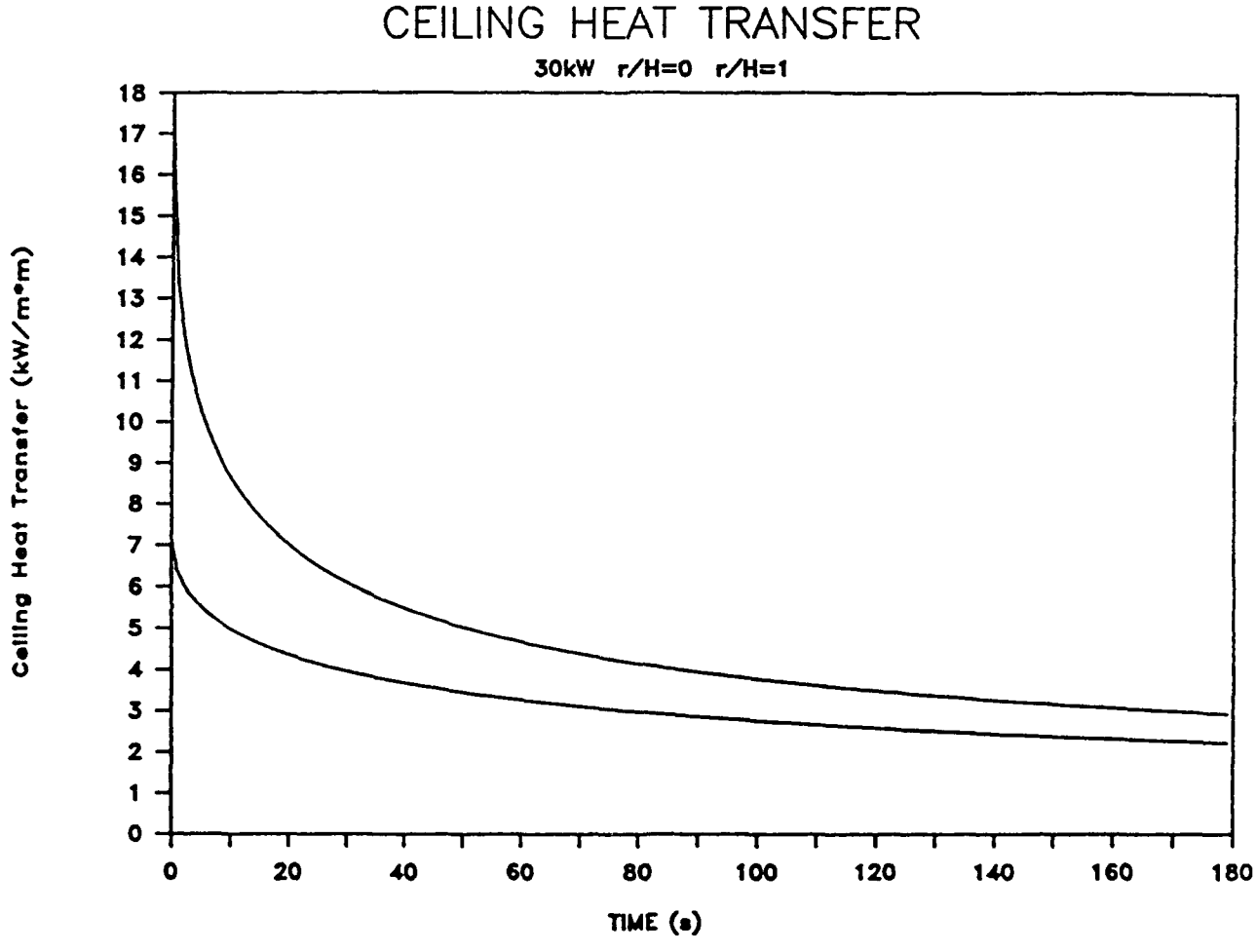

Fig. 29 Calculated Ceiling Heat Transfer Decay for 30 kW Fire at r/H = 0, 1

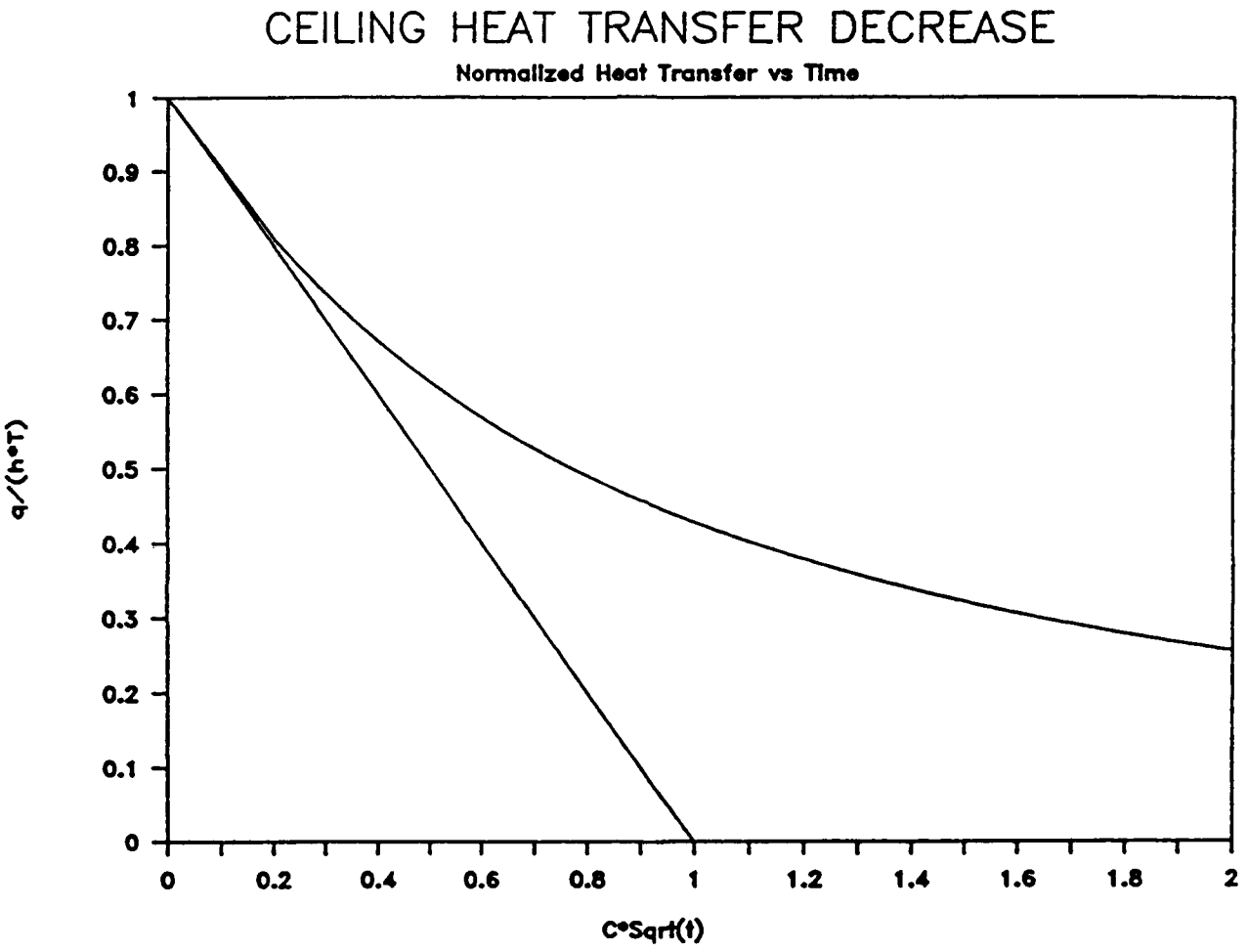

Fig. 30 Normalized Solution and Small Time Approximation.

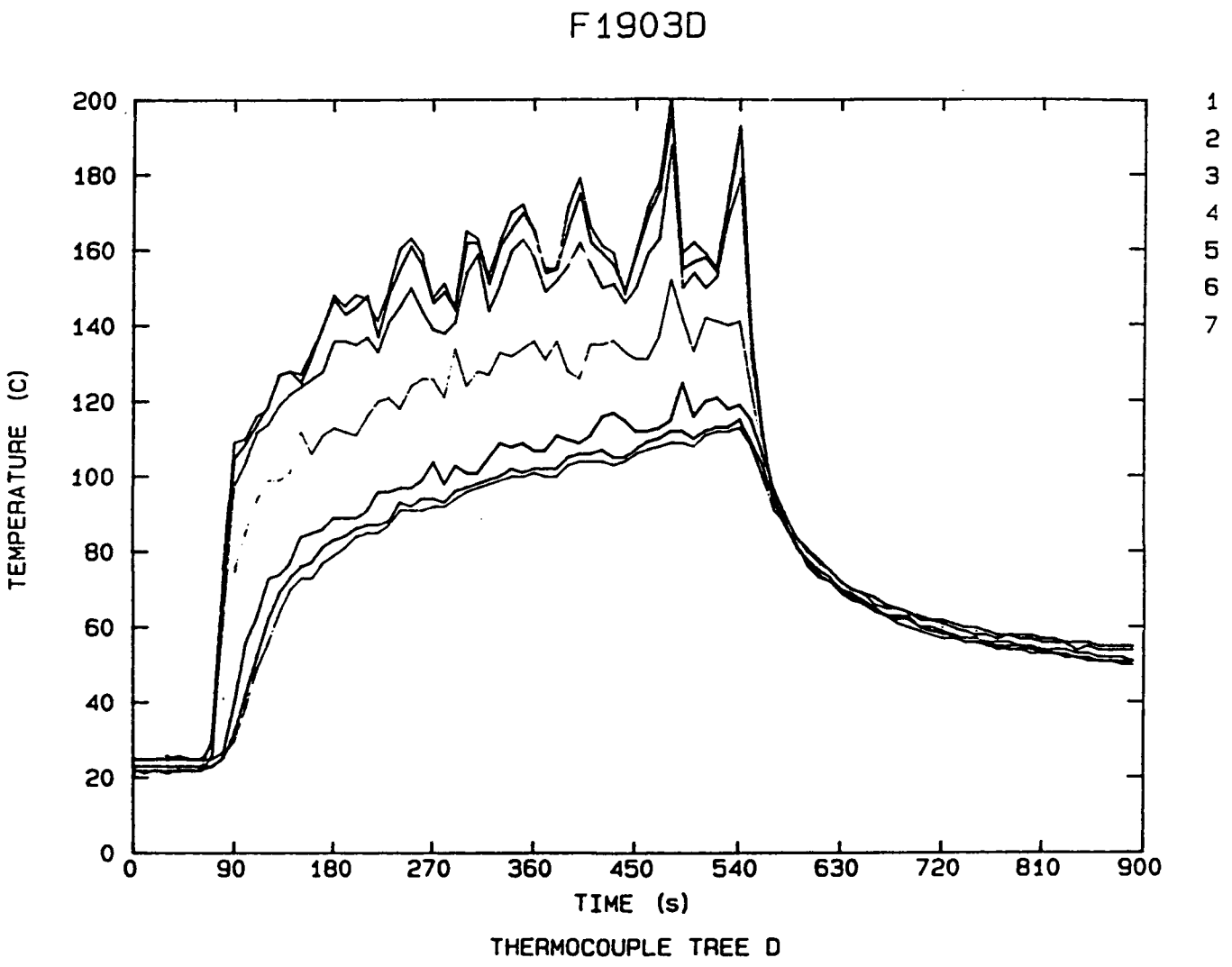

Fig. 31 Gas Temperature-Time Trace, TC Tree D, 40 kW Fire

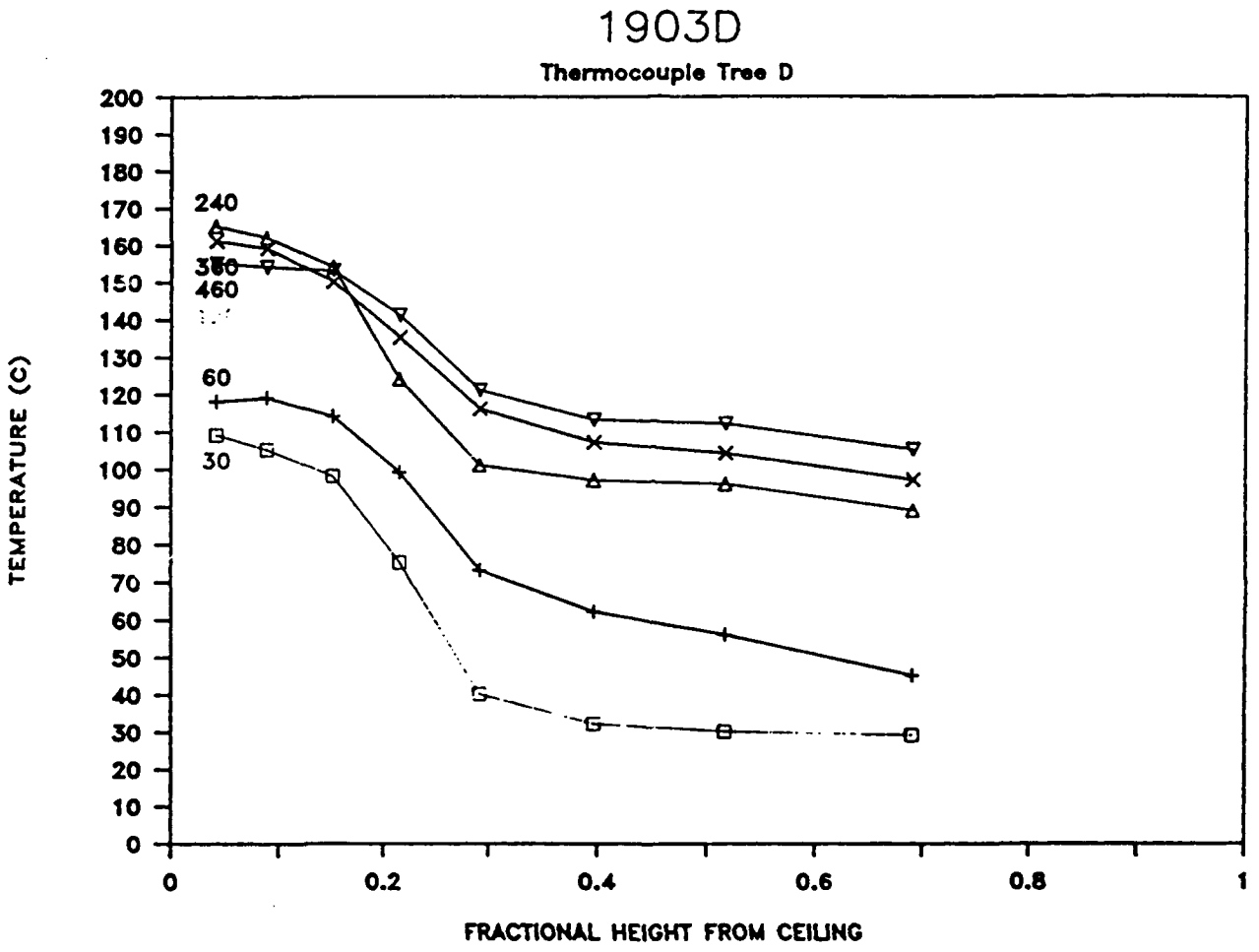

Fig. 32 Vertical Temperature Profiles (selected times)

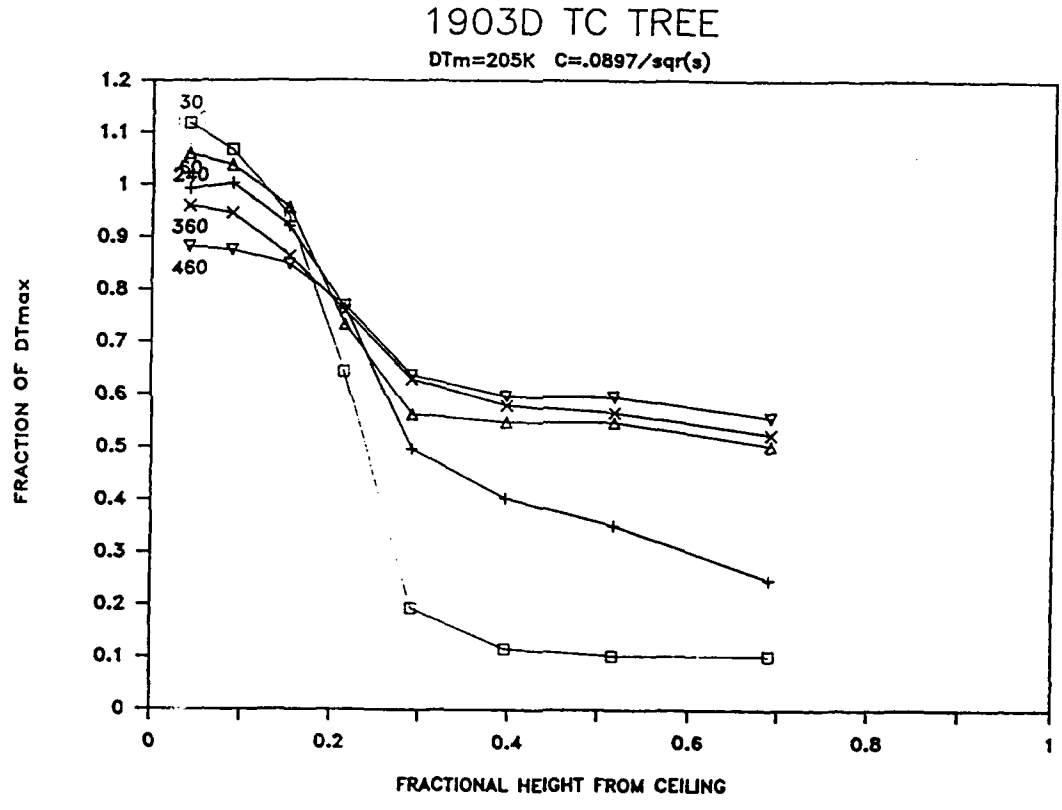

Fig. 33 Normalized Temperature Profile

APPENDIX

APPENDIX

Table: Instrumentation

Channel No.	Description		Location
0	TC	North Wall, Interior	0.3 m above floor, 0.3 m east of cabin centerline
1	TC	Tree A	.0413 m from ceiling
2	TC	(centerline, 1.22 m from east wall)	.0889 m from ceiling
3	TC	(centerline, 1.22 m from east wall)	.152 m from ceiling
4	TC	(centerline, 1.22 m from east wall)	.216 m from ceiling
5	TC	(centerline, 1.22 m from east wall)	.292 m from ceiling
6	TC	(centerline, 1.22 m from east wall)	.397 m from ceiling
7	TC	(centerline, 1.22 m from east wall)	.518 m from ceiling
8	TC	Ventilation Exhaust	West End
9	TC	Tree B	.0413 m from ceiling
10	TC	(.61 m from east and south walls)	.0889 m from ceiling
11	TC	(.61 m from east and south walls)	.152 m from ceiling
12	TC	(.61 m from east and south walls)	.216 m from ceiling
13	TC	(.61 m from east and south walls)	.292 m from ceiling
14	TC	(.61 m from east and south walls)	.397 m from ceiling
15	TC	(.61 m from east and south walls)	.518 m from ceiling
16	TC	Ventilation Exhaust	East End
17	TC	Tree D	.0413 m from ceiling
18	TC	(1.83 m from east, .30 m from south walls)	.0889 m from ceiling
19	TC	(1.83 m from east, .30 m from south walls)	.152 m from ceiling
20	TC	(1.83 m from east, .30 m from south walls)	.216 m from ceiling
21	TC	(1.83 m from east, .30 m from south walls)	.292 m from ceiling
22	TC	(1.83 m from east, .30 m from south walls)	.397 m from ceiling
23	TC	(1.83 m from east, .30 m from south walls)	.518 m from ceiling
24	TC	(1.83 m from east, .30 m from south walls)	.690 m from ceiling
25	TC	Tree C	.0413 m from ceiling
26	TC	(centerline, 0.3 m from east wall)	.0889 m from ceiling
27	TC	(centerline, 0.3 m from east wall)	.152 m from ceiling
28	TC	(centerline, 0.3 m from east wall)	.216 m from ceiling
29	TC	(centerline, 0.3 m from east wall)	.292 m from ceiling
30	TC	(centerline, 0.3 m from east wall)	.397 m from ceiling

Channel No.	Description		Location
31	TC	(centerline, 0.3 m from east wall)	.518 m from ceiling
32	TC	(centerline, 0.3 m from east wall)	.690 m from ceiling
33	TC	Ceiling "T1" Centerline	0.61 m from east wall
34	TC	Ceiling "T2" 0.30 m from north	0.91 from east wall
35	TC	Ceiling "T3" Centerline	1.83 m from east wall
36	TC	Ceiling "T4" 0.30 m from north	1.83 m from east wall
37	TC	East Wall, Interior 0.61 m above floor	0.3 m north of centerline
38	TC	North Wall, Interior 0.30 m below ceiling	0.3 m east of cabin centerline
39	TC	North Wall, Interior 0.76 m above floor	0.76 m from east wall
40	HF	North Wall, Exterior 0.17 m below ceiling	2.15 m from east wall
41	TC_{HF}	North Wall, Exterior 0.17 m below ceiling	2.15 m from east wall
42	HF	North Wall, Exterior 0.22 m above floor	2.16 m from east wall
43	TC_{HF}	North Wall, Exterior 0.22 m above floor	2.16 m from east wall
44	HF	North Wall, Exterior 0.22 m above floor	0.30 m from east wall
45	TC_{HF}	North Wall, Exterior 0.22 m above floor	0.30 m from east wall
46	HF	North Wall, Exterior 0.21 m below ceiling	0.32 m from east wall
47	TC_{HF}	North Wall, Exterior 0.21 m below ceiling	0.32 m from east wall
48	V	Inlet flow velocity, east half	
49	V	Inlet flow velocity, west half	
50	Δp	Cabin Static Pressure Differential	
51	O_2	Cabin O_2 Concentration	various locations
52	CO	Cabin CO Concentration	various locations
53	CO_2	Cabin CO_2 Concentration	various locations
54	O_2	Exhaust gas O_2 Concentration	
55			
56			
57			
58			
59			

TC - thermocouple chromel-alumel 0.25 mm D wire (on trees - TC's faced away from fire)

HF - foil type heat flow sensors (RdF Corporation 20480-3)

TC_{HF} - copper constantan thermocouples (integral part of heat flow sensor)

V - linearized, temp. compensated hot film anemometer (Omega FMA 603V) cross section was traversed at various fan settings in order to convert single, centerline velocity value into a flow rate. (Profile fitted nicely into 1/7 power. Re → 10^4 for all conditions).

The following sheets contain the reduced data for run F1202. See preceding table in Appendix for detailed descriptions of channel numbers, locations from Figure 1 and Appendix, units from axes on remaining figures.

1202A

TIME (s)	CHANNEL 1	2	3	4	5	6	7
0	27	27	27	26	26	26	26
10	27	27	27	26	26	26	26
20	27	27	27	26	27	26	26
30	27	27	27	26	26	26	26
40	27	27	27	26	26	26	26
50	27	27	27	26	26	26	26
60	27	27	27	26	26	27	26
70	27	27	27	27	27	29	27
80	59	73	43	32	31	35	28
90	71	99	70	46	40	44	32
100	82	111	79	55	48	52	39
110	94	124	78	62	55	54	45
120	93	124	87	65	58	58	50
130	93	122	90	70	61	60	54
140	99	127	89	71	64	61	58
150	102	134	93	73	66	63	59
160	109	136	91	74	67	66	61
170	103	127	109	86	70	68	63
180	113	145	104	80	71	69	65
190	102	124	107	85	74	71	68
200	109	148	120	88	78	76	70
210	111	130	115	97	82	76	71
220	122	154	126	92	80	78	73
230	108	142	118	93	82	81	74
240	121	141	123	101	88	78	78
250	123	149	119	97	84	81	75
260	119	140	123	101	87	81	77
270	132	158	121	98	85	82	78
280	118	139	118	98	88	85	79
290	127	157	133	103	89	82	80
300	115	134	117	95	86	84	79
310	125	155	128	101	89	83	81
320	128	156	133	99	86	83	81
330	123	141	123	99	86	82	81
340	117	144	122	98	87	85	81
350	129	158	125	102	91	84	81
360	128	144	129	109	90	86	82
370	126	154	128	108	92	86	83
380	129	155	126	105	92	87	84
390	136	163	135	102	92	87	86
400	126	144	120	99	90	88	84
410	135	159	123	102	93	88	85
420	139	168	135	103	94	88	86
430	126	142	123	102	92	88	86
440	125	149	121	104	92	90	87

TIME (s)	1	2	3	4	5	6	7
450	139	167	130	106	94	91	87
460	134	154	140	108	93	90	88
470	125	144	126	107	93	93	87
480	134	159	143	114	97	91	89
490	118	125	115	103	93	83	86
500	103	102	97	93	85	76	80
510	94	92	88	84	78	72	75
520	89	85	81	77	73	68	70
530	82	79	76	73	70	65	67
540	77	74	72	69	67	63	64
550	74	71	69	67	64	61	61
560	71	69	67	65	62	59	60
570	68	66	64	62	60	57	57
580	66	64	63	61	58	56	56
590	64	62	61	59	58	55	55
600	63	61	59	58	56	54	54
610	62	60	58	56	55	53	53
620	62	59	57	55	54	53	51
630	60	58	56	54	53	51	51
640	59	56	55	53	52	51	50
650	58	56	54	53	52	50	49
660	56	55	53	52	51	50	49
670	56	54	53	52	51	49	48
680	54	53	53	51	50	49	48
690	53	53	52	51	50	48	47
700	53	53	52	50	49	48	46
710	53	52	51	49	48	48	46
720	52	51	51	49	49	47	45
730	52	51	50	49	48	46	45
740	52	51	50	48	48	46	45
750	51	50	49	47	47	46	45
760	50	51	49	48	47	46	44
770	51	50	49	47	47	45	44
780	51	50	48	47	47	45	44
790	51	49	48	47	46	45	43
800	51	50	47	47	46	45	43
810	51	49	47	46	46	44	43
820	50	49	47	46	46	45	43
830	49	48	48	47	46	44	43
840	49	48	48	46	45	44	43
850	49	48	47	45	45	44	43
860	49	48	47	45	45	43	42
870	51	48	46	45	44	43	42
880	49	47	46	45	44	43	42
890	48	47	47	44	44	43	42

1202B

TIME (s)	CHANNEL 9	10	11	12	13	14
0	27	27	27	27	27	27
10	27	27	27	28	27	27
20	27	27	27	27	27	27
30	27	27	27	28	27	27
40	28	27	27	28	27	27
50	28	27	27	27	27	27
60	27	27	27	27	27	27
70	28	28	28	28	28	27
80	52	46	42	37	33	32
90	65	62	59	53	42	39
100	74	71	69	57	49	48
110	81	77	77	60	53	51
120	84	81	80	63	57	54
130	88	86	82	69	60	57
140	90	86	85	70	62	60
150	93	89	85	71	65	61
160	93	89	86	73	66	63
170	95	92	89	79	71	67
180	99	95	89	82	74	69
190	93	92	91	82	74	71
200	97	94	91	89	82	74
210	94	96	96	91	82	77
220	102	99	95	94	84	79
230	99	96	95	89	81	77
240	109	105	103	94	86	79
250	105	101	98	93	87	80
260	108	104	103	95	87	82
270	110	105	100	94	86	83
280	101	100	98	94	84	81
290	111	107	105	100	90	85
300	103	100	98	92	85	82
310	110	105	101	97	91	85
320	112	108	104	99	91	84
330	109	107	103	96	88	84
340	106	102	99	93	88	83
350	113	108	107	99	92	86
360	110	110	106	96	91	86
370	114	111	106	96	90	86
380	113	112	112	100	91	86
390	120	117	112	100	92	88
400	111	110	107	95	89	86
410	116	113	111	101	95	89
420	121	115	113	104	92	89
430	112	111	106	99	90	88
440	113	109	106	99	92	87

TIME (s)	9	10	11	12	13	14
450	121	114	114	104	93	88
460	121	117	115	110	95	90
470	113	110	108	101	93	88
480	119	115	112	108	104	94
490	107	104	99	95	92	86
500	91	90	88	85	83	81
510	82	81	81	78	77	77
520	78	77	76	74	74	72
530	73	73	72	71	70	67
540	70	69	69	67	66	64
550	68	67	66	64	63	62
560	65	64	63	62	62	60
570	62	62	61	61	60	58
580	61	60	60	59	58	58
590	59	59	58	57	57	56
600	58	57	57	56	56	54
610	58	56	56	55	54	53
620	57	55	55	54	53	53
630	55	54	54	53	53	52
640	54	54	53	53	52	51
650	54	53	52	52	51	50
660	53	52	51	51	51	50
670	53	51	51	51	50	49
680	53	51	50	50	49	49
690	52	51	50	50	49	48
700	52	50	50	50	49	48
710	51	50	49	49	48	48
720	50	49	49	49	48	47
730	50	49	49	49	48	47
740	50	49	49	49	47	47
750	50	49	49	48	47	46
760	49	48	48	48	47	46
770	49	48	48	48	46	46
780	48	48	48	48	46	45
790	48	47	47	47	46	45
800	47	47	47	47	46	45
810	47	47	47	47	46	45
820	47	47	46	46	46	45
830	48	46	46	46	46	45
840	47	46	46	46	45	45
850	48	46	46	46	45	44
860	46	46	46	46	45	44
870	46	45	46	46	45	44
880	46	45	45	46	45	44
890	46	45	45	45	45	43

1202D

TIME (s)	CHANNEL 17	18	19	20	21	22	23
0	28	28	28	28	28	28	27
10	28	28	28	28	28	28	27
20	28	28	28	28	28	28	27
30	28	28	28	28	28	28	27
40	28	28	28	28	28	28	27
50	28	27	28	28	28	28	27
60	28	27	28	28	28	27	28
70	46	38	34	30	29	28	28
80	83	80	64	41	31	30	30
90	98	96	79	53	41	37	33
100	111	108	81	59	48	44	40
110	121	116	90	64	53	51	46
120	126	122	88	66	58	56	52
130	130	121	90	69	61	60	55
140	135	128	93	72	64	62	58
150	136	130	97	76	67	65	61
160	132	129	98	75	69	67	64
170	134	130	104	83	72	69	66
180	141	137	118	87	74	71	68
190	130	127	113	88	76	72	69
200	135	132	112	92	80	74	71
210	132	132	117	94	81	75	73
220	146	138	115	93	83	77	74
230	137	130	117	96	84	79	76
240	138	135	118	99	88	82	77
250	143	141	125	101	87	82	78
260	142	140	121	105	89	82	79
270	147	143	126	105	87	82	79
280	139	135	124	99	88	84	81
290	152	151	139	104	90	85	81
300	145	136	117	97	88	85	82
310	142	137	117	98	89	87	83
320	153	148	130	99	89	86	83
330	155	151	131	103	89	88	83
340	140	135	123	102	92	87	83
350	152	149	134	106	93	88	84
360	161	156	130	109	92	88	84
370	147	142	127	112	92	89	86
380	155	149	126	102	93	89	85
390	166	160	130	107	93	89	86
400	154	146	113	101	94	89	85
410	152	148	129	105	93	90	87
420	164	157	137	114	95	90	87
430	157	146	119	106	95	90	87
440	154	143	123	103	94	90	87

TIME (s)	17	18	19	20	21	22	23
450	160	154	129	103	95	91	88
460	158	150	125	113	97	92	90
470	154	149	120	105	96	92	89
480	158	154	137	110	99	93	90
490	120	118	109	99	94	89	86
500	103	101	95	91	88	84	81
510	93	91	87	82	80	75	74
520	86	84	81	77	76	72	71
530	80	78	75	73	71	68	67
540	76	74	72	70	68	66	65
550	73	71	69	67	65	63	62
560	71	68	66	64	63	61	60
570	68	66	64	62	61	59	58
580	65	64	62	60	60	58	57
590	63	62	60	59	58	57	56
600	61	61	59	58	57	55	55
610	61	60	59	56	56	54	54
620	60	59	57	55	55	54	53
630	59	58	56	55	54	53	52
640	58	56	55	54	53	52	52
650	57	56	55	53	52	52	51
660	56	55	54	52	52	51	50
670	56	54	53	52	51	50	50
680	56	54	53	51	51	50	50
690	55	53	52	51	50	49	49
700	53	52	51	50	50	49	48
710	53	52	51	50	49	48	48
720	53	51	51	49	49	48	48
730	53	50	51	49	49	48	48
740	52	50	50	49	48	48	47
750	51	50	49	49	48	47	47
760	52	50	49	48	48	47	47
770	52	49	49	48	47	47	47
780	51	49	49	48	47	47	46
790	51	48	49	48	47	47	46
800	50	48	48	47	47	46	46
810	50	48	48	47	47	46	46
820	50	48	48	47	47	46	46
830	49	48	47	47	46	45	45
840	49	47	47	46	46	45	45
850	49	47	48	46	46	45	45
860	50	47	47	46	46	45	45
870	49	47	47	46	46	45	44
880	49	46	47	46	46	45	44
890	49	46	46	46	45	45	44

1202C

	TIME	CHANNEL					
24	(s)	25	26	27	28	29	30
27	0	27	27	27	27	27	27
27	10	27	27	27	27	27	27
27	20	27	27	27	27	27	27
27	30	27	27	27	27	27	27
27	40	27	27	27	27	27	27
27	50	27	27	27	27	27	27
27	60	27	27	27	27	27	27
28	70	28	28	28	27	27	27
31	80	52	51	49	42	37	33
33	90	69	66	62	52	43	38
36	100	78	76	71	59	49	43
40	110	84	82	82	65	53	47
44	120	87	86	82	66	57	52
49	130	89	89	88	73	59	55
52	140	90	93	90	72	60	57
54	150	95	95	93	73	62	60
57	160	97	96	95	74	65	62
59	170	94	96	94	79	68	64
61	180	98	98	98	89	74	66
63	190	95	96	97	85	73	68
65	200	104	104	106	93	78	70
67	210	97	99	99	91	79	72
69	220	103	106	105	98	84	75
70	230	109	107	104	97	84	76
70	240	102	104	103	97	84	77
72	250	110	111	111	101	91	77
73	260	105	108	106	97	85	78
73	270	112	113	112	100	86	79
74	280	115	110	108	100	87	80
76	290	110	112	111	101	89	82
76	300	104	106	104	96	85	80
76	310	112	112	111	101	88	83
77	320	115	113	113	100	87	83
78	330	107	113	110	98	87	83
78	340	116	115	111	103	90	84
79	350	117	118	114	103	89	84
80	360	110	113	111	102	90	83
80	370	116	115	113	106	92	85
80	380	121	119	116	104	91	86
81	390	115	118	116	105	91	85
81	400	112	113	112	100	89	85
81	410	119	118	115	105	95	86
82	420	121	124	121	105	93	86
82	430	111	115	112	102	91	86
83	440	123	118	117	108	93	86

24	TIME (s)	25	26	27	28	29	30
83	450	123	121	117	105	94	87
84	460	117	120	118	108	93	87
85	470	112	114	112	105	96	87
84	480	121	121	122	113	98	90
80	490	104	104	102	96	89	85
77	500	91	91	90	87	83	80
72	510	83	83	83	81	78	76
69	520	78	78	77	76	74	71
65	530	75	74	73	72	70	68
63	540	71	70	69	69	67	65
61	550	68	67	66	66	65	62
59	560	66	65	64	64	62	60
58	570	64	64	63	62	61	59
57	580	63	63	62	61	59	57
56	590	61	60	60	59	57	55
55	600	60	59	58	58	56	54
54	610	58	58	57	57	55	53
53	620	58	57	56	56	54	53
53	630	57	56	55	55	54	52
52	640	56	55	54	54	53	51
51	650	54	54	53	53	52	51
51	660	53	53	52	53	51	50
50	670	52	52	52	52	50	49
50	680	53	52	51	51	50	49
49	690	52	51	51	51	50	48
49	700	52	51	51	50	49	48
48	710	51	50	50	50	48	48
48	720	51	50	49	49	48	47
48	730	50	49	49	49	48	47
47	740	49	49	48	48	47	47
47	750	49	48	48	48	47	46
47	760	49	48	48	48	47	46
47	770	49	48	48	48	47	46
47	780	49	48	47	47	46	45
46	790	48	47	47	47	46	45
46	800	48	47	47	46	46	45
46	810	48	47	47	46	45	45
46	820	47	47	46	47	46	45
45	830	48	46	46	46	45	45
45	840	47	46	46	46	45	44
45	850	47	46	46	46	45	44
45	860	47	46	46	46	44	44
45	870	47	46	46	46	44	44
44	880	46	46	45	45	44	43
45	890	46	45	45	45	44	43

1202T

31	32	TIME (s)	CHANNEL 33	34	35	36
27	26	0	27	28	29	29
26	26	10	27	28	29	29
26	26	20	27	28	29	29
27	26	30	27	28	29	29
26	26	40	27	28	29	29
27	26	50	27	28	29	29
27	26	60	27	28	29	29
28	27	70	30	34	112	58
30	28	80	38	49	132	83
33	30	90	45	62	161	93
40	34	100	50	66	166	103
44	39	110	56	71	164	108
49	45	120	57	77	169	116
51	48	130	58	78	172	121
55	51	140	60	79	187	120
58	54	150	62	80	184	120
61	56	160	63	83	183	123
62	58	170	61	80	160	114
63	61	180	65	85	157	109
65	61	190	63	80	155	134
67	65	200	69	88	175	121
69	65	210	65	82	182	127
70	68	220	68	86	150	111
72	68	230	68	87	205	135
73	71	240	66	83	169	113
72	71	250	72	91	202	120
75	73	260	69	87	192	124
75	73	270	73	87	155	115
76	72	280	74	95	204	143
77	74	290	73	90	158	120
75	73	300	72	91	170	148
78	75	310	74	95	189	143
78	75	320	75	95	201	125
78	75	330	73	88	154	116
79	76	340	74	99	217	145
79	77	350	77	99	182	126
79	77	360	75	89	172	119
80	76	370	77	97	214	142
81	78	380	78	99	225	146
81	79	390	78	94	177	132
81	77	400	77	96	176	138
83	79	410	78	101	247	148
82	80	420	81	100	188	127
81	79	430	77	93	171	130
83	80	440	81	102	217	150

31	32	TIME (s)	33	34	35	36
83	81	450	82	104	215	152
83	80	460	80	98	173	132
84	80	470	81	98	179	145
87	82	480	83	101	162	130
81	79	490	74	86	130	104
76	75	500	68	77	111	92
73	71	510	65	72	108	86
69	67	520	62	69	103	81
64	63	530	60	66	100	78
62	60	540	59	64	98	76
61	57	550	57	63	95	74
58	56	560	56	61	93	72
57	54	570	55	60	91	71
55	53	580	54	59	89	69
54	51	590	54	58	88	68
53	50	600	53	58	87	68
51	50	610	52	57	82	67
51	49	620	52	57	83	66
51	49	630	51	56	82	65
50	48	640	51	56	82	64
49	48	650	50	55	81	64
49	47	660	50	55	80	63
48	47	670	50	54	79	63
48	46	680	50	54	78	62
47	46	690	49	54	75	62
47	45	700	49	54	75	62
46	45	710	49	53	74	61
45	44	720	49	53	74	61
45	44	730	48	53	73	61
45	44	740	48	52	72	60
45	44	750	48	32	72	60
45	44	760	48	52	71	59
44	43	770	47	52	71	59
44	43	780	47	52	68	59
44	43	790	47	51	69	59
44	43	800	47	51	70	59
44	42	810	47	51	68	58
43	42	820	47	51	66	58
44	42	830	46	51	67	58
43	42	840	46	50	64	57
43	42	850	46	50	65	56
43	42	860	46	50	66	56
42	42	870	46	50	65	56
42	41	880	46	50	63	56
42	41	890	46	50	65	55

1202W

1202H

TIME (s)	37	38	39	0	TIME (s)	40
0	23	24	25	25	0	3.070
10	23	24	25	25	10	2.218
20	23	24	25	25	20	1.706
30	23	24	25	25	30	1.535
40	23	24	25	24	40	3.241
50	23	24	24	25	50	2.900
60	23	24	24	25	60	2.729
70	23	24	25	25	70	4.776
80	25	25	27	26	80	8.700
90	26	25	28	27	90	9.552
100	27	27	30	28	100	12.111
110	29	28	32	30	110	13.305
120	30	29	34	31	120	20.299
130	32	30	36	33	130	25.246
140	33	32	38	34	140	20.469
150	34	33	39	35	150	24.734
160	36	34	41	37	160	26.440
170	37	36	43	38	170	26.610
180	38	37	44	39	180	31.045
190	39	38	47	40	190	43.668
200	41	39	49	41	200	34.286
210	42	41	51	42	210	51.174
220	43	42	52	43	220	41.792
230	44	43	54	44	230	56.803
240	45	44	55	45	240	39.915
250	46	45	57	46	250	49.638
260	47	46	58	47	260	54.756
270	48	47	59	47	270	44.180
280	49	48	61	48	280	55.609
290	50	49	62	49	290	54.244
300	51	50	63	49	300	60.044
310	51	50	63	50	310	71.984
320	52	51	64	51	320	82.901
330	53	52	65	51	330	65.332
340	53	52	66	52	340	62.091
350	54	53	66	52	350	61.408
360	55	54	67	52	360	60.385
370	55	54	68	53	370	67.549
380	56	55	68	53	380	76.249
390	56	55	68	54	390	73.861
400	57	56	69	54	400	75.055
410	57	56	69	54	410	80.343
420	58	57	70	55	420	68.231
430	58	57	70	55	430	82.731
440	59	57	71	55	440	110.1938

TIME (s)	37	38	39	0	TIME (s)	40
450	59	58	71	56	450	82.901
460	60	58	71	56	460	91.260
470	60	58	72	56	470	79.490
480	61	59	72	57	480	84.095
490	60	58	71	56	490	73.178
500	60	58	69	55	500	65.332
510	59	57	68	54	510	65.161
520	58	56	66	53	520	59.873
530	57	56	65	52	530	65.332
540	56	55	63	51	540	55.097
550	55	54	62	50	550	53.391
560	54	53	60	49	560	53.391
570	54	52	59	48	570	54.415
580	53	51	58	48	580	55.097
590	52	50	56	47	590	38.551
600	51	49	55	46	600	43.839
610	50	49	54	45	610	41.109
620	50	48	53	45	620	40.257
630	49	47	52	44	630	44.009
640	48	46	51	43	640	38.551
650	48	46	50	43	650	32.581
660	47	45	49	42	660	34.286
670	46	45	49	42	670	33.092
680	46	44	48	41	680	29.169
690	45	43	47	41	690	32.922
700	45	43	46	40	700	24.904
710	44	42	46	40	710	25.928
720	44	42	45	39	720	32.581
730	43	41	44	39	730	30.192
740	43	41	44	39	740	22.005
750	42	41	43	38	750	20.811
760	42	40	43	38	760	19.617
770	42	40	42	38	770	21.493
780	41	39	42	38	780	18.593
790	41	39	41	37	790	20.128
800	40	39	41	37	800	23.369
810	40	38	41	37	810	26.781
820	40	38	40	36	820	20.128
830	39	38	40	36	830	17.228
840	39	37	40	36	840	15.011
850	39	37	39	36	850	15.011
860	38	37	39	36	860	23.540
870	38	37	39	36	870	15.352
880	38	36	38	35	880	13.135
890	38	36	38	35	890	22.858

1202J

41	42	43	TIME (s)	44	45
2	1.896	0	0	1.046	0
2	1.896	0	10	1.046	0
2	3.102	0	20	1.394	0
2	2.930	0	30	1.220	0
2	2.585	0	40	1.917	0
2	2.585	0	50	1.743	0
2	2.413	0	60	2.440	0
2	2.930	0	70	1.220	0
4	3.619	0	80	1.743	0
6	3.964	1	90	1.917	0
8	5.170	1	100	2.265	0
10	6.032	2	110	2.788	0
12	6.377	3	120	3.311	0
15	6.549	4	130	3.834	1
17	7.239	5	140	4.356	1
20	10.341	6	150	3.659	2
22	9.479	7	160	5.228	3
25	10.858	8	170	6.099	3
27	11.892	9	180	5.925	4
30	10.858	10	190	7.144	5
32	15.167	11	200	6.273	5
34	14.133	12	210	7.144	6
36	13.960	13	220	5.750	7
38	19.476	14	230	10.107	8
40	17.924	15	240	7.841	9
42	16.373	16	250	9.235	10
43	16.890	17	260	14.115	10
45	19.476	18	270	12.546	11
46	22.233	18	280	15.160	12
48	17.924	19	290	13.418	13
49	20.510	20	300	14.463	13
51	24.646	21	310	19.342	14
52	24.818	22	320	18.471	15
54	23.267	23	330	15.334	15
55	23.784	24	340	15.334	16
56	28.955	24	350	14.637	17
57	24.474	25	360	22.130	17
58	28.782	26	370	25.093	18
59	29.127	26	380	20.388	18
60	25.163	27	390	20.039	19
61	28.265	28	400	17.425	20
62	28.265	28	410	15.857	20
63	27.748	29	420	20.388	21
64	28.782	30	430	24.918	21
64	31.368	30	440	30.494	21

41	42	43	TIME (s)	44	45
66	32.574	31	450	30.146	22
66	30.161	31	460	26.487	22
67	29.299	32	470	21.782	23
67	33.781	32	480	21.956	23
67	33.091	32	490	21.782	24
65	28.782	33	500	23.350	24
64	33.264	32	510	30.843	24
62	30.506	32	520	27.881	24
60	38.951	32	530	25.441	24
59	27.748	32	540	26.312	23
57	27.231	31	550	18.994	23
55	24.474	31	560	19.168	23
53	23.612	30	570	20.039	23
51	26.370	30	580	21.956	22
49	26.887	29	590	21.782	22
48	22.923	29	600	20.213	21
46	27.576	28	610	21.956	21
44	21.716	28	620	23.350	21
42	23.957	27	630	23.524	20
41	22.405	26	640	22.653	20
39	34.642	26	650	19.691	19
38	19.820	25	660	16.554	19
37	22.578	25	670	19.516	19
35	24.474	24	680	14.986	18
34	23.440	24	690	12.546	18
33	20.165	23	700	15.857	17
32	19.648	23	710	17.425	17
31	23.612	22	720	17.251	17
30	20.682	22	730	18.257	16
29	21.027	21	740	19.865	16
28	16.029	21	750	15.334	16
27	16.546	20	760	16.554	15
26	23.440	20	770	16.206	15
25	17.235	19	780	16.380	15
25	17.063	19	790	12.372	14
24	18.958	18	800	14.812	14
23	15.684	18	810	14.115	14
23	15.856	18	820	16.728	13
22	13.788	17	830	10.630	13
21	15.511	17	840	12.546	13
21	14.305	17	850	14.812	12
20	13.788	16	860	9.235	12
20	14.650	16	870	12.721	12
19	12.237	16	880	11.849	12
19	14.133	15	890	11.501	12

1202K

46	47	TIME (s)	48	49	50
2.737	1	0	0.502	0.510	0.240
3.592	1	10	0.527	0.528	0.244
1.710	1	20	0.536	0.510	0.241
2.395	1	30	0.556	0.487	0.244
2.566	1	40	0.504	0.532	0.251
2.052	1	50	0.510	0.480	0.246
2.052	1	60	0.512	0.517	0.279
3.250	1	70	0.532	0.501	0.536
3.079	2	80	0.468	0.518	0.451
3.250	2	90	0.447	0.512	0.419
4.789	2	100	0.516	0.496	0.390
4.447	3	110	0.508	0.530	0.395
4.276	3	120	0.497	0.483	0.360
4.789	4	130	0.479	0.485	0.334
5.815	5	140	0.481	0.505	0.328
9.407	5	150	0.501	0.486	0.331
6.157	6	160	0.527	0.507	0.322
6.157	7	170	0.500	0.499	0.363
7.697	8	180	0.479	0.508	0.337
8.723	8	190	0.550	0.482	0.290
8.723	9	200	0.479	0.468	0.306
9.065	10	210	0.533	0.489	0.339
11.973	10	220	0.517	0.553	0.293
13.683	11	230	0.518	0.467	0.293
9.407	12	240	0.504	0.504	0.309
9.749	12	250	0.486	0.521	0.282
11.802	13	260	0.482	0.510	0.297
14.025	13	270	0.489	0.514	0.273
10.262	14	280	0.508	0.428	0.289
10.947	14	290	0.508	0.486	0.250
13.170	15	300	0.543	0.461	0.240
12.315	16	310	0.486	0.507	0.299
15.223	16	320	0.530	0.468	0.296
16.078	17	330	0.511	0.458	0.299
14.196	17	340	0.521	0.473	0.297
12.657	18	350	0.519	0.486	0.279
16.249	18	360	0.515	0.515	0.293
22.577	19	370	0.500	0.508	0.275
14.025	19	380	0.535	0.460	0.268
16.249	19	390	0.516	0.496	0.273
18.472	20	400	0.519	0.514	0.247
14.367	20	410	0.536	0.491	0.307
20.012	21	420	0.538	0.476	0.289
19.670	21	430	0.532	0.464	0.266
20.012	21	440	0.531	0.493	0.293

46	47	TIME (s)	48	49	50
19.670	22	450	0.532	0.502	0.278
20.867	22	460	0.518	0.497	0.262
21.038	22	470	0.515	0.505	0.292
20.867	23	480	0.520	0.513	0.058
20.525	23	490	0.522	0.512	0.112
22.920	23	500	0.527	0.504	0.140
26.169	23	510	0.499	0.511	0.159
19.328	23	520	0.526	0.501	0.177
22.064	22	530	0.500	0.514	0.191
22.406	22	540	0.508	0.511	0.201
23.433	22	550	0.540	0.513	0.212
16.762	21	560	0.473	0.542	0.219
16.762	21	570	0.513	0.492	0.220
18.301	21	580	0.530	0.514	0.226
18.643	20	590	0.534	0.518	0.232
20.012	20	600	0.523	0.493	0.234
20.183	19	610	0.501	0.508	0.239
14.881	19	620	0.510	0.532	0.242
14.710	18	630	0.514	0.494	0.244
12.657	18	640	0.510	0.475	0.245
17.617	18	650	0.505	0.504	0.245
12.999	17	660	0.521	0.483	0.248
16.762	17	670	0.516	0.476	0.249
12.315	17	680	0.534	0.480	0.251
14.710	16	690	0.560	0.483	0.255
17.959	16	700	0.515	0.477	0.251
21.209	16	710	0.507	0.524	0.254
12.315	15	720	0.510	0.476	0.253
15.907	15	730	0.537	0.488	0.254
14.710	15	740	0.489	0.537	0.253
13.512	14	750	0.471	0.461	0.256
17.446	14	760	0.499	0.545	0.256
11.631	14	770	0.487	0.511	0.253
12.144	14	780	0.523	0.513	0.255
9.749	13	790	0.534	0.461	0.252
11.460	13	800	0.479	0.503	0.256
13.170	13	810	0.531	0.509	0.257
10.434	13	820	0.544	0.517	0.257
9.065	13	830	0.534	0.531	0.259
12.486	12	840	0.525	0.482	0.257
11.631	12	850	0.517	0.501	0.257
10.776	12	860	0.490	0.511	0.258
13.854	12	870	0.524	0.532	0.259
11.631	12	880	0.551	0.494	0.259
9.749	11	890	0.561	0.514	0.261

Chapter 3. Effect of Venting Through Small Hatches Near The Ceiling on Counterflow-Ventilated Enclosure Fires

King-Mon Tu, William Rinkinen
Center for Fire Research
National Institute of Standards and Technology

and

Bernard McCaffrey
University of Maryland
Baltimore, MD

1.0 Introduction

The work described herein involves the extended study of the effects of forced ventilation on the fire environment in an enclosed volume. A unique aspect concerns the direction of the ventilation flow which is opposed to the buoyancy forces of the fire-generated hot gases, that is, fresh air is forced into the enclosure at the ceiling and exhausted at the floor of the otherwise sealed "box".

In Chapter 2, using the same facility without hatches at both of the two end walls, the complete baseline thermal field in the enclosure as a function of fire size and ventilation rate was measured. The conclusions indicated that variations of the ventilation rate within ranges considered had little effect on the ability of the system to remove promptly the thermal energy generated by the fire. The ventilation did little to prevent the buoyancy forces from tending to keep the enclosure quite stratified. Most of the heat released by the fire was absorbed by the ceiling above the fire.

Recently, with additional equipment, the chemical species concentrations at various positions throughout the enclosure were measured for the present ventilation configuration and range of ventilation flow rates. The spatial distribution of combustion products in the vertical direction was found to be similar to that of the stratified temperature distribution. This environment can be broadly described as strongly buoyant, weakly forced-ventilated. This chapter describes changes in the enclosure environment brought about by the installation of hatches at the two end walls of the box close to the ceiling. Results of changes in the thermal field and chemical species concentrations will be compared to the baseline results.

2.0 Experimental

The enclosure was the same as that described in Chapter 2, with dimensions of 4.8x2.4x1.2 m high composed of two 2.4x2.4x1.2 m high test chambers which were airtight clamped together. The test chambers were made of galvanized steel sheet and containing a ceiling and floor plenum constructed of calcium silicate board (marinite) which allowed for two separate pairs of air inlet configuration positions in the ceiling and a single pair for exhaust in the floor. The inlet and outlet slits run the full length of the longer dimension of the box. (See Fig. 1) For the experiments described here 32 simulated seats of aluminum and marinite were symmetrically arranged in the box. The fire, a constant feed of propane through a diffusive burner at the floor, was located in the geometric center of the enclosure and exhibited heat release rates between 10 and 60 kW. Ventilation flow rates varied between three and six minutes for one enclosure volume exchange. Approximately 60

channels of data were recorded in time during each test. Complete details of this facility are contained in Chapter 2.

3.0 Results

In order to evaluate the effects of introducing the hatches the baseline environment in the case of no hatches must first be established. Assuming complete combustion of propane, the reaction with excess dry air, x, is illustrated in the following:

$$C_3H_8 + 5(1+x)[O_2+3.76N_2] = 3CO_2 + 4H_2O + 5xO_2 + 5(1+x)3.76N_2 \quad (1)$$

The mole fraction of CO_2 in the exhaust is $[CO_2]=3/(25.8+23.8x)$ (2)

The mole fraction of O_2 in the exhaust is $[O_2] =5x/(25.8+23.8x)$ (3)

In the limit of large excess air (large x), the mole fraction of O_2 in the exhaust is 0.21 which represents initial conditions in tests. Measurements in the exhaust were obtained as oxygen depletion ($0.21-[O_2]$). From equation 3 this depleted value will be:

$$C\ 21 - [O_2] = 5.42/(25.8+23.8x) \text{ and hence, what will be called} \quad (4)$$

the "concentration" is defined as through use of equations (2) and (4) as:

$$[CO_2]/3 = (0.21-[O_2])/5.42 = 1/(25.8 + 23.8x) \quad (5)$$

A similar analysis can be used to develop an approximate relation between combustion products and propane supply. Within the notation of Equation (1), the following identity can be stated

$$\frac{Q/\Delta H \rho_f}{\dot{V}} = \frac{[C_3H_8]}{5\ (1+x)\ [O_2+3.76N_2]} \tag{6}$$

where Q is the heat release rate of the fire, ΔH is the propane heat of combustion, ρ_f is the propane supply density, and V is the volumetric supply rate of air. Combining Equations (6) and (1), and recognizing that each mole of propane stoichiometrically yields three moles of CO_2 resulted in the following

$$\frac{Q/\Delta H \rho_f}{\dot{V}} = \frac{[CO_2]/3}{3\ [CO_2] + 4\ [H_2O] + 5\ x\ [O_2] + 5\ (1+x)\ 3.76\ [N_2] - [CO_2]/3} \tag{7}$$

Using the same methodology used to get Equations (2) and (3), Equation (7) can be reduced to

$$\frac{Q/\Delta H \rho_f}{\dot{V}} = \frac{[CO_2]/3}{25.5 + 23.8x} \tag{8}$$

The right hand side of Equation (8) is almost identical to the right hand side of Equation (5) except for a small change in the first term of the denominator. Thus, in the absence of sources and sinks, after the transient, the

the average concentration for the box or the well stirred reactor result is approximately equal to the volume flow rate of propane to that of the air ventilation volume flow rate ($\dot{V}$),

$$\frac{Q/\Delta H\rho_f}{\dot{V}} = \frac{Q(kW)/(46343*1.92)(kJ/m^3)}{14.5m^3 \ / \ 60 \ / \ t(min)} = 4.7*10^{-5}*Q(kw)*t(min) \qquad (9)$$

where t is the time for one enclosure air change. Pagni, et al [1], have generalized the above analysis including the transient portions.

Figure 2 shows a scatter plot of all the baseline data for CO_2 (+) and O_2 (□) gaseous concentration as defined in Equation (5) for five positions in the enclosure with no hatches and also for an additional O_2 (Δ) sample in the exhaust gas. If the analyses and experiments were perfect, corresponding CO_2 and O_2 points would coincide. Obviously, positions near the ceiling exhibit higher gaseous concentrations, whereas data from lower points in the box have similar gaseous concentration values to those in the exhaust. The abscissa of Figure 2 is the non-dimensional generation to ventilation rates ratio described by Equation (9) and the straight line shows a calculation of what a well stirred reactor would exhibit. The baseline data in Figure 2 are steady state values and represent concentration averages of the test data from 450s to 800s. The data plot in Figure 2 also provides a consistency check since these concentration values are results from two independent instruments. Note that the small amount of CO and soot present in these experiments hardly affects the accuracy of the equality. The extent of agreement can also be observed in Figure 2 by comparing any pair of data sets. For clarity in subsequent plotting and analysis we can observe the average of the two "concentrations", Equation 5, as representative of that particular point.

Figure 3 contains all the test data as seen in Figure 2 and shows the vertical distribution of the normalized gaseous concentrations in the box. The abscissa in Fig. 3 is termed "Normalized Concentration". From the results of Fig. 2 we can factor out first order effects of fire size and ventilation rate by dividing the Concentration by the right hand side of Eq. 9. The scale then varies about the value of 1, the well stirred result. Obviously data from near the ceiling will have values higher than the well stirred result while those near the floor will have lower values. The filled symbols are results for the "wall" ventilation configuration (Fig. 1) and the others correspond to the "central" ventilation configuration. In general the "wall" yields higher concentrations for the centerline positions shown in figure 3. It is not clear from Figure 3 whether these higher centerline concentrations are due to a simple local increase in dilution since the source of the fresh air is closer to the sampling position (the cold air in the wall case could travel down adjacent to the wall and exit at the floor) or to a more complex flow pattern. The data symbols represent averages of the data at the particular position; the bars represent high and low values and the number below the symbols is the number of data sets. In general the lower end of the bar corresponds to longer ventilation times and the upper end of the range corresponds to higher heat release experiments. These second order effects then would dictate steady state concentrations varying with Q to somewhat greater than a linear relation and the variation with ventilation time to a somewhat less than a linear relation. Again one might speculate that with lower flow velocities in the longer time cases there is less penetration through the hot upper layers yielding more dilution.

Figure 4 shows the vertical distribution of a scaled temperature profile $(T-T_0)/Q$ which is the average of the four thermocouple tree results in the enclosure. The divergence of the circles and squares as the ceiling is approached is evident from Fig. 4. (Based on the temperature distribution seen on Fig. 4 perhaps a linear with height profile would be more appropriate than a two layer, hot-cold, model to capture the essentials for fire in an enclosure with small ventilation.) The advantage of venting from the top of the cabin can be quantified from the results on Fig. 4. $(T-T_0)/Q = 4$ at the ceiling area and $(T-T_0)/Q = 1$ at the floor area, obviously a factor of 4 or more in thermal energy exchange can be realized by venting at the ceiling versus the floor provided the overall thermal field is not disturbed by the venting, as is the case here. Similarly, one foresees the same advantage is available in consideration of conserved scalars like chemical species and, to first approximation, smoke. Figure 4 further shows that in the mid-level regions, a tripling of the heat release does not quite triple the temperature difference. This effect gets somewhat larger at the enclosure upper levels.

Figure 5 shows the steady state vertical temperature profiles for thermocouple trees A, B, C and D in the enclosure with no hatches. Only near the ceiling, the top few thermocouples, is the thermocouple tree position relative to the fire important. Below this ceiling jet the temperature readings in any horizontal slice are almost identical for the four thermocouple locations.

Figure 6 shows the steady state vertical temperature profiles for thermocouple trees A, B, C and D in the enclosure with the largest pair of hatches (0.0465 m^2 or 15cm x 30cm for each hatch) cut at both of the end walls. Figure 6 and Figure 5 are almost identical, illustrating the insensitivity of the thermal field to the introduction of hatches. This is probably due to the fact that the ceiling receives much of the heat from the fire and can easily reheat the gases to make up for the small amount of thermal energy lost by flow of gases through the hatches.

Figure 7 illustrates the reduction in gaseous concentrations in the enclosure for both the upper and lower positions as a function of hatch size. Selected data are presented in Figure 7. Test results indicate that for the two smallest size hatches (7.5X15 cm each hatch) placed at the top center of the two end walls, a 7% reduction in concentration at the top position (ceiling) and a 16% reduction in concentration in the exhaust (floor) of CO_2 and O_2 occurred. For the next larger size hatches (15X15 cm each hatch) the reductions in concentrations increase to 16% at the top and 24% in the exhaust. For hatch sizes doubled again (15x30 cm each hatch) in the enclosure, the reductions in concentrations increase to 22% at the top and 40% in the exhaust respectively.

The flow of gases through the vent can be estimated by a simple hydraulic calculation if the pressure difference across the cabin is known. For example, with 7.5X15 cm hatches, a differential pressure of about 5 N/m^2 was measured at about the mid height of the box. This would lead to a flow of about 0.04 kg/s out the hatches. For the next larger size hatches (15x15 cm

each hatch), the pressure differential dropped to about 1 N/m^2 thus reducing the velocity by half but, since the hatch area has doubled, the mass flow rate out of the hatches is still about the same. Taking the mass flow rate of about 0.04 kg/s and multiplying by a C_p and the result of Fig. 4 at the ceiling, namely $\Delta T=4xQ$, will yield an thermal energy flow of about 0.1 to 0.2 times Q. That is, between 10% and 20% of the thermal energy released by the fire was being vented at these late, steady state times. For the nominal 3 minute exchange times for these test runs the system ventilation flow is about 2 1/2 times the hatch flow or about 0.1 kg/s. From Fig. 4 at $z/H = 0$ the thermal energy exchange will be reduced by a factor of four in comparison to the ceiling. Both of these are small in comparison to the amount of gas moved by the fire plume entrainment. An estimate of the amount of air entrainment for a 30kW fire to a height of about 1 m is about 0.3 kg/s[3]. Therefore mixing of the gases in the cabin by the fire plume is a dominant force driving gas flow within the cabin. (Note that for a 30kW fire only about 0.01 kg/s is required for combustion). For a source of smoke and toxic products not coming from an entraining fire in the open area of the cabin, as for example, in a fire located in a lavatory or hidden behind walls or other compartments, the situation could be quite different.

4.0 Conclusions

For the situation considered here, i.e. vent holes of the given size placed near the center of the end walls near the ceiling, steady state results indicate:

1) a negligible effect on gas, ceiling and wall temperatures

2) throughout the enclosure the CO_2 concentration is less and the O_2 concentration is greater.

5.0 References

1. Pagni, P., Alvares, N., and Foote, K., Defining Characteristic Times in Forced Ventilation Enclosure Fires, American Society for Testing and Materials, STP 983 (1988).

2. McCaffrey, B., Momentum Implications for Buoyant Diffusion Flames, Combustion and Flame 52, 149 (1983).

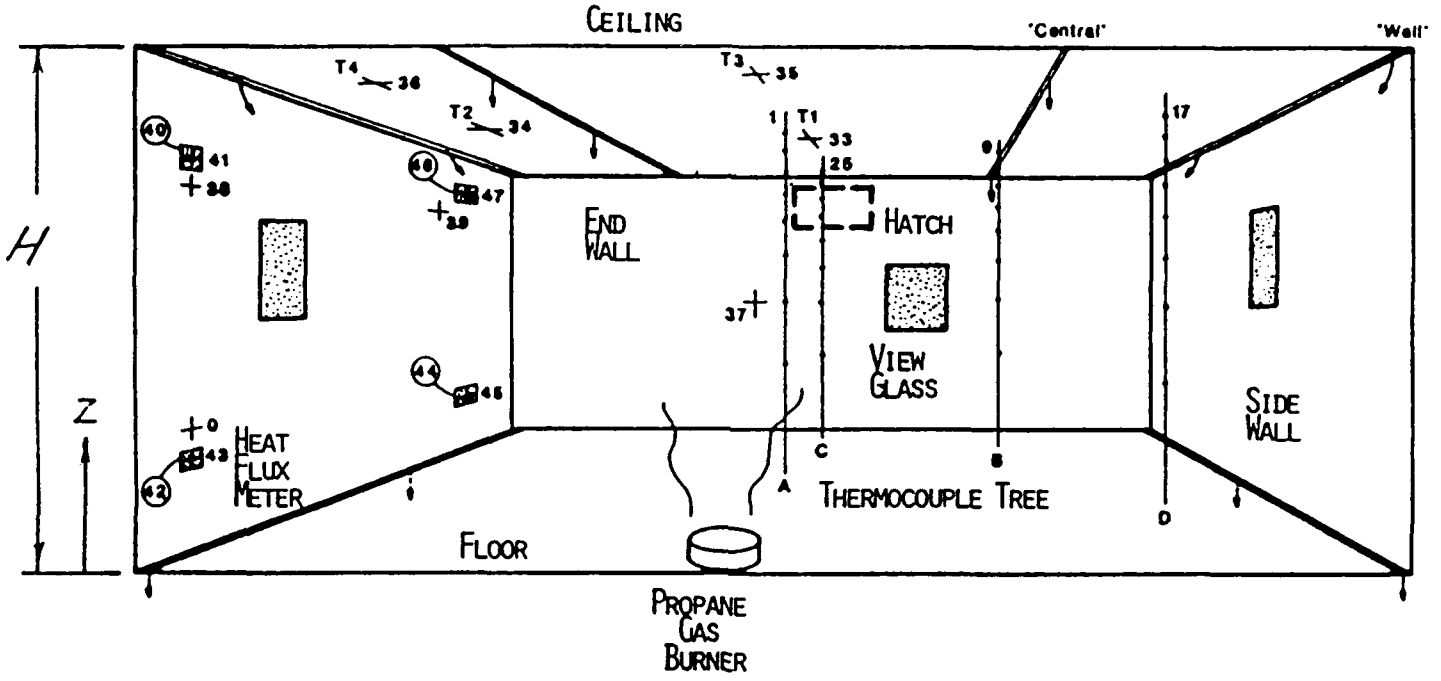

Fig. 1 Interior View of One-Half of Symmetric Enclosure (Seats Not Shown)

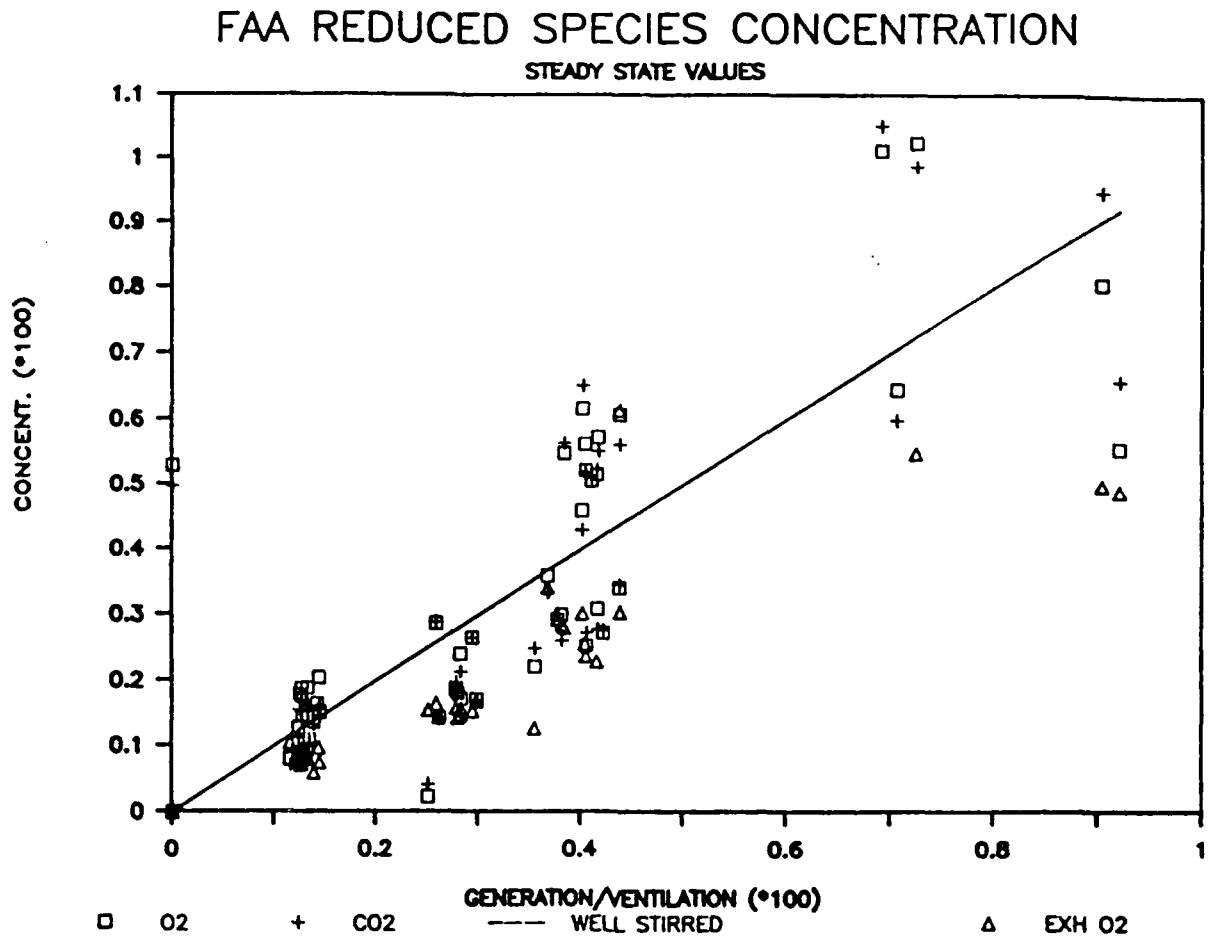

Fig. 2 Gas Concentrations at Steady State

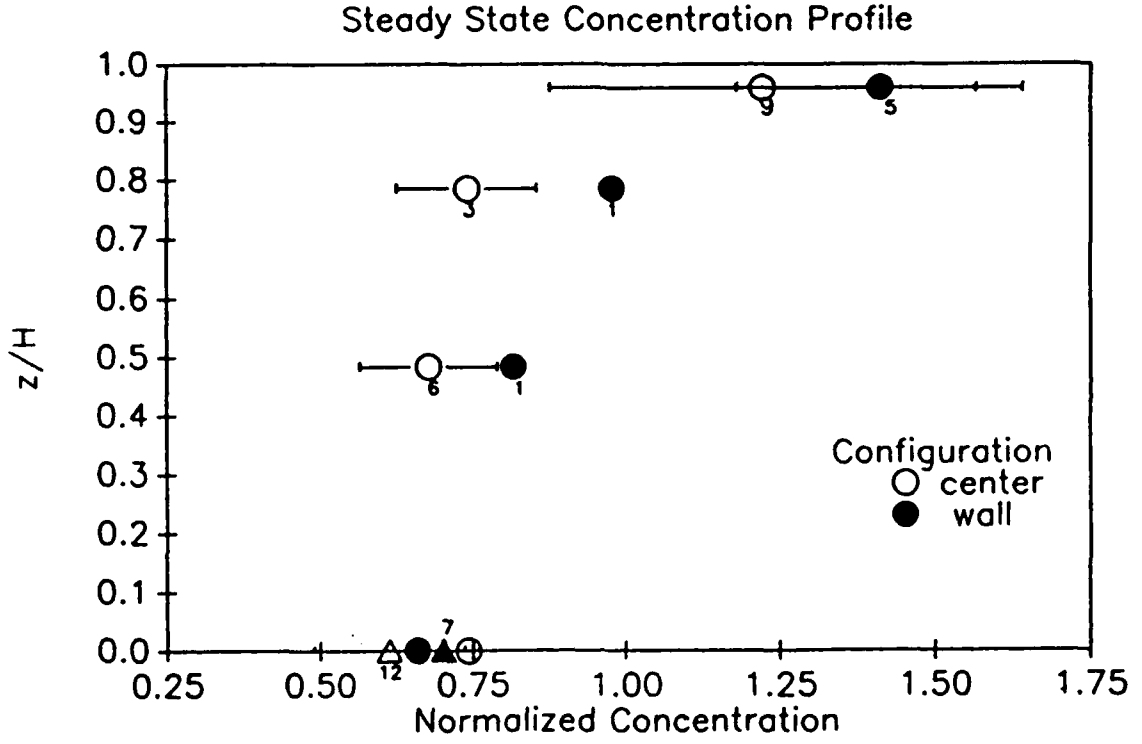

Fig. 3 Vertical Species Distribution

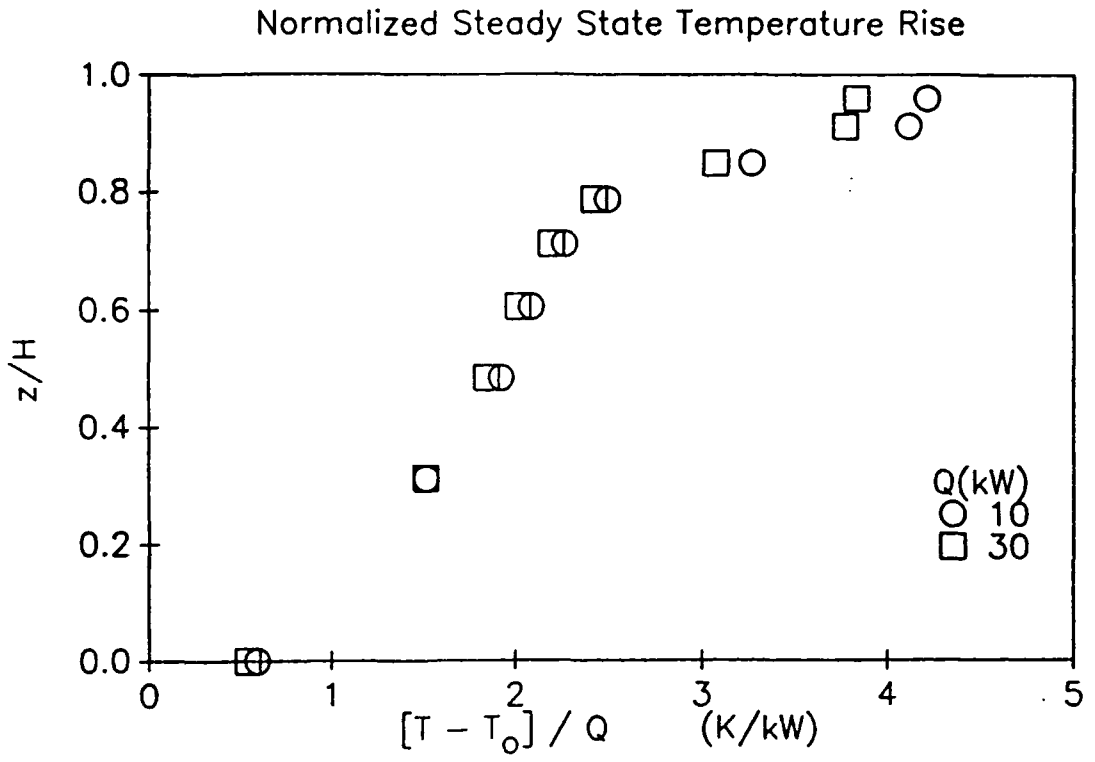

Fig. 4 Vertical Temperature Distribution

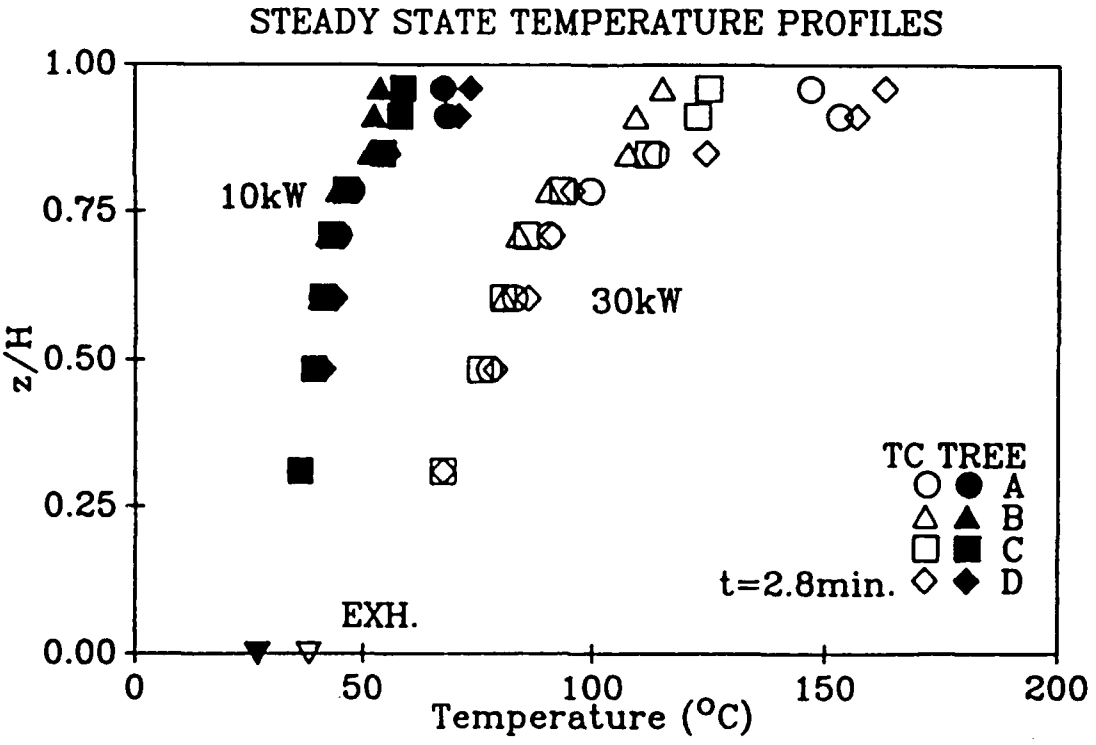

Fig. 5 Temperature Profile (No Hatch)

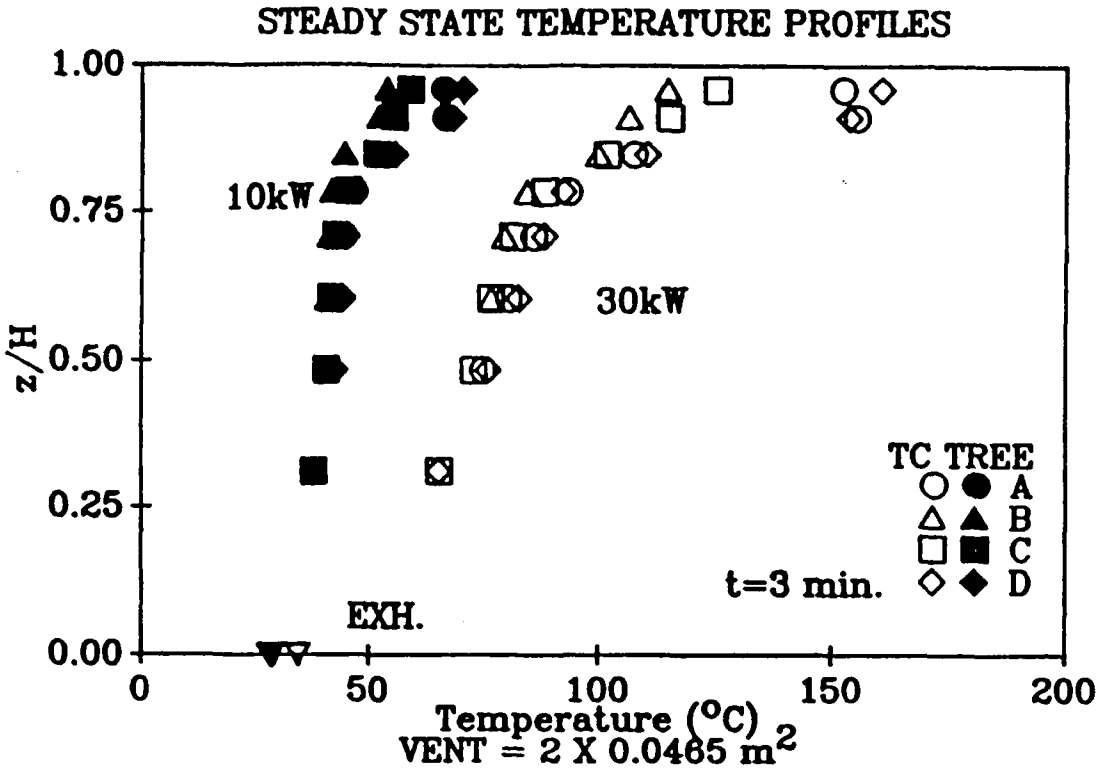

Fig. 6 Temperature Profile (With Hatch)

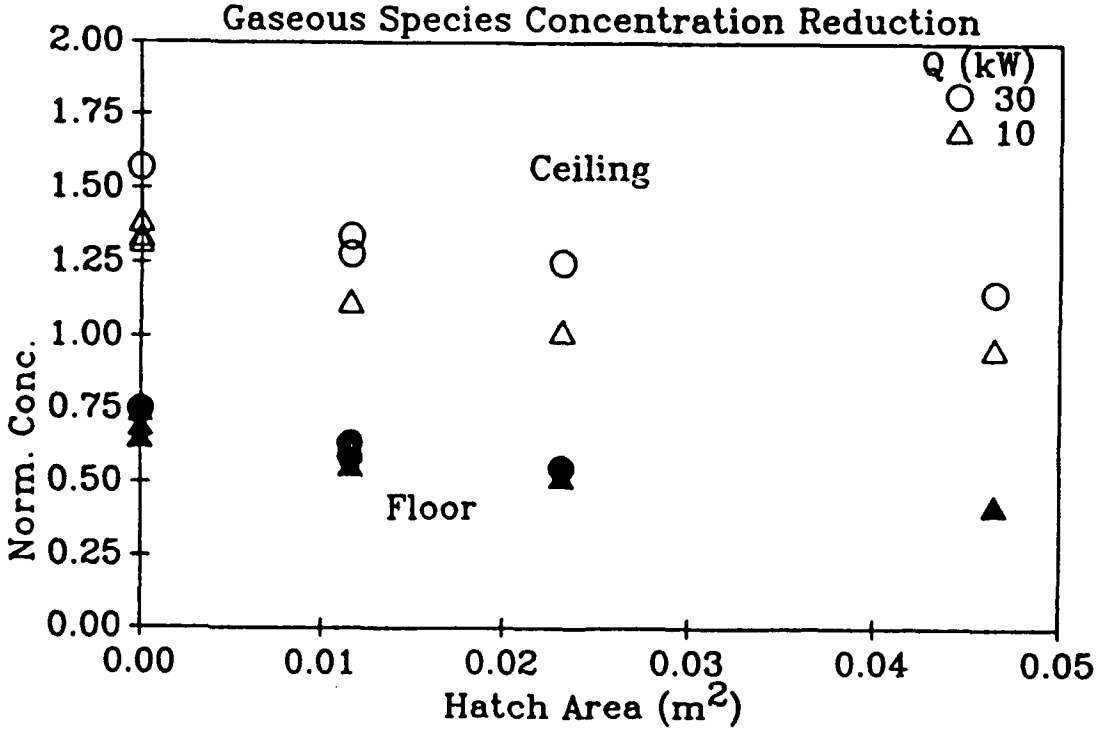

Fig. 7 Species Concentration Decrease, Ceiling and Floor

Chapter 4. Effect of Reversing the Supply Ventilation Air Direction on the Fire Environment in Aircraft Cabins

by

Bernard McCaffrey
University of Maryland
Baltimore, MD

King-Mon Tu and William Rinkinen
Center for Fire Research
National Institute of Standards and Technology

The normal direction for aircraft cabin ventilation is from top-to-bottom; that is, fresh air is forced in at the ceiling and exhausted near the floor. The data and analysis in Chapter 2 indicate that changes in the rate of top-to-bottom ventilation had little effect on the thermal environment produced by a fire in a reduced-scale simulated cabin section. Most of the energy of the fire (C_3H_8 burning in a pool configuration) is initially absorbed by the ceiling above the fire and is not exhausted through the floor vents. This is a consequence of buoyancy forces keeping the hottest and most heavily concentrated smoke and combustion products near the ceiling. The temperature and concentrations fall linearly with decreasing height for the remaining portion of the cabin. Laterally, or in each strata, the gases are quite uniform in temperature. The concentrations of conserved species (CO_2, O_2 depletion) rise and fall almost in direct proportion to ventilation time, which is defined as the time for one complete airchange.

The introduction of hatches near the ceiling of the cabin as a possible remedial action is discussed in Chapter 3. Three rectangular hatches of increasingly larger area were cut into both end walls of the reduced-scale

simulated cabin section and the temperature and chemical species concentration were mapped. The forced ventilation system was operated in the normal top-to-bottom mode. Steady state results indicated that the presence of the hatches had a negligible effect on gas, ceiling and wall temperatures but a significant effect on the values of species concentrations both near the ceiling and the floor. For a set of modest hatches (each of area 0.0465 m^2) reductions in concentrations of 40% and 22% were observed in the exhaust and at the ceiling, respectively.

The current study examines the effects of reversing the direction of the forced ventilation; that is, fresh air is forced in at the floor and exhausted at the ceiling. Experiments were conducted in the same reduced-scale cabin section described in Chapter 2. Although the sizes and positions of the ventilation openings remained unchanged, their roles (inlet/outlet) were interchanged by completely interchanging the supply and exhaust system (i.e. fans, ductworks) external to the reduced-scale cabin. The general flow pattern is now from bottom-to-top, in the same direction as the fire-pumped gases and opposite that of the normal air flow in a passenger aircraft. Comparing the data in Figure 1 (reversed flow) with that in Figure 2 (normal flow), significant reductions in gas temperature throughout the test period are evident, especially the mid to lower cabin positions.

Figure 3 shows the "steady state" spatial average of the gas temperatures measured at common heights on the four thermocouple trees. The "steady state" values are arbitrarily defined as the average of data from 700 to 800 seconds. Except for the uppermost 2 or 3 thermocouple positions, the variance

associated with the spatial average is very small and, therefore, the reported averages are highly representative of the temperatures recorded at each of the four thermocouple trees. Figure 4 is the same data normalized by heat release rate, Q, for ease of interpretation. In contrast to the case of ceiling to floor ventilation, reversed flow data do not scale with the simple first power of Q. The reduction in temperature rise is of the order of 60% for about three-quarters of the height of the cabin. The temperature rise reduction then decreases to about 15% near the ceiling and is slightly lower for the ceiling thermocouples themselves (not shown).

Explicit dependence of gas temperature on ventilation rate can be seen in Figure 5 both for the normal flow mode and for three ventilation rates in the reversed flow mode. The rate of ventilation appears to have a greater effect for the reversed flow situation.

Reductions in chemical species concentrations displayed in Figure 6 are greater than temperature rise reductions in the mid level strata. Although the concentrations are lower in the reversed flow case, the "contaminated" upper layer is thicker and more uniform, indicating that the reversed ventilation flow was "sweeping" the combustion products up to the ceiling.

Figure 7 shows, for the reversed flow mode, the effect of ventilation rate on the "steady state" output of three smoke meters. We see in this figure clearing effects associated with increased ventilation rates.

To put the reversed flow results into perspective, consider Figure 8 which combines the gaseous species concentration results of two fire sizes, 10 kW and 30 kW for (1) Normal Flow Ventilation Mode, and (2) Reversed Flow Ventilation Mode, with (i) no hatches (area = 0 m^2), and (ii) one set of hatches (area = 0.0465 m^2 each hatch). For the given hatch size, the reversed flow gas concentrations are significantly lower than the corresponding normal flow gas concentrations. Indeed, the gas concentrations of reversed flow with no hatch are lower than the results of normal flow with the largest hatch. Also, recall that reversed flow ventilation improved the thermal environment (Figures. 1 and 2), whereas normal flow ventilation had a negligible effect on the temperature data (Chapter 3).

Conclusions

The following conclusions are drawn from this model study of fire environment in aircraft cabins under forced ventilation conditions:

1. Reversing the ventilation flow direction caused a large decrease in both the temperature and the gas concentrations in the test article.

2. The introduction of two 152 mm by 305 mm hatches near the ceiling of the test article had essentially no impact on the verticle temperature profile. It did cause a significant reduction in the gas concentrations.

3. Doubling the ventilation time from 3 to 6 minutes per air exchange had very little impact on the temperature profile. It did decrease the light transmission through the cabin due to smoke. Normally, the combustion product concentration increased linearly with fire size and decreased linearly with ventilation rate.

4. The temperature rise at any elevation was found to be proportional to the total heat release rate.

All the experiments upon which these conclusions were based were performed with a gas burner which had a fixed heat release rate. In an actual aircraft

cabin fire, the heat release rate itself would also be affect by the ventilation conditions.

Acknowledgement

We are grateful to the technical support and advice given by Dr. James Quintiere and Dr. David Evans of the Center for Fire Research and Dr. Thor I. Eklund of the FAA during the course of this work, and acknowledge the sponsor from the FAA Technical Center, Fire Safety Branch to carry out this problem.

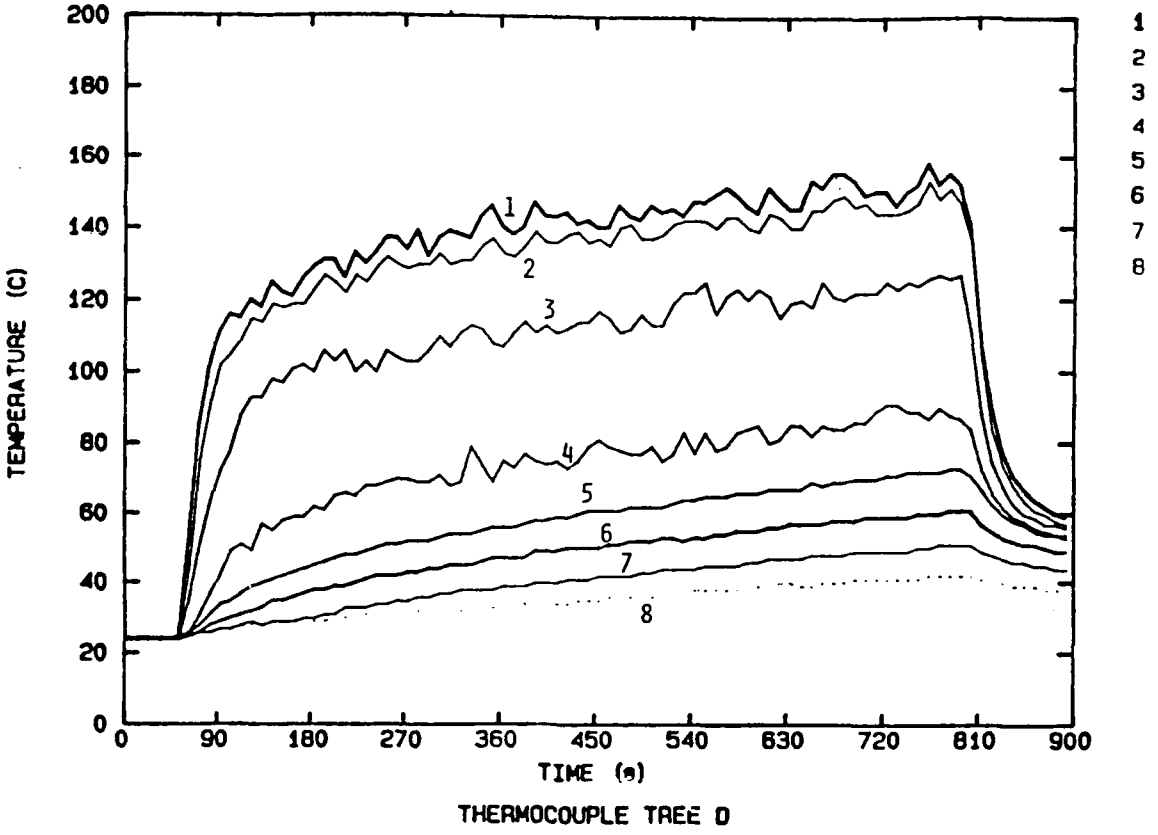

Fig. 1 TC Tree "D" Time History: REVERSED FLOW

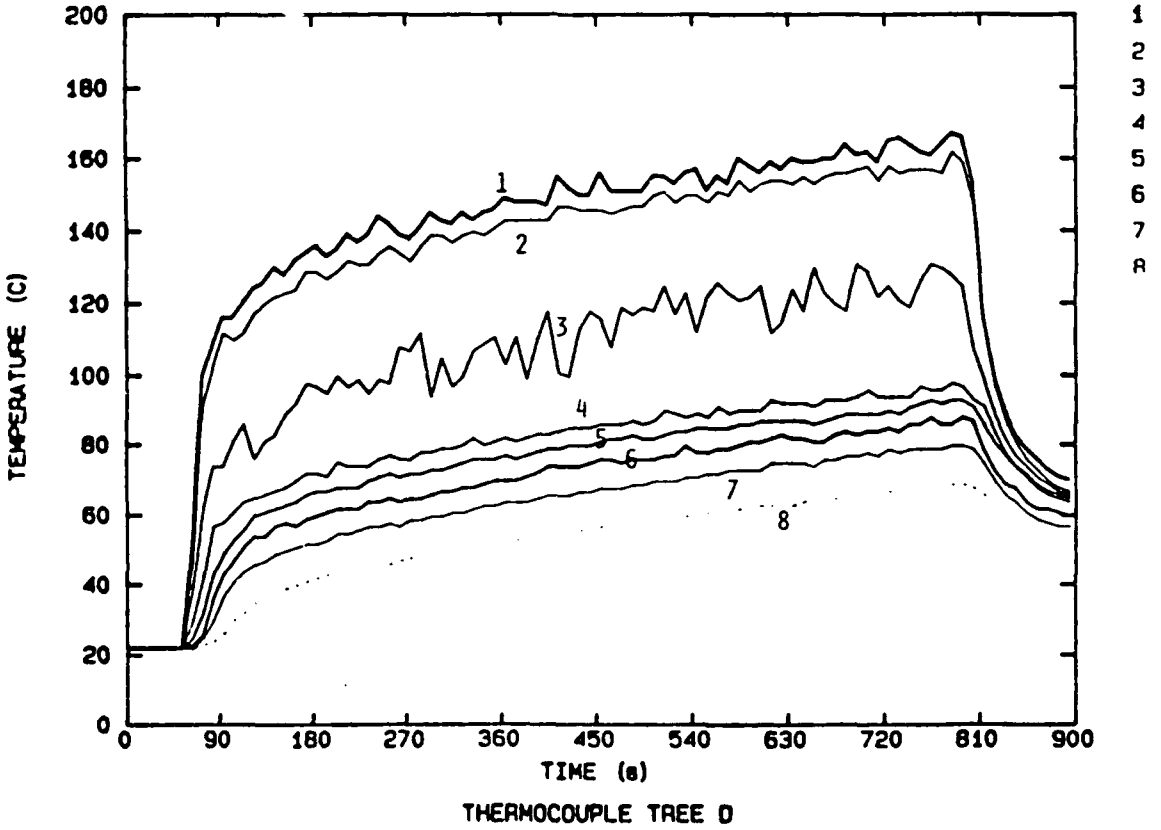

Fig. 2 TC Tree "D" Time History: NORMAL FLOW

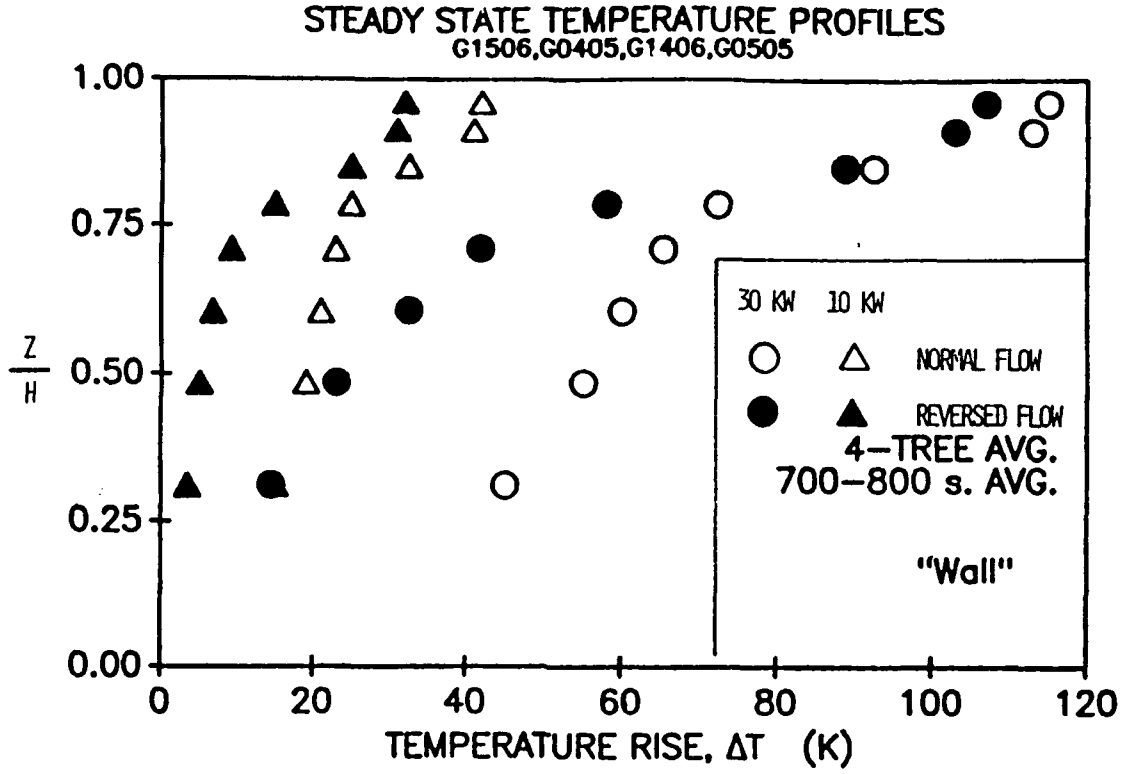

Fig. 3 Temperature Profiles: Reverse vs Normal Flow

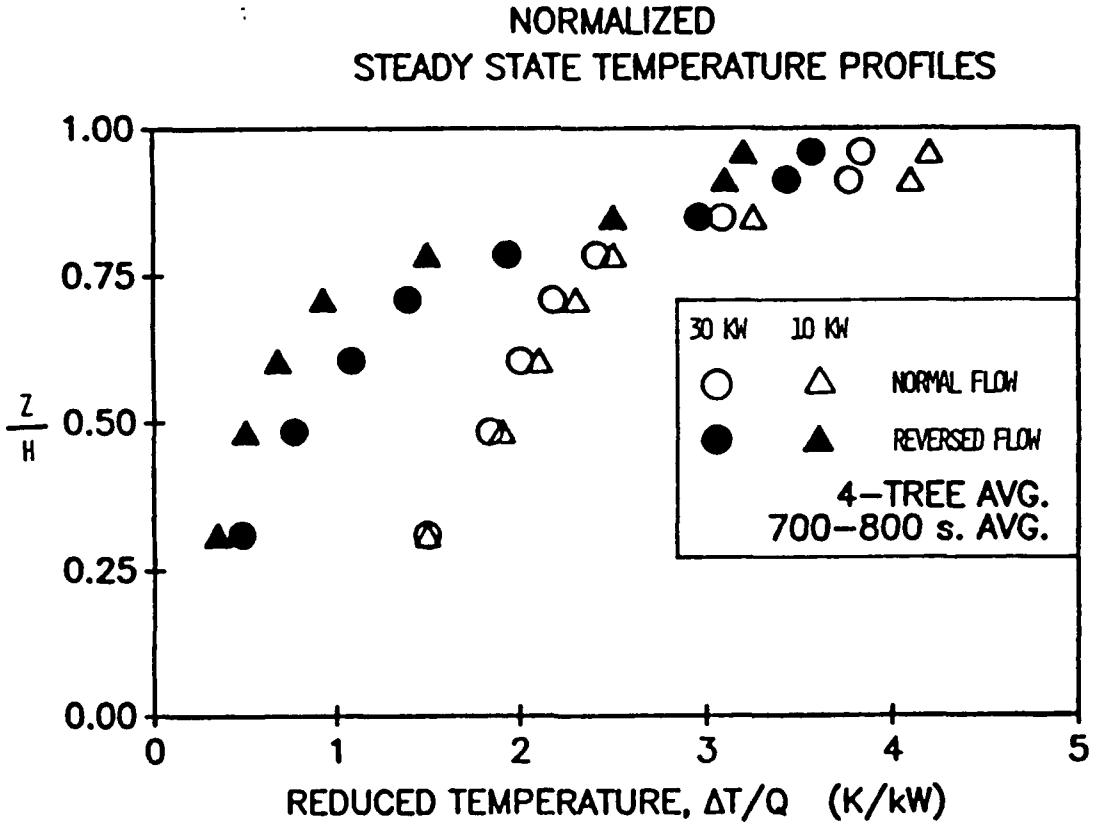

Fig. 4 Normalized Profiles: Reverse vs Normal Flow

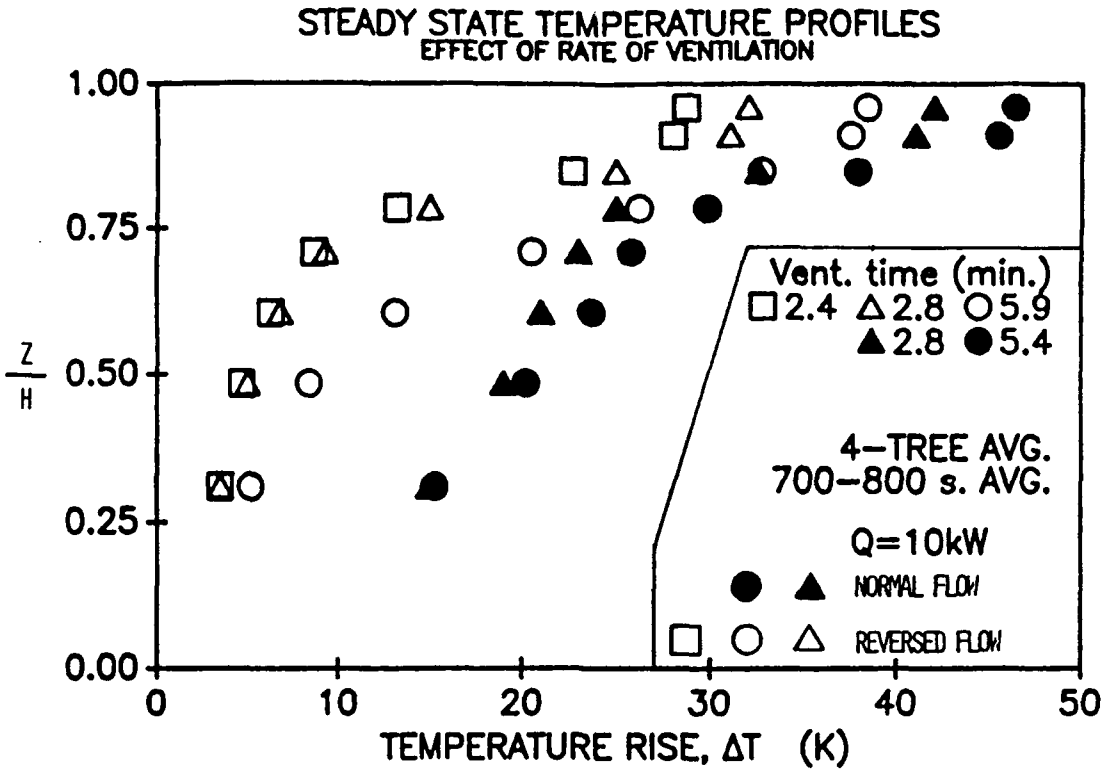

Fig. 5 Effect of Ventilation

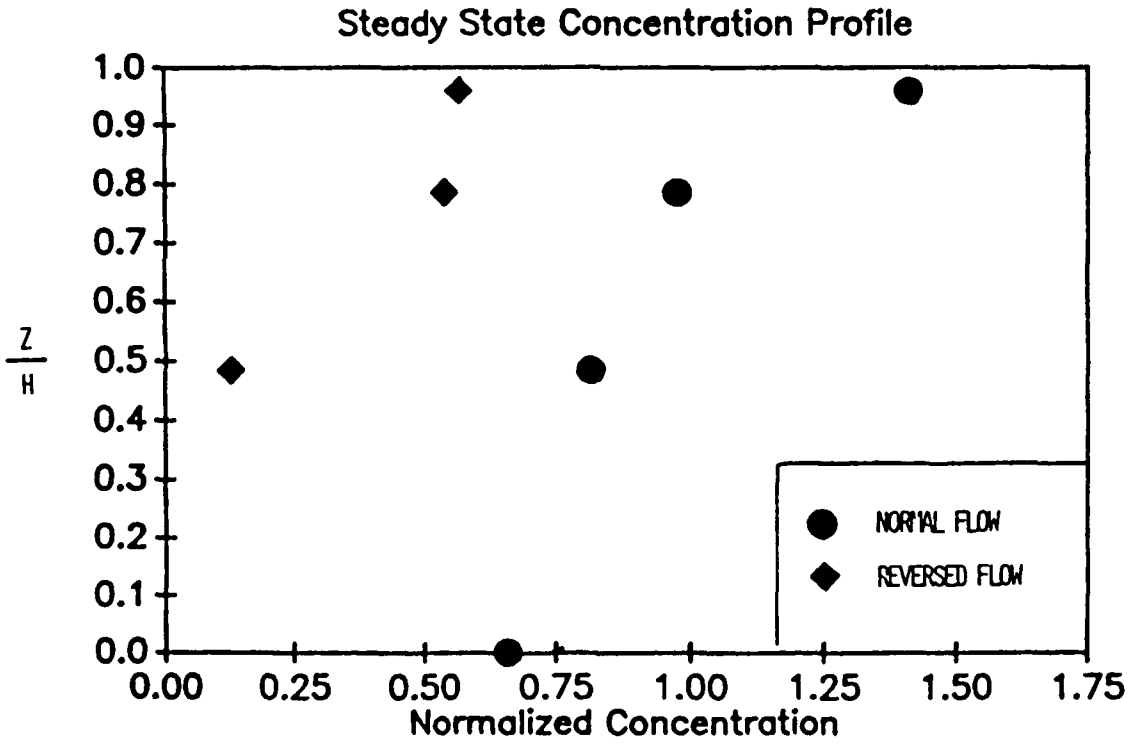

Fig. 6 Chemical Species: Reverse vs Normal Flow

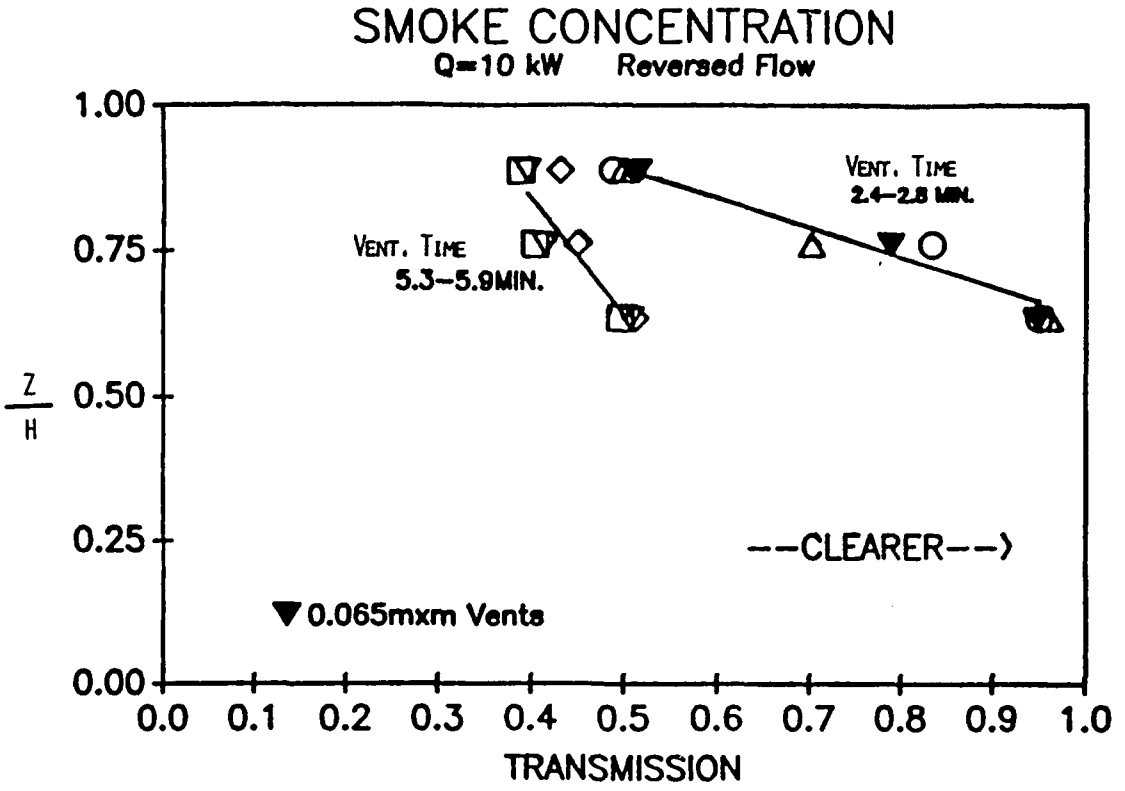

Fig. 7 Effect of Ventilation Rate on Smoke (Reversed Mode)

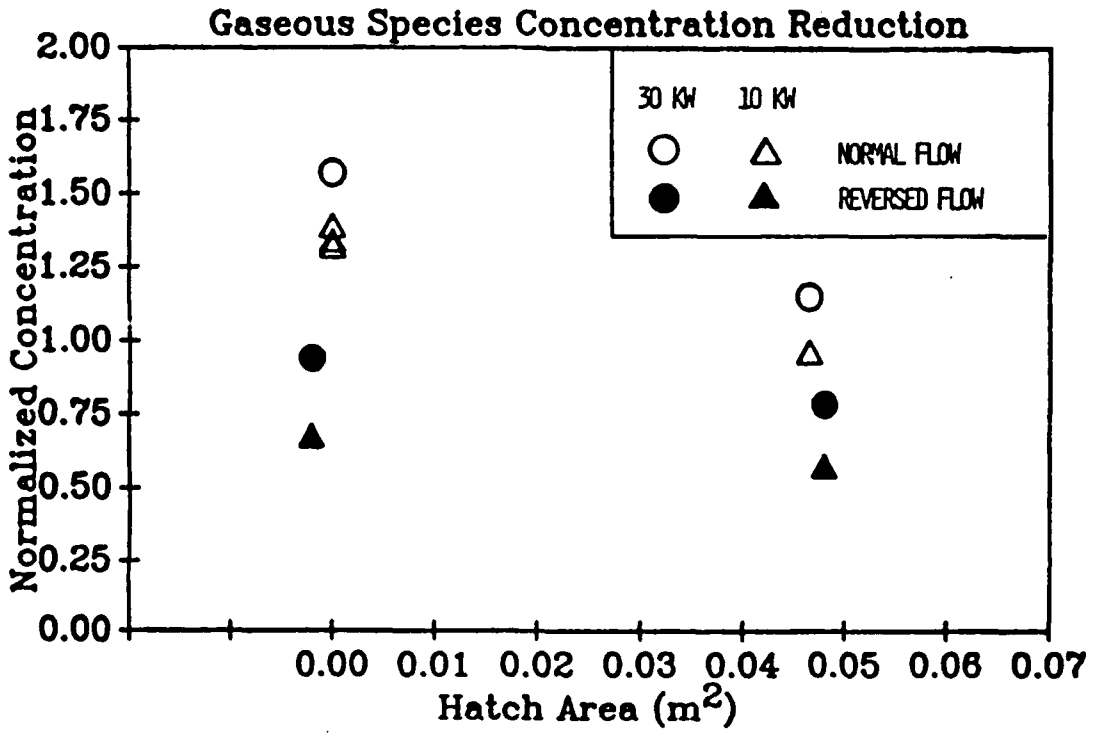

Fig. 8 Efficacy of Venting and Reversing Flow

☆U.S. GOVERNMENT PRINTING OFFICE: 1993 - 704-078/60225